



U.S. DEPARTMENT OF
ENERGY

PNNL-22130

Prepared for the U.S. Department of Energy
Under Contract DE-AC05-76RL01830

STOMP-HYDT-KE

A Numerical Simulator for the Production of Natural Gas Hydrate using Guest Molecule Exchange with CO₂ and N₂

Revision 1.0

M.D. White

December 2012



Pacific Northwest
NATIONAL LABORATORY

DISCLAIMER

This report was prepared as an account of work sponsored by an agency of the United States Government. Neither the United States Government nor any agency thereof, nor Battelle Memorial Institute, nor any of their employees, makes **any warranty, express or implied, or assumes any legal liability or responsibility for the accuracy, completeness, or usefulness of any information, apparatus, product, or process disclosed, or represents that its use would not infringe privately owned rights.** Reference herein to any specific commercial product, process, or service by trade name, trademark, manufacturer, or otherwise does not necessarily constitute or imply its endorsement, recommendation, or favoring by the United States Government or any agency thereof, or Battelle Memorial Institute. The views and opinions of authors expressed herein do not necessarily state or reflect those of the United States Government or any agency thereof.

PACIFIC NORTHWEST NATIONAL LABORATORY
operated by
BATTELLE
for the
UNITED STATES DEPARTMENT OF ENERGY
under Contract DE-AC05-76RL01830

Printed in the United States of America

Available to DOE and DOE contractors from the
Office of Scientific and Technical Information,
P.O. Box 62, Oak Ridge, TN 37831-0062;
ph: (865) 576-8401
fax: (865) 576-5728
email: reports@adonis.osti.gov

Available to the public from the National Technical Information Service,
U.S. Department of Commerce, 5285 Port Royal Rd., Springfield, VA 22161
ph: (800) 553-6847
fax: (703) 605-6900
email: orders@ntis.fedworld.gov
online ordering: <http://www.ntis.gov/ordering.htm>

STOMP-HYDT-KE

A Numerical Simulator for the Production of Natural Gas Hydrate using Guest Molecule Exchange with CO₂ and N₂

Revision 1.0

M.D. White

December 2012

Prepared for
the U.S. Department of Energy
under Contract DE-AC05-76RL01830

Pacific Northwest National Laboratory
Richland, Washington 99352

Preface

This STOMP (Subsurface Transport Over Multiple Phases) guide document describes the theory and application of the STOMP-HYDT-KE operational mode. This operational mode of the STOMP simulator is designed to solve problems involving the production of natural gas hydrates from geologic accumulations, using depressurization, thermal stimulation, inhibitor injection or guest molecule exchange technologies. One unique feature of the STOMP-HYDT-KE operational mode is its capabilities for ternary hydrates of CH₄, CO₂, and N₂ mixtures, which is reflected in the “HYDT” part of the simulator name. Another unique feature of the simulator is that it tracks mobile and gas-hydrate components of the hydrate formers (i.e., CH₄, CO₂, and N₂) independently, with transfer between the mobile and gas hydrate fractions occurring via kinetic exchange. This kinetic feature of the code is also reflected in the “KE” part of the simulator name. This manuscript is intended to document the theory and application of the STOMP-HYDT-KE to the production of natural gas hydrates and is expected to evolve as new applications of the simulator are realized. Currently the document is not intended to serve as a user’s guide, as it is void of input formatting instructions, except for the input files included in the problem descriptions.

The STOMP-HYDT-KE simulator is written in Fortran 90 with dynamic memory allocation. The code can be configured for either a banded or conjugate gradient linear system solver. The simulator is provided as source code to encourage the open exchange of scientific and mathematical ideas, but this requires that the user compile and link the code into an executable. In writing this manuscript the authors have assumed that the reader is familiar with numerical simulation of multifluid subsurface flow and reactive transport and with the computing environment on which they plan to compile and execute the STOMP-HYDT-KE simulator. The simulator is maintained following a configuration management plan as a collection of source code files. Assembly of the library files into a single source code or executable occurs through a software maintenance utility. Version numbers are assigned to individual files in the STOMP library of files and those version numbers are reported to standard output and the “output” file for the active files in the executable at the conclusion of the execution. The memory requirements for executing the STOMP-HYDT-KE simulator is dependent on the complexity of the physical system to be modeled and the size and dimensionality of the computational domain. Likewise, execution speed depends on the problem complexity, size and dimensionality of the computational domain, and computer performance.

Summary

Hydrates of natural gas occur in geologic deposits under conditions where a source of natural gas seeps into aquifers with low temperatures and high pressures. Natural gas sources can be biogenic, created by biological activity in sediments, and/or thermogenic, created by geochemical processes deeper in the earth. Geologic settings with low-temperature and high-pressure conditions, sufficient to create natural gas hydrates, have been located under the Arctic permafrost and beneath the ocean floor. Whereas estimates vary the energy content of methane stored in gas hydrate form probably exceeds all other known fossil fuels. The potential energy resource of natural gas hydrates held in geologic accumulations, using lower volumetric estimates, is sufficient to meet the world demand for natural gas for nearly eight decades, at current rates of increase. As with other unconventional energy resources, the challenge is to economically produce the natural gas fuel. The gas hydrate challenge is principally technical. Meeting that challenge will require innovation, but more importantly, scientific research to understand the resource and its characteristics in porous media. The thermodynamic complexity of gas hydrate systems makes numerical simulation a particularly attractive research tool for understanding production strategies and experimental observations. Simply stated, producing natural gas from gas hydrate deposits requires releasing CH₄ from solid gas hydrate. The conventional way to release CH₄ is to dissociate the hydrate by changing the pressure and temperature conditions to those where the hydrate is unstable. Alternatively, the guest-molecule exchange technology releases CH₄ by replacing it with more thermodynamically stable molecules (e.g., CO₂, N₂). This technology has three advantageous: 1) it sequesters greenhouse gas, 2) it potentially releases energy via an exothermic reaction, and 3) it retains the hydraulic and mechanical stability of the hydrate reservoir. Numerical simulation of the production of gas hydrates from geologic deposits requires accounting for coupled processes: multfluid flow, mobile and immobile phase appearances and disappearances, heat transfer, and multicomponent thermodynamics.

The U.S. Department of Energy (DOE), through the National Environmental Technology Laboratory (NETL) and the Korea National Gas Hydrate Program, through the Korea Institute for Geosciences and Mineral Resources (KIGAM) has requested the development of numerical simulation capabilities for the production of natural gas hydrates from geologic deposits. Funding from both agencies via the Korea-U.S. Gas Hydrate Joint Program has supported the development of a series of STOMP-HYD simulators by the Pacific Northwest National Laboratory¹ (PNNL). The first simulator in the series, STOMP-HYD, was capable of simulating four production technologies: 1) depressurization, 2) thermal stimulation, 3) inhibitor injection and 4) CO₂ exchange. This simulator assumed equilibrium conditions between the mobile and hydrate components of the hydrate formers, CH₄ and CO₂. Experiments conducted at the Korea Institute of Geoscience and Mineral Resources (KIGAM), however, demonstrated that guest molecule exchange was a kinetic process, with respect to the time scales for flow through geologic media. The second simulator in the series, STOMP-HYD-KE, extended the capabilities of STOMP-HYD, by solving separate conservation equations for the mobile and hydrate components of the hydrate formers, CH₄ and CO₂. Hydrate formers transitioned between mobile and hydrate forms via hydrate formation, dissociation, and exchange; where, all three mechanisms were controlled via kinetic rates. The STOMP-HYDT-KE simulator extends the capabilities of its predecessor by including a third hydrate former, N₂. As with the two other hydrate formers, CH₄ and CO₂, the mobile and hydrate components of N₂ are solved separately. In its full capability configuration, the STOMP-HYDT-KE solves nine conservation equations at each grid cell: 1) energy, 2) water mass, 3) mobile CH₄ mass, 4) hydrate CH₄ mass, 3) mobile CO₂ mass, 4) hydrate CO₂ mass, 3) mobile N₂ mass, 4) hydrate N₂ mass, and 9) inhibitor mass. The modular design of the simulator allows for one or two of the hydrate formers and/or the inhibitor to be eliminated from the solution. The transition between STOMP-HYD-KE and STOMP-HYDT-KE involved two significant changes in the code: 1) equation of state module and 2) ternary hydrate equilibria. This manuscript documents the incremental changes that were

¹ Pacific Northwest National Laboratory is operated for the U.S. Department of Energy by Battelle Memorial Institute

made to develop the STOMP-HYDT-KE simulator from the STOMP-HYD-KE simulator and demonstrates the simulator application via a series of benchmarking problems.

KEYWORDS: natural gas hydrate; depressurization; thermal stimulation; inhibitor injection; guest molecule exchange; CO₂; CH₄; N₂; numerical simulation; STOMP

Acknowledgments

Development, verification and documentation of the STOMP-HYDT-KE by the Pacific Northwest National Laboratory (PNNL) was funded by the U.S. Department of Energy (DOE) Office of Fossil Energy, through the National Energy Technology Laboratory (NETL) and by the Korea Natural Gas Hydrate Program, through the Korea Institute of Geoscience and Mineral Resources (KIGAM).

Lou Capitanio
Office of Fossil Energy
U.S. Department of Energy
Washington, DC 20585
202-586-5098

Ray Boswell
National Energy Technology Laboratory
P.O. Box 880
U.S. Department of Energy
Morgantown, WV 26507
304-285-4541

Seung-Ho Kim
Gas Hydrate R&D Organization
124 Gwahang-no Yuseong-gu
Daejeon 305-350 Korea
+82 42 868 3360

Se-Joon Kim
Korea Institute of Geoscience and Mineral Resources
124 Gwahang-no Yuseong-gu
Daejeon 305-350 Korea
+82 42 868 3214

Nomenclature

Roman Symbols

a	Peng-Robinson parameter, J/kmol [$\text{m L}^2/\text{n t}^2$]
A_n	Avagadro's number, molecules/kmol [$1/\text{n}$]
b	Peng-Robinson parameter, m^3/kmol [L^3/n]
c	Peneloux volume correction parameter, m^3/kmol [L^3/n]
D	molecular diffusion coefficient, m^2/s [L^2/t]
g	acceleration of gravity, m/s^2 [L/t^2]
h	enthalpy, J/kg [L^2/t^2]
H	Henry's coefficient, Pa [$\text{m}/\text{L t}^2$]
\mathbf{J}	diffusive flux vector, $\text{kg}/\text{m}^2 \text{ s}$ [$\text{m}/\text{L}^2 \text{ t}$]
k_{ij}	binary interaction parameter
\mathbf{k}_e	effective thermal conductivity vector, $\text{W}/\text{m K}$ [$\text{L}/\text{t}^3 \text{ T}$]
K_e	kinetic guest molecule exchange parameter, kg/s [m/t]
K_f	kinetic formation parameter, $\text{kg}/\text{Pa s}$ [L t]
k_r	relative permeability
m	mass source rate, kg/s [m/t]
m_h^i	hydrate mass of component i , kg [m]
M	molecular weight, kg/kmol [m/n]
n^{H_2O}	hydration number
N_{lc}	number of large-cage molecules
N_{sc}	number of small-cage molecules
P	pressure, Pa [$\text{m}/\text{L s}^2$]
P_{CO_2,CH_4}	pressure at tabulated CO_2 and CH_4 mole fractions, Pa [$\text{m}/\text{L s}^2$]
P_g^i	gas partial pressure of component i , Pa [$\text{m}/\text{L s}^2$]
P_{gn}	maximum of gas and nonaqueous-liquid pressures, Pa [$\text{m}/\text{L s}^2$]
q	energy source rate or power, W [L^2/t^3]
R	ideal gas constant, J/kmol K [$\text{m L}^2/\text{n t}^2 \text{ T}$]
s	saturation
t	time, s [t]
T	temperature, C [T]
T_{CO_2,CH_4}	temperature at tabulated CO_2 and CH_4 mole fractions, C [T]
u	internal energy, J/kg [L^2/t^2]
V	molar volume, m^3/kmol [L^3/n]
\mathbf{V}	volumetric flux or Darcy velocity vector, m/s [L/t]

V_{uc}	sI unit-cell volume, m ³ [L ³]
x_i	nonaqueous-liquid phase mole fraction of component i
y_i	gas phase mole fraction of component i
z	total gas and nonaqueous-liquid mole fraction
\mathbf{z}	gravitational unit vector
Z	compressibility factor
Z_{RA}	Rackett compressibility factor

Greek Symbols

β	capillary head scaling factor
φ_e^i	gas former mole fraction in equilibrium with hydrate of component i
φ_g^i	gas former mole fraction in equilibrium with mobile phases of component i
φ_h^i	hydrate former mole fraction of component i
φ_m^i	mobile former mole fraction of component i
η	component volumetric density, kg/m ³ [m/L ³]
μ	viscosity, Pa s [m/L t]
ρ	density, kg/m ³ [m/L ³]
τ	tortuosity factor
ν	specific molar volume, m ³ /kmol [L ³ /n]
Φ	fugacity coefficient
ϕ	porosity
χ	mole fraction
ψ_b^s	total-salt mass fraction in brine
ψ_h^i	hydrate mole fraction of formers of component i
ω	mass fraction or acentric factor

Subscripts

c	critical point
e	nonwetting fluid entry
g	gas phase (mobile)
gn	gas or nonaqueous phase
h	hydrate phase (immobile)
i	ice phase (immobile)
l	aqueous phase (mobile)
lc	large cage
mp	Webb matching point
n	nonaqueous-liquid phase (mobile)

<i>na</i>	total nonaqueous phases
<i>od</i>	oven dried conditions
<i>p</i>	precipitated salt phase (immobile)
<i>r</i>	residual
<i>sc</i>	small cage
<i>t</i>	total liquid (mobile)
γ	phase index

Superscripts

<i>c</i>	CO ₂ component
<i>i</i>	component index
<i>j</i>	component index
<i>m</i>	CH ₄ component
<i>n</i>	N ₂ component
<i>s</i>	salt/inhibitor component
<i>w</i>	water component

Contents

Preface.....	iii
Summary.....	v
Acknowledgments.....	vii
Nomenclature.....	ix
1.0 Introduction.....	1.1
2.0 Mathematical Model.....	2.1
2.1 Equation of State.....	2.1
2.1.1 Tabular Data for Gas and Nonaqueous-Liquid Equilibria.....	2.1
2.1.2 Interpolation Algorithm for Tabular Data of Gas and Nonaqueous-Liquid Equilibria.....	2.3
2.1.3 Gas and Nonaqueous-Liquid Density.....	2.6
2.1.4 Aqueous Composition and Density.....	2.7
2.1.5 Ice Composition and Density.....	2.8
2.1.6 Hydrate Composition and Density.....	2.8
2.1.7 EOS Discussion.....	2.11
2.2 Conservation Equations.....	2.11
2.3 Constitutive Equations.....	2.13
2.3.1 Aqueous Viscosity.....	2.13
2.3.2 Gas Viscosity.....	2.13
2.3.3 Nonaqueous-Liquid Viscosity.....	2.13
2.3.4 Aqueous Diffusion Coefficients.....	2.13
2.3.5 Gas Diffusion Coefficients.....	2.14
2.3.6 Nonaqueous-Liquid Diffusion Coefficients.....	2.14
2.3.7 Aqueous Thermal Conductivity.....	2.14
2.3.8 Gas Thermal Conductivity.....	2.14
2.3.9 Nonaqueous-Liquid Thermal Conductivity.....	2.14
2.3.10 Ice Thermal Conductivity.....	2.14
2.3.11 Hydrate Thermal Conductivity.....	2.14
2.3.12 Aqueous Enthalpy and Internal Energy.....	2.15
2.3.13 Gas Enthalpy and Internal Energy.....	2.15
2.3.14 Nonaqueous-Liquid Enthalpy and Internal Energy.....	2.15
2.3.15 Ice Enthalpy and Internal Energy.....	2.15
2.3.16 Hydrate Enthalpy and Internal Energy.....	2.15
2.4 Numerical Solution.....	2.16
2.5 Initial Conditions.....	2.19
3.0 Demonstration Problems.....	3.22
3.1 Verification Problems.....	3.22

3.1.1	Transition to Equilibrium without Hydrates: TTE1	3.22
3.1.2	Transition to Equilibrium from Hydrate and Mobile Phase Non-equilibria: TTE23.26	
3.1.3	Transition to Equilibrium from Hydrate and Mobile Phase Equilibria: TTE3	3.30
3.1.4	Transition to Equilibrium from Hydrate and Mobile Phase Equilibria: TTE4	3.34
3.2	Benchmark Problems.....	3.38
3.2.1	Mixed CO ₂ and N ₂ Gas Flow through a CH ₄ Hydrate Bearing Column	3.38
3.3	Validation Problems.....	3.42
3.3.1	KIGAM 2006 Experiment	3.42
4.0	References	4.1

Figures

Figure 1. Phase Envelope Elements (adopted from Pedersen and Christensen, 2007).....	2.2
Figure 2. Phase Envelope for Mixtures of CH ₄ , CO ₂ , and N ₂	2.3
Figure 3. Modified Bicubic Spline Interpolation Scheme on CO ₂ and CH ₄ Mole Fraction of Formers	2.4
Figure 4. Phase Envelope Interpolated versus Computed.....	2.5
Figure 5. Former Mole Fraction of CO ₂ in Hydrate versus CO ₂ and CH ₄ Former Mole Fraction in Gas under Equilibrium Conditions at 4°C.....	2.9
Figure 6. Former Mole Fraction of CH ₄ in Hydrate versus CO ₂ and CH ₄ Former Mole Fraction in Gas under Equilibrium Conditions at 4°C.....	2.9
Figure 7. Former Mole Fraction of N ₂ in Hydrate versus CO ₂ and CH ₄ Former Mole Fraction in Gas under Equilibrium Conditions at 4°C.....	2.10
Figure 8. Hydrate Density versus CO ₂ and CH ₄ Former Mole Fraction in Gas under Equilibrium Conditions at 4°C	2.11
Figure 9. Transition to Equilibrium (TTE1) for Gas Pressure, Aqueous Pressure, Temperature, and Aqueous Saturation	3.23
Figure 10. Transition to Equilibrium (TTE1) for Gas Mass Fractions of Hydrate Formers.....	3.23
Figure 11. Transition to Equilibrium (TTE2) for Gas Pressure, Aqueous Pressure, Temperature, and Aqueous Saturation.....	3.27
Figure 12. Transition to Equilibrium (TTE1) for Gas Mass Fractions of Hydrate Formers.....	3.27
Figure 13. Transition to Equilibrium (TTE3) for Aqueous Saturation, Hydrate Saturation, Gas Saturation, Temperature, and Gas Pressure	3.31
Figure 14. Transition to Equilibrium (TTE3) for Hydrate Mass Fractions and Gas Mole Fraction of Formers.....	3.31
Figure 15. Transition to Equilibrium (TTE3) for Aqueous Saturation, Hydrate Saturation, Gas Saturation, Temperature, and Gas Pressure	3.35
Figure 16. Transition to Equilibrium (TTE3) for Hydrate Mass Fractions and Gas Mole Fraction of Formers.....	3.35
Figure 17. Profiles of Hydrate Saturation at 0, 10, 50, 100, 500, 1000, and 3600 s	3.39
Figure 18. Profiles of CO ₂ Hydrate Mass Fraction at 0, 10, 50, 100, 500, 1000, and 3600 s	3.39
Figure 19. Profiles of CH ₄ Hydrate Mass Fraction at 0, 10, 50, 100, 500, 1000, and 3600 s	3.40
Figure 20. Profiles of N ₂ Hydrate Mass Fraction at 0, 10, 50, 100, 500, 1000, and 3600 s.....	3.40
Figure 21. Profiles of Aqueous Saturation at 0, 10, 50, 100, 500, 1000, and 3600 s.....	3.41
Figure 22. Profiles of Gas Saturation at 0, 10, 50, 100, 500, 1000, and 3600 s	3.41
Figure 23. Profiles of Temperature at 0, 10, 50, 100, 500, 1000, and 3600 s	3.42
Figure 24. Experimental Apparatus	3.43
Figure 25. Soil Grain Size Distribution	3.44
Figure 26. Drained Water Mass versus Time during the Gas Flooding Simulation for the Constant Pressure and Constant Flow Rate Scenarios.....	3.47
Figure 27. Gas Mass Flow Rate versus Time during the Gas Flooding Simulation for the Constant Pressure and Constant Flow Rate Scenarios.....	3.47

Figure 28. Pressure and Saturation Profiles versus Column Height at the End of the Gas Flooding Simulation for the Constant Pressure and Constant Flow Rate Scenarios.....	3.48
Figure 29. Temperature and Pressure Profiles versus Column Height at the End of the First Pressurization Simulation of the Hydrate Formation Stage	3.49
Figure 30. Temperature and Pressure versus Time during the Temperature Reduction to 1°C Simulation of the Hydrate Formation Stage	3.49
Figure 31. Aqueous, Gas, and Hydrate Saturation versus Time during the Temperature Reduction to 1°C Simulation of the Hydrate Formation Stage	3.50
Figure 32. Integrated CH ₄ and Water Mass versus Time during the Temperature Reduction to 1°C Simulation of the Hydrate Formation Stage	3.50
Figure 33. Hydrate, Gas, Nonaqueous-Liquid, and Aqueous Saturation versus Time at the Column Top, Middle and Bottom for Cycle 1 of the Swapping at Constant Flow Rate Simulation.....	3.52
Figure 34. CO ₂ Mass Fraction in Hydrate, Gas, Nonaqueous-Liquid and Aqueous versus Time at the Column Top, Middle and Bottom for Cycle 1 of the Swapping at Constant Flow Rate Simulation.....	3.53
Figure 35. CH ₄ Mass Fraction in Hydrate, Gas, Nonaqueous-Liquid and Aqueous versus Time at the Column Top, Middle and Bottom for Cycle 1 of the Swapping at Constant Flow Rate Simulation.....	3.53
Figure 36. N ₂ Mass Fraction in Hydrate, Gas, Nonaqueous-Liquid and Aqueous versus Time at the Column Top, Middle and Bottom for Cycle 1 of the Swapping at Constant Flow Rate Simulation.....	3.54
Figure 37. Differential Total and Hydrate CO ₂ , CH ₄ , and N ₂ Mass versus Time at the Column Top, Middle and Bottom for Cycle 1 of the Swapping at Constant Flow Rate Simulation	3.54
Figure 38. CO ₂ , CH ₄ , N ₂ , Gas, and Nonaqueous-Liquid Mass Crossing the Bottom Surface versus Time for Cycle 1 of the Swapping at Constant Flow Rate Simulation.....	3.55
Figure 39. Hydrate, Gas, Nonaqueous-Liquid, and Aqueous Saturation versus Time at the Column Top, Middle and Bottom for Cycle 2 of the Swapping at Constant Flow Rate Simulation.....	3.56
Figure 40. CO ₂ Mass Fraction in Hydrate, Gas, Nonaqueous-Liquid and Aqueous versus Time at the Column Top, Middle and Bottom for Cycle 2 of the Swapping at Constant Flow Rate Simulation.....	3.57
Figure 41. CH ₄ Mass Fraction in Hydrate, Gas, Nonaqueous-Liquid and Aqueous versus Time at the Column Top, Middle and Bottom for Cycle 2 of the Swapping at Constant Flow Rate Simulation.....	3.57
Figure 42. N ₂ Mass Fraction in Hydrate, Gas, Nonaqueous-Liquid and Aqueous versus Time at the Column Top, Middle and Bottom for Cycle 2 of the Swapping at Constant Flow Rate Simulation.....	3.58
Figure 43. Differential Total and Hydrate CO ₂ , CH ₄ , and N ₂ Mass versus Time at the Column Top, Middle and Bottom for Cycle 2 of the Swapping at Constant Flow Rate Simulation	3.58
Figure 44. CO ₂ , CH ₄ , N ₂ , Gas, and Nonaqueous-Liquid Mass Crossing the Bottom Surface versus Time for Cycle 2 of the Swapping at Constant Flow Rate Simulation.....	3.59
Figure 45. Hydrate, Gas, Nonaqueous-Liquid, and Aqueous Saturation versus Time at the Column Top, Middle and Bottom for Cycle 3 of the Swapping at Constant Flow Rate Simulation.....	3.59
Figure 46. CO ₂ Mass Fraction in Hydrate, Gas, Nonaqueous-Liquid and Aqueous versus Time at the Column Top, Middle and Bottom for Cycle 3 of the Swapping at Constant Flow Rate Simulation.....	3.60

Figure 47. CH ₄ Mass Fraction in Hydrate, Gas, Nonaqueous-Liquid and Aqueous versus Time at the Column Top, Middle and Bottom for Cycle 3 of the Swapping at Constant Flow Rate Simulation.....	3.60
Figure 48. N ₂ Mass Fraction in Hydrate, Gas, Nonaqueous-Liquid and Aqueous versus Time at the Column Top, Middle and Bottom for Cycle 3 of the Swapping at Constant Flow Rate Simulation.....	3.61
Figure 49. Differential Total and Hydrate CO ₂ , CH ₄ , and N ₂ Mass versus Time at the Column Top, Middle and Bottom for Cycle 3 of the Swapping at Constant Flow Rate Simulation	3.61
Figure 50. CO ₂ , CH ₄ , N ₂ , Gas, and Nonaqueous-Liquid Mass Crossing the Bottom Surface versus Time for Cycle 3 of the Swapping at Constant Flow Rate Simulation.....	3.62

Tables

Table 1a. Primary Variable Sets and Phase Conditions without Hydrate	2.16
Table 1b. Primary Variable Sets and Phase Conditions with Hydrate.....	2.17
Table 2a. Initial Condition, Flash Condition, and Phase Condition Chart.....	2.20
without Nonaqueous-Liquid Conditions.....	2.20
Table 2b. Initial Condition, Flash Condition, and Phase Condition Chart	2.21
with Nonaqueous-Liquid Conditions.....	2.21
Table 3. Initial Conditions for the Transition to Equilibrium without Hydrates Problem: TTE1	3.22
Table 4. Initial Conditions for the Transition to Equilibrium from Hydrate and Mobile Phase Non-equilibria: TTE2	3.26
Table 5. Initial Conditions for the Transition to Equilibrium from Hydrate and Mobile Phase Equilibria: TTE3.....	3.30
Table 6. Initial Conditions for the Transition to Equilibrium from Hydrate and Mobile Phase Equilibria: TTE4.....	3.34
Table 7. Initial Conditions for the Mixed CO ₂ and N ₂ Gas Flow.....	3.38
through a CH ₄ Hydrate Bearing Column Problem.....	3.38
Table 8. Experimental Apparatus and Petrophysical Properties	3.44
Table 9. Soil Hydraulic Characteristics	3.45

1.0 Introduction

Gas hydrates are clathrated compounds in which water molecules encapsulate a guest molecule within a lattice structure. The lattice structure of gas hydrates form under low temperature, high-pressure conditions via hydrogen bonding between water molecules. Gas hydrates with CH₄ (methane) guest molecules are abundant as geologic accumulations in offshore and permafrost environments where sufficiently low temperature and high-pressure conditions exist. From an energy resource perspective, these geologic accumulations of natural gas hydrates represent a significant component of the world's organic carbon sources. Recent surveys by the United States Geological Survey (USGS) have estimated that reserves of methane in hydrate form exceed the all other fossil fuel forms of organic carbon (Booth et al., 1996). Under geologic environmental conditions, the lattice structure of a gas hydrate depends primarily on the guest molecule (Englezos, 1993; and Sloan, 1998). Pure and mixture compositions of the three hydrate formers; CH₄, CO₂, and N₂, form sl hydrate structures under geologic temperature and pressure conditions (Sloan, 1998). The equilibrium composition of hydrates depends on temperature, pressure, and composition hydrate formers in the mobile phases (i.e., aqueous, nonaqueous-liquid, and gas). The nonaqueous-liquid for the ternary CH₄-CO₂-N₂ system would be an immiscible CO₂-rich liquid phase.

Natural gas can be produced from geologic accumulations of natural gas hydrates either by dissociating the clathrated structure, yielding liquid water and gaseous methane, or by replacing the CH₄ molecule with another guest. Conventional approaches to producing natural gas hydrate are through clathrate dissociation: 1) thermal stimulation, 2) depressurization, and 3) inhibitor injection. The thermal stimulation approach involves raising the hydrate temperature above the stability point, causing the hydrate to dissociate. Thermal stimulation requires a continuous energy source to overcome the endothermic heat of dissociation. Depressurization involves lowering the hydrate pressure below the stability point, causing the hydrate to dissociate. Depressurization results in rapid hydrate dissociation, but with an associate drop in the hydrate temperature. Without an external heat source, depressurization lowers the hydrate temperature to a new equilibrium condition, halting the depressurization process. Inhibitor injection involves the injection of an organic or inorganic compound that shifts the hydrate equilibrium point to lower temperatures for isobaric conditions. As with depressurization, inhibitor injection could require additional inhibitor or a heat source to compensate for the decrease in hydrate temperature with dissociation.

The concept of exchanging CO₂ with CH₄ as guest molecules in geologic accumulations of natural gas hydrates as a production technology was first advanced by Ohgaki et al. (1996). This concept was then extended to ethane hydrates by Nakano et al. (1998). Their original concept involved injecting CO₂ gas into an aqueous-gas-hydrate system and allowing the CO₂ and CH₄ to equilibrate. The greater chemical affinity for CO₂ over CH₄ in the hydrate structure, as evidenced by the higher heat of formation and equilibrium temperature, yields a mixed CO₂-CH₄ hydrate. Resulting equilibrium concentrations of CO₂ are greater than CH₄ in the hydrate phase and less than CH₄ in the gas phase. If this molecular exchange technology can be realized for field production of geologic accumulations of natural gas hydrates, it could offer two secondary benefits; mechanical stability and mitigating global warming. If the exchange process is conducted without significant hydrate dissociation the mechanical stability of the hydrate-bearing formation could be maintained. The exchange technology would additionally represent a nearly neutral carbon process, sequestering one molecule of CO₂ for each produced molecule of CH₄, which could then be burned to produce energy and CO₂. The inclusion of N₂ into the guest-molecule exchange process is currently being considered, because of the additional control that a third component gives to the hydrate equilibria.

Since the original studies by Ohgaki et al. (1996), Hirohama et al. (1996), and Komai et al. (1997), the CO₂-CH₄ exchange technology has been investigated by others. Smith et al. (2001) assessed the feasibility of exchanging CO₂ with CH₄ in geologic accumulations of gas hydrate by examining the thermodynamic potential for the exchange as a function of pore sizes. This study concluded that the replacement of CH₄ by CO₂ in geologic accumulations of gas hydrate is less thermodynamically favored as pore size decreases. Rice

(2003; 2006) has proposed a methane hydrate production scheme for suboceanic deposits that yields hydrogen and carbon dioxide. In this scheme methane hydrate is produced using conventional technologies (e.g., thermal stimulation, depressurization) and the captured CO₂ is sequestered on the ocean floor or in the suboceanic sediments in hydrate form. Whereas Rice's scheme involves CO₂ sequestration in hydrate form, the CO₂-CH₄ molecular exchange is indirect, requiring hydrate dissociation and subsequent reformation. McGrail et al. (2004) proposed a concept for exchanging CO₂ with CH₄ in geologic deposits of gas hydrate by injecting a micro-emulsion of liquid CO₂ and water. The micro-emulsion is designed to provide sensible heat to dissociate the CH₄ hydrate, taking advantage of the higher heat of formation for the CO₂ hydrate versus the CH₄ hydrate. This technology was demonstrated in laboratory columns and numerically simulated (White and McGrail, 2006). Castaldi et al. (2007) investigated the technical feasibility of a down-hole combustion method for producing natural gas hydrate and sequestering CO₂. The details of replacing CO₂ with CH₄ in the hydrate structure was left unspecified, other than requiring a balance in the rates of CH₄ hydrate dissociation and CO₂ hydrate formation. The thermodynamics of this approach are favorable, but the implementation remains a technical challenge.

A previous investigation by the authors considered the production of natural gas hydrates from geologic deposits using CO₂ injection for a five-spot well configuration (White and McGrail, 2008). This paper described the numerical theory for both an equilibrium and kinetic exchange numerical simulator, however; only the equilibrium version of the simulator had been implemented at that time. Simulations of CO₂ injected as liquid, subcritical gas, aqueous dissolved CO₂, and supercritical gas yielded rapid formation of secondary hydrate, when the formation remained within the hydrate stability region. This paper investigates the application of the kinetic exchange and formation implementation of the STOMP-HYD simulator to the CO₂ injection scenario to understand the impact of exchange kinetics, formation kinetics, and bound-water limits on the injectivity of hydrate-bearing formations in the arctic.

2.0 Mathematical Model

The first simulator in the STOMP hydrate series, STOMP-HYD, solves five conservation equations at each grid cell: 1) energy, 2) water mass, 3) CH₄ mass, 4) CO₂ mass, and 5) inhibitor mass, and assumes equilibrium conditions between the mobile and hydrate phases. With its kinetic formulation, the second simulator in the STOMP hydrate series, STOMP-HYD-KE, solves seven conservation equations at each grid cell: 1) energy, 2) water mass, 3) mobile CH₄ mass, 4) hydrate CH₄ mass, 5) mobile CO₂ mass, 6) hydrate CO₂ mass, and 7) inhibitor mass. The subject simulator, STOMP-HYDT-KE, solves nine conservation equations at each grid cell: 1) energy, 2) water mass, 3) mobile CH₄ mass, 4) hydrate CH₄ mass, 5) mobile CO₂ mass, 6) hydrate CO₂ mass, 7) mobile N₂ mass, 8) hydrate N₂ mass, and 9) inhibitor mass. The simulator name reflects its origin and capabilities; first STOMP as being a member of the STOMP suite of simulators, second HYDT for ternary hydrates, and third KE for kinetic exchange. The mobile phases are aqueous, nonaqueous-liquid and gas. Equilibria are assumed for the components in the mobile phases. Non-equilibria are allowed for the hydrate-former components between the mobile and hydrate phases. Differences between the non-equilibria and equilibria concentrations of the hydrate formers drive the system towards equilibrium, using kinetic rates for guest molecule exchange, hydrate formation, and hydrate dissociation. In addition to allowing disequilibrium conditions between the mobile and hydrate phases, the STOMP-HYD-KE simulator additionally considers a lower limit on mobile water available for forming hydrate. This model assumes that not all of the mobile phase water is available for forming hydrate and once the water content has fallen below this level, additional hydrate formation is halted even though there may be sufficient hydrate formers and the system is within hydrate stability conditions.

2.1 Equation of State

In the previous STOMP hydrate simulators component concentrations in the mobile phases were computed via simple solubility relationships. For STOMP-HYDT-KE mobile phase equilibria were computed using a combination of the Peng-Robinson equation of state for the nonaqueous-liquid and gas phases, and Henry's law for the aqueous phase. The objective in formulating the equation-of-state (EOS) algorithms was to create a scheme that was accurate and computationally efficient. In developing the EOS algorithms it was assumed that water would be ignored in the Peng-Robinson EOS for the nonaqueous-liquid and gas phases. Water concentration in the gas phase would be made via a secondary calculation, based on the water vapor pressure, and water concentration in the nonaqueous-liquid phase was ignored. For the temperature and pressure ranges of interest for hydrate production scenarios, the CH₄-CO₂-N₂ system is rather complex, with the mixture critical point being near or within the hydrate stability temperature and pressure zone. The first attempt at developing an EOS algorithm for this the CH₄-CO₂-N₂ system followed the classical flash calculation, given molar concentrations of the three components (Pedersen and Christensen, 2007). The outcomes of a flash calculation are the number of phases, the molar fractions of each phase, and the molar compositions of each phase. The classical approach for determining the number of phases is to compute the dew and bubble points for the mixture mole fractions, using fugacity coefficients computed from a cubic EOS, such as Peng-Robinson (Pedersen and Christensen, 2007). A typical phase envelope diagram is depicted in Figure 1, showing the dew- and bubble-point branches, critical point, cricondenbar point, and cricondenthem point.

2.1.1 Tabular Data for Gas and Nonaqueous-Liquid Equilibria

Dew and bubble point determinations require the solution to a nonlinear system of equations. For dew point calculations, an initial guess at the liquid phase composition is required and for bubble point calculations, an initial guess at the gas phase composition is required. For the CH₄-CO₂-N₂ system, an accurate initial guess is

essential to the success of finding a solution, especially near the critical point of the mixture. The potential for an excessive number of Newton-Raphson iterations or a non-convergent solution, made the classical approach not a viable option. Michelsen (1980) proposed a method for computing the phase envelope, including the critical point, the cricondentherm (the maximum temperature), and cricondenbar (the maximum pressure), that involved using a previous phase envelope point to compute the next point on the phase envelope. Using the Michelsen (1980) approach it was possible to generate phase envelopes over the entire range of mixture concentrations, starting with a temperature of -50°C . Phase envelope shapes as a function of mixture concentration, computed from a modified Michelsen scheme (1980), are shown in Figure 2. The curves were generated using two paths, one starting at -50°C on the dew-point branch, ending at the cricondentherm, and the second starting at -50°C on the bubble-point branch, ending at the cricondentherm.

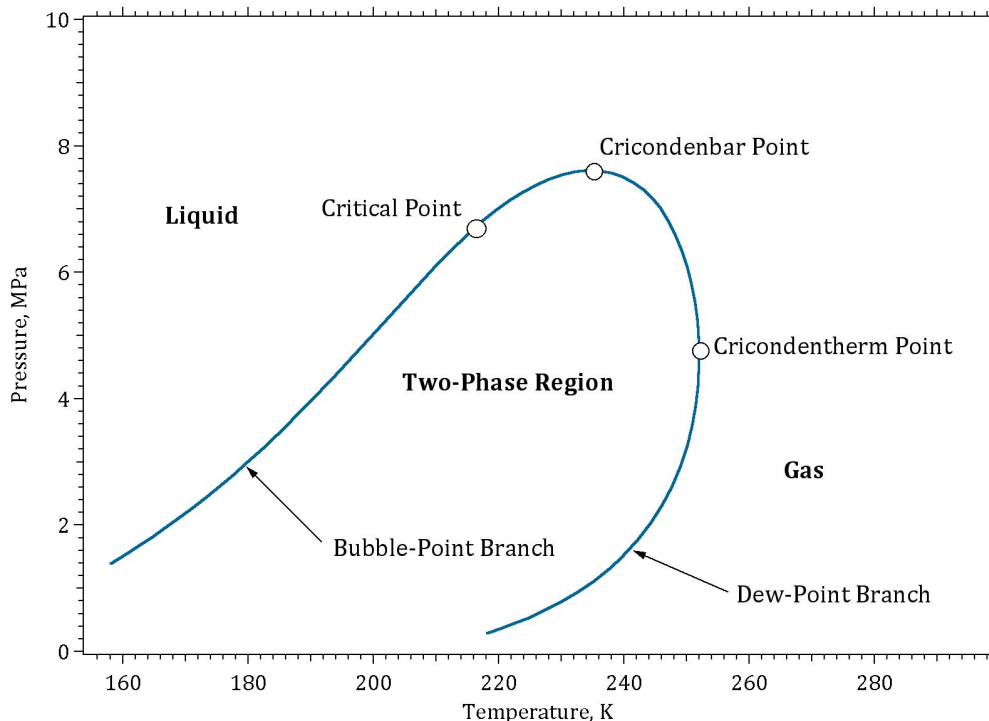


Figure 1. Phase Envelope Elements (adopted from Pedersen and Christensen, 2007)

Phase envelopes were generated for CO_2 molar fractions of at least 0.20 for 0.1 increments in molar fractions of all three hydrate formers, yielding a total of 45 phase envelopes, expressed as pressure as a function of temperature. To ensure convergence phase envelope calculations were generated using a 0.1°C step in temperature. Computing from the lower temperature value to the cricondentherm point on both the dew- and bubble-point branches created single-valued functions for pressure. A third curve was generated from the lower temperature point at -50°C along a vapor molar fraction of 0.5. The intersection of this line with the dew- and bubble-point branches determined the mixture critical point. The phase envelope data were stored in a property file for each of the 45 phase-equilibria compositions. The data for each mixture composition comprised the critical temperature and pressure, cricondenbar temperature and pressure, cricondentherm temperature and pressure. Then for each branch of the phase envelope there were 51 points of temperature, pressure, second derivative of pressure with respect to temperature, K -factor (K_i) for each component, and second derivative of the K_i for each component with respect to temperature. The tabular data is then used to develop cubic splines temperature versus pressure and temperature versus the K_i for each component on the two branches of the phase envelope for a given composition of mobile hydrate formers.

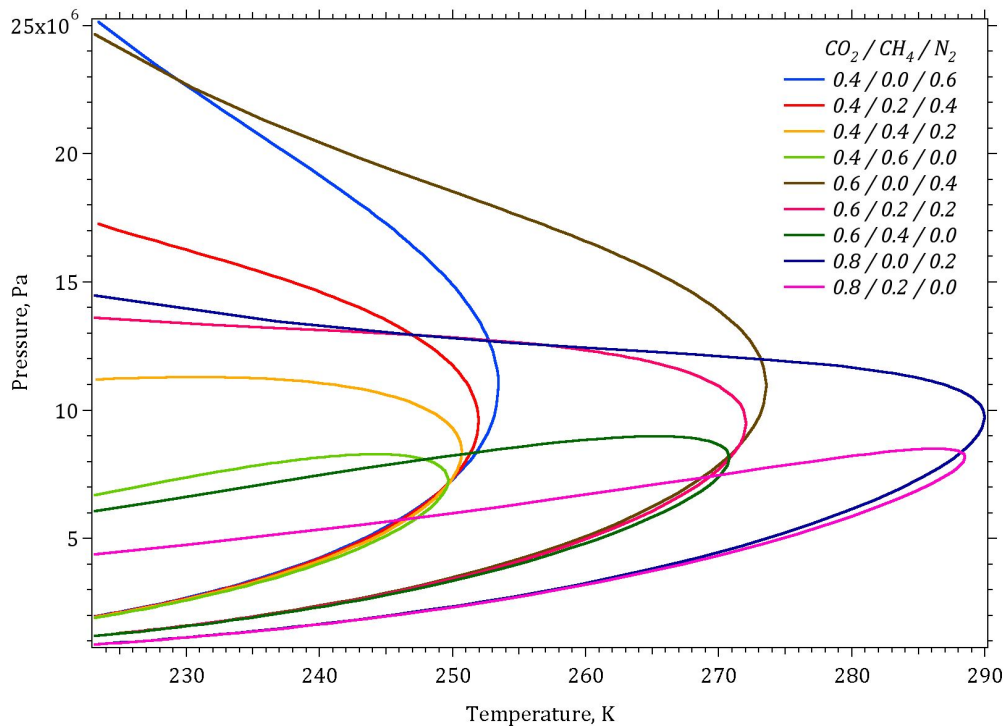


Figure 2. Phase Envelope for Mixtures of CH₄, CO₂, and N₂

The two-phase region between the dew- and bubble point branches of the phase envelope is discretized by temperature and pressure. Temperature is discretized into 25 evenly spaced points, with the inclusion of the critical and cricondentherm temperatures, making a possible 27 temperature points. Pressure discretization is determined by locating pressure points on the dew- and bubble-point branches of the phase envelope. All none unique pressures are included, yielding a potential of 53 pressure points. For each temperature and pressure point combination eight values are required; the molar fraction of gas (b), second partial derivative of b with respect to pressure, K_i for each component, and the second partial derivative of K_i with respect to pressure for each component. The b and K_i data and second partial derivatives were computed for each temperature and pressure point using the classical two-phase flash calculation with the Peng-Robinson cubic equation of state (Pedersen and Christensen, 2007). The second partial derivative values stored in the table will be used for a bi-cubic spline interpolation for the two-phase region. The phase envelope and two-phase data table for the CH₄-CO₂-N₂ system comprises just under 400,000 data points.

2.1.2 Interpolation Algorithm for Tabular Data of Gas and Nonaqueous-Liquid Equilibria

The EOS yields the number of phases, the molar fraction of phases, and the composition of each phase, as a function of temperature, pressure, and composition of hydrate formers. The data table contains both branches of the phase envelope, stored in form convenient for cubic spline interpolation, and the two-phase region, stored in a form convenient for bi-cubic spline interpolation for a discrete number of compositions of hydrate formers. What remains is to develop scheme to interpolate across the tabulated compositions of hydrate formers. The phase envelopes, shown in Figure 1, vary in shape with composition of hydrate formers. Some compositions yield phase envelopes with the critical, cricondenbar, and cricondentherm coexisting, others with cricondenbar being greater than the critical pressure, and others with the cricondentherm being greater than the critical temperature.

The scheme that was chosen to interpolate between the tabulated compositions of hydrate formers was one where an interpolated cricondentherm temperature was first computed using a modified bicubic spline interpolation on the CO₂ and CH₄ mole fractions of formers. The mole fraction of formers sum to 1.0, which means that tabular data are only stored for tabular combinations of CO₂ and CH₄ mole fractions that sum to 1.0 or less. Cubic splines at the five nearest tabulated values of CO₂ mole fractions are created as a function of CH₄ concentration (i.e., the green dots and lines in Figure 3). The green dots above the CO₂ and CH₄ mole fraction diagonal (i.e., zero-N₂ diagonal) are set to be equivalent to their reflected counter part, as shown by the dashed black arrow in Figure 3. A cubic spline along the zero-N₂ diagonal is additionally created if the CH₄ mole fraction intersects the zero-N₂ diagonal within the range of CO₂ cubic splines (i.e., the blue dots and lines in Figure 3). Each of these cubic splines is interpolated at the CH₄ mole fraction, creating the red dots in Figure 3. A final cubic spline is created using the red dots, and then interpolated at the CO₂ mole fraction, yielding the interpolated value shown as a black dot in Figure 3.

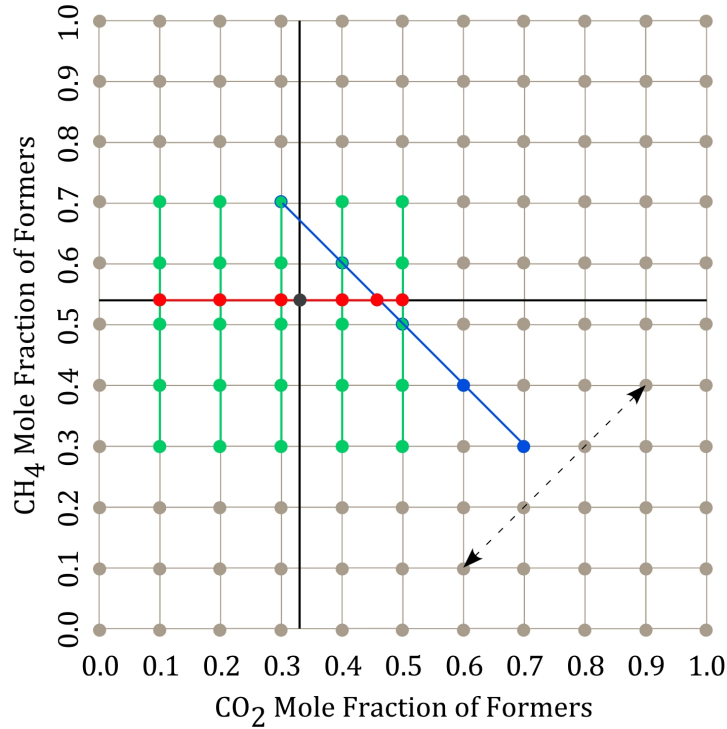


Figure 3. Modified Bicubic Spline Interpolation Scheme on CO₂ and CH₄ Mole Fraction of Formers

Interpolated pressures on the two branches of the phase envelope, were then computed using the modified bicubic spline interpolation on the CO₂ and CH₄ mole fractions of formers, but with the temperature scaled according to the cricondentherm temperature of the mixture:

$$T_{CO_2,CH_4} = T_{CO_2,CH_4}^{cricondentherm} \left(\frac{T}{T_{mixture}^{cricondentherm}} \right) \quad (1)$$

where, temperature is expressed in °K. To verify the interpolation scheme, the phase envelope for a mixture of 0.65 CO₂, 0.15 CH₄, 0.20 N₂ was computed using the Michelsen scheme (1980), and the subject interpolation scheme, using tabulated values at four neighboring molar concentration ratios. As shown in Figure 4, the phase envelopes from the two calculation approaches are in good agreement, with the interpolation scheme avoiding the convergence pitfalls of the classical approach.

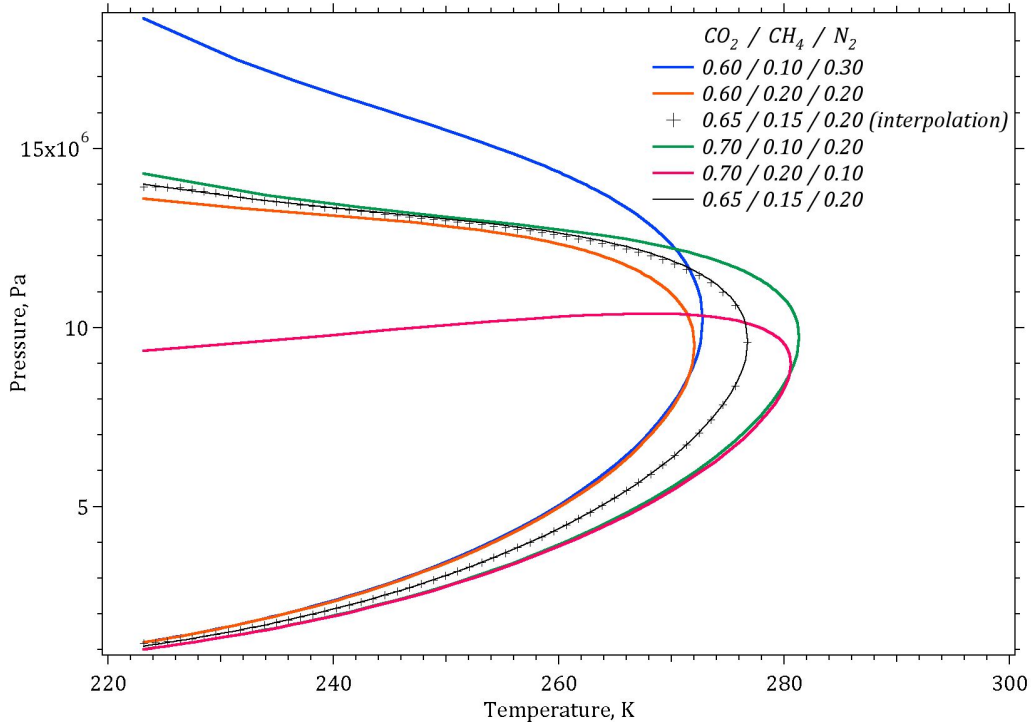


Figure 4. Phase Envelope Interpolated versus Computed

Development of the entire phase envelope is not required for every EOS calculation. The first stage of an EOS calculation, however, does require the determination of the existing phases. This determination uses the following procedure:

1. Modified bicubic spline interpolation with the hydrate-former mole fraction of CO_2 and CH_4 to determine the mixture cricondentherm temperature.
2. Cubic spline interpolation on the dew-point branch up to the cricondentherm temperature to determine the lower phase-envelope pressure for the four neighboring tabulated values of hydrate-former mole fraction of CO_2 and CH_4 , with the temperature scaled according to Eqn. (1).
3. Cubic spline interpolation on the bubble-point branch down to the cricondentherm temperature to determine the upper phase-envelope pressure for the four neighboring tabulated values of hydrate-former mole fraction of CO_2 and CH_4 , with the temperature scaled according to Eqn. (1).
4. Modified bicubic spline interpolation with the hydrate-former mole fraction of CO_2 and CH_4 to determine the mixture lower phase-envelope pressure.
5. Modified bicubic spline interpolation with the hydrate-former mole fraction of CO_2 and CH_4 to determine the mixture upper phase-envelope pressure.
6. Phase determination using the following checks:
 - a. If the temperature is above the mixture cricondentherm temperature, then only gas phase exists.
 - b. If the temperature is below the mixture cricondentherm temperature and the pressure is below the lower phase-envelope pressure, then only gas phase exists.
 - c. If the temperature is below the mixture cricondentherm temperature and the pressure is above the upper phase-envelope pressure, then only liquid phase exists.
 - d. If the temperature is below the mixture cricondentherm temperature and the pressure is between the lower and upper phase envelope pressures, then both liquid and gas a phase exist.
7. For two-phase conditions conduct the following additional steps:

- a. Bi-cubic spline interpolation for b and K_i for the four neighboring tabulated values of hydrate-former mole fraction of CO_2 and CH_4 , with the temperature scaled according to Eqn. (1) and the pressure scaled according to Eqn. (2).
- b. Modified bicubic spline interpolation with the hydrate-former mole fraction of CO_2 and CH_4 to determine the mixture b and K_i .

$$P_{\text{CO}_2, \text{CH}_4} = P \left[\frac{\left(P_{\text{CO}_2, \text{CH}_4}^{\text{upper}} - P_{\text{CO}_2, \text{CH}_4}^{\text{lower}} \right)}{\left(P_{\text{mixture}}^{\text{upper}} - P_{\text{mixture}}^{\text{lower}} \right)} \right] + P_{\text{CO}_2, \text{CH}_4}^{\text{lower}} \quad (2)$$

The superscript upper in Eqn. (2) refers to the bubble-point branch of the phase envelope, and the superscript lower refers to the dew-point branch. The upper and lower pressures for the tabulated values of hydrate-former compositions are determined using temperatures scaled per Eqn. (1) from the cubic spline coefficients stored in the data table. The cubic-spline calculation is relatively rapid, as the constructed cubic spline is stored in memory, via the data table.

2.1.3 Gas and Nonaqueous-Liquid Density

The interpolation scheme described above establishes the existing phases among the gas-only, nonaqueous-liquid-only, and two-phase options. In the gas-only case the Peng-Robinson equation of state with the Peneloux volume correction (Pedersen and Christensen, 2007) is then used to determine the gas density:

$$P = \frac{RT}{V-b} - \frac{a(T)}{(V+c)(V+2c+b) + (b+c)(V-b)} \quad (3a)$$

$$a(T) = 0.45724 \left(\frac{R^2 T_c^2}{P_c} \right) \left[1 + m \left(1 - \sqrt{\frac{T}{T_c}} \right) \right]^2 \quad (3b)$$

$$m = 0.37464 + 1.54226 \omega - 0.26992 \omega^2 \quad (3c)$$

$$b = \frac{0.07780 RT_c}{P_c} \quad (3d)$$

$$c = \frac{0.40768 RT_c (0.29441 - Z_{RA})}{P_c} \quad (3e)$$

$$Z_{RA} = 0.29056 - 0.08775 \omega \quad (3f)$$

The Peng-Robinson equation with the Peneloux volume correction, Eqn. (3a) is solved directly using the Nickalls (1993) algorithm for cubic equations, yielding three molar volume solutions. For the gas-only case, the maximum molar volume root is chosen as the solution. Classical mixing rules (Elliot and Lira) are used to determine the coefficients in Eqn. (3):

$$a = \sum_{i=1}^n \sum_{j=1}^n \chi_i \chi_j \sqrt{a_i a_j} (1 - k_{ij}) \quad (4a)$$

$$b = \sum_{i=1}^n \chi_i b_i \quad (4b)$$

For the liquid only, the Peng-Robinson equation, with the Peneloux volume correction is used, Eqn. (3) and (4), but the minimum molar volume root is chosen from the Nickalls (1993) cubic equation solution. In the two-phase case the Peng-Robinson equation, with the Peneloux volume correction is used, Eqn. (3) and (4), with the gas and liquid compositions determined by the molar fraction of gas and K-factors:

$$y_i = \chi_g^i = \frac{z_i K_i}{1 + \beta (K_i - 1)} \quad (5a)$$

$$x_i = \chi_n^i = \frac{z_i}{1 + \beta (K_i - 1)} \quad (5b)$$

Two notations are used in Eqn. (5) to indicate gas and liquid. The first notation uses y to indicate gas molar fractions and x to indicate liquid molar fractions and the subscript i to indicate the component. The second notation uses χ to indicate molar fractions; the subscript g and n to indicate gas and nonaqueous-liquid phases; and the superscript i to indicate the component. The first notation is used for the Peng-Robinson equations and the second notation is used otherwise throughout this document.

2.1.4 Aqueous Composition and Density

Aqueous phase concentrations are computed from the gas phase component fugacity and Henry's constant, that includes the effect of temperature and salinity (Battistelli et al., 1997):

$$\chi_l^i = \frac{\Phi_i P_g^i}{H^i} \quad (6)$$

In the liquid-only case the gas phase concentration is that at the bubble point for the system temperature. Gas phase component fugacity is computed using the Peng-Robinson equation of state and the gas component mole fractions:

$$\ln(\Phi_i) = -\ln(Z - B) + (Z - 1) \frac{b_i}{b} - \frac{A}{2^{1.5} B} \left[\frac{1}{a} \left(2 \sqrt{a_i} \sum_{j=1}^n z_j \sqrt{a_j} (1 - k_{ij}) \right) - \frac{b_j}{b} \right] \ln \left(\frac{Z + (\sqrt{2} + 1) B}{Z - (\sqrt{2} - 1) B} \right) \quad (7a)$$

$$A = \frac{a(T) P}{R^2 T^2} \quad (7b)$$

$$B = \frac{bP}{RT} \quad (7c)$$

2.1.5 Ice Composition and Density

Ice is assumed to only comprise water. Ice density is computed from a polynomial function in terms of absolute temperature (ASHRAE, 1977).

2.1.6 Hydrate Composition and Density

The kinetic formulation of STOMP-HYDT-KE allows for non-equilibrium conditions between the mobile fluids and hydrate. Hydrate compositions under equilibrium conditions are determined from the gas molar concentration of hydrate formers and temperature or pressure, using tabular data generated from the cell potential method (Garapati and Anderson; 2009, 2010). The tabular data can be used to determine the equilibrium pressure, given the temperature and gas mole fraction of hydrate formers, or the equilibrium temperature, given the pressure and gas mole fraction of hydrate formers. The cell potential method yields small and large cage occupancies for each of the hydrate formers, which are included in the tabular data. The ternary (i.e., CH₄-CO₂-N₂) hydrate equilibrium table comprises 66 ratios of mole fractions of hydrate formers, incremented by 0.1, with each mole fraction ratio having 115 temperature/pressure points. For each hydrate former mole fraction ratio and temperature point the table includes the following data: temperature, pressure, small-cage occupancy of CO₂, small-cage occupancy of CH₄, small-cage occupancy of N₂, large-cage occupancy of CO₂, large-cage occupancy of CH₄, and large-cage occupancy of N₂. The modified bicubic spline interpolation (Press et al., 1986), shown in Figure 3, on the mole fractions of CO₂ and CH₄ of formers is used to determine mixture values of the tabular data. Hydrate mole fractions are computed from the small- and large-cage occupancies, assuming an ideal sI clathrated structure (Sloan, 1998):

$$\chi_h^i = \left(1 - \chi_h^{H_2O}\right) \psi_h^i \quad (8a)$$

$$\chi_h^{H_2O} = \frac{n^{H_2O}}{1 + n^{H_2O}} \quad (8b)$$

$$n^{H_2O} = \frac{23}{\left(\sum_{i=1}^n y_{sc}^i + 3 \sum_{i=1}^n y_{lc}^i\right)} \quad (8c)$$

$$\psi_h^i = \frac{(y_{sc}^i + 3 y_{lc}^i)}{\left(\sum_{i=1}^n y_{sc}^i + 3 \sum_{i=1}^n y_{lc}^i\right)} \quad (8d)$$

Plots of former mole fractions of CO₂, CH₄, and N₂ in the hydrate are shown against the CO₂ and CH₄ former mole fractions in the gas under equilibrium conditions, in Figures 5 through 7, respectively.

If equilibrium conditions were assumed between the hydrate and mobile phases, then hydrate would occur when either the system temperature was below the hydrate equilibrium temperature, or the total vapor pressure of the hydrate formers was greater than the hydrate equilibrium pressure. The STOMP-HYDT-KE simulator, however, allows non-equilibrium conditions between the mobile phases and hydrate, which means

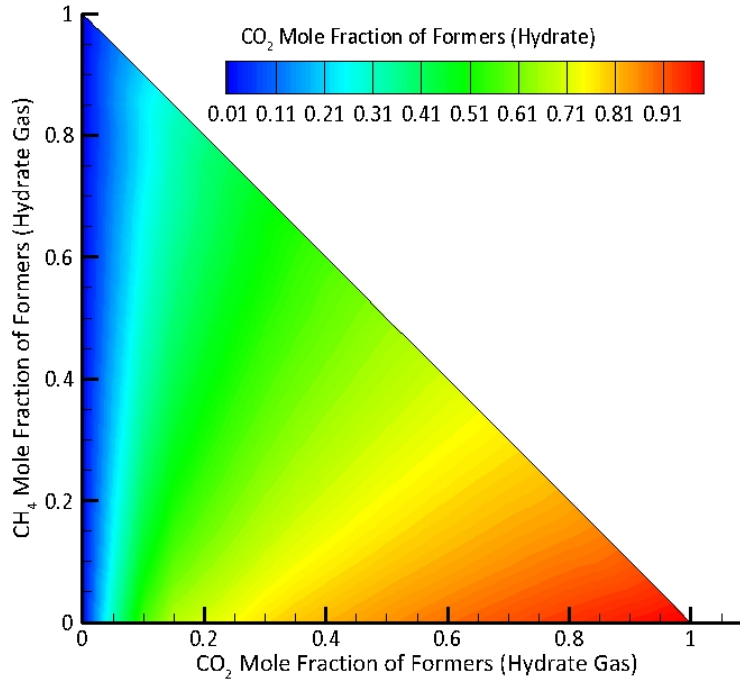


Figure 5. Former Mole Fraction of CO₂ in Hydrate versus CO₂ and CH₄ Former Mole Fraction in Gas under Equilibrium Conditions at 4°C

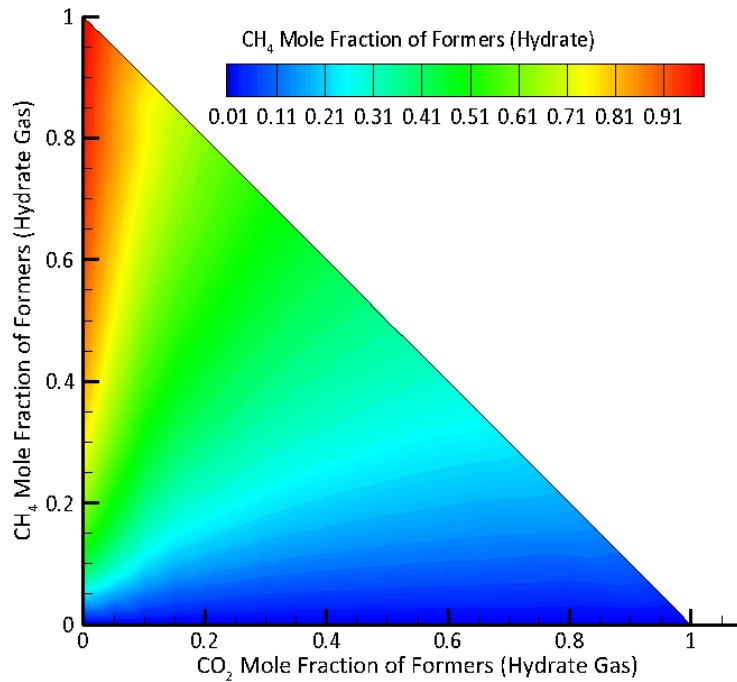


Figure 6. Former Mole Fraction of CH₄ in Hydrate versus CO₂ and CH₄ Former Mole Fraction in Gas under Equilibrium Conditions at 4°C

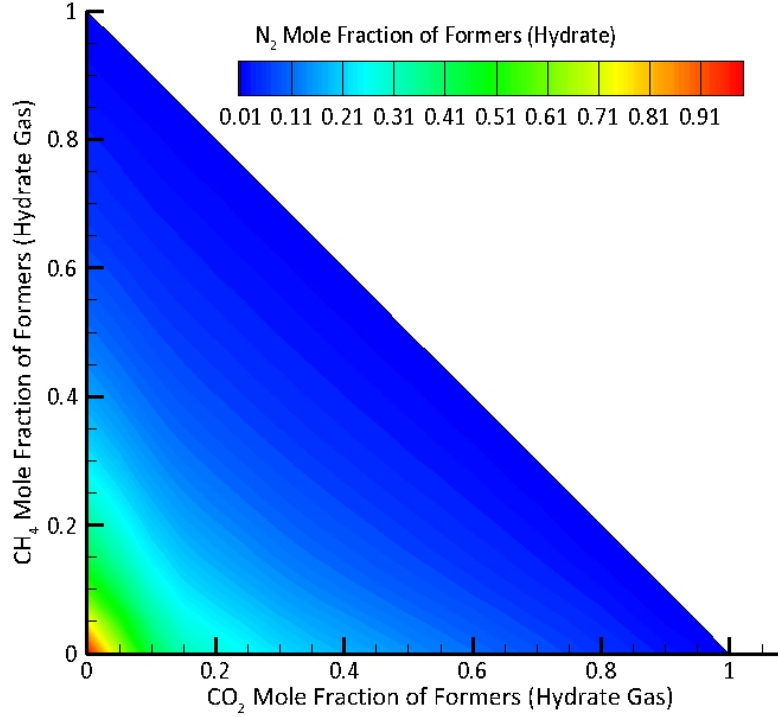


Figure 7. Former Mole Fraction of N₂ in Hydrate versus CO₂ and CH₄ Former Mole Fraction in Gas under Equilibrium Conditions at 4°C

that hydrate can exist under conditions outside of the stability zone, and conversely hydrate can be absent under conditions within the stability zone. When the system is outside of the stability zone and hydrate exists, the total vapor pressure of the hydrate formers in equilibrium with the hydrate, will be greater than the total vapor pressure of hydrate formers in equilibrium with the mobile phases. This difference in total vapor pressure drives hydrate dissociation. When the total vapor pressure of hydrate formers is greater in the mobile phase than the hydrate phase, then this difference drives hydrate formation. Differences in component vapor pressures between the mobile and hydrate phases drive exchange of guest molecules.

Hydrate density is computed according to (Sloan, 1998), assuming a sI hydrate crystal cell structure and the interpolated values of small- and large cage occupancies:

$$\rho_h = \frac{N^{H2O} M^{H2O} + \sum_{i=1}^n \left(y_{sc}^i N_{sc} + y_{lc}^i N_{lc} \right) M^i}{A_n V_{uc}} \quad (9)$$

$$N^{H2O} = 46 \text{ molecules}; N_{sc} = 2 \text{ molecules}; N_{lc} = 6 \text{ molecules};$$

$$A_n = 6.023 \times 10^{26} \text{ molecules / kmol}; V_{uc} = 1.728 \times 10^{-27} \text{ m}^3$$

Hydrate density as a function of the CO₂ and CH₄ former mole fraction in gas under equilibrium conditions at 4°C is shown in Figure 8, with pure CH₄ hydrate having the lowest density and pure CO₂ hydrate the highest.

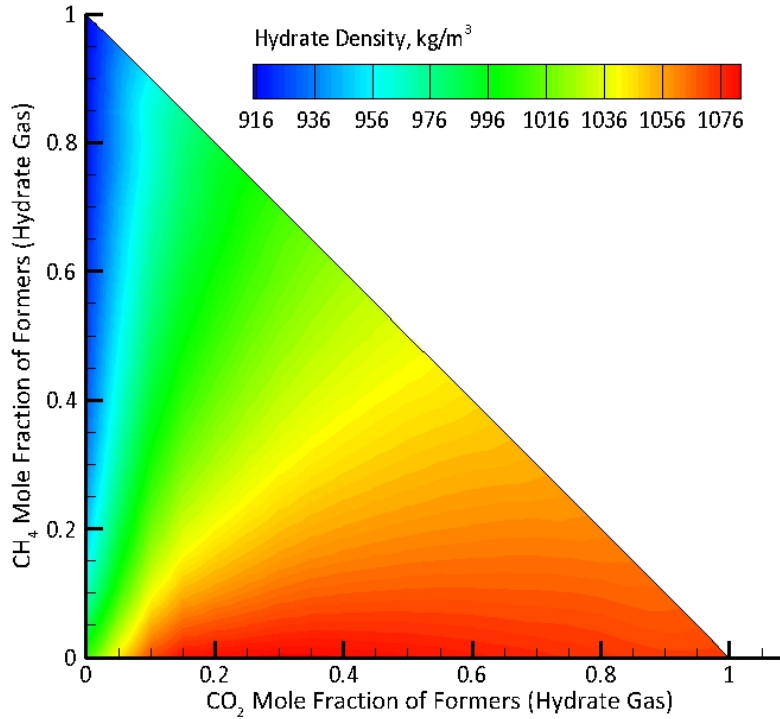


Figure 8. Hydrate Density versus CO₂ and CH₄ Former Mole Fraction in Gas under Equilibrium Conditions at 4 °C

2.1.7 EOS Discussion

The equation of state identifies the existing phase, composition of those phases, and density of those phases. The STOMP-HYDT-KE simulator considers three mobile phases: aqueous, gas, and nonaqueous-liquid; and three immobile phases: hydrate, ice, and precipitated salt. The mobile phases are assumed to be in thermodynamic equilibrium. Equilibrium between the aqueous phase and gas and nonaqueous-liquid phases is computed via solubility models. Equilibrium between the gas and nonaqueous-liquid phases is computed via a hybrid tabular interpolation and Peng-Robinson cubic equation of state. In this scheme, interpolation of tabular data is used to determine phase occurrences and compositions and the Peng-Robinson cubic equation of state is used to determine phase density. Direct, non-iterative calculations of properties is computational the most efficient approach. Molar fractions of the total amount of hydrate formers in the gas and nonaqueous-liquid phases (i.e., feed compositions) provide direct calculation paths for all secondary variables as will be described below.

2.2 Conservation Equations

The conservation equations equate the change in the conserved quantity within a volume over time with the net flux of the conserved quantity into the volume plus any net source of the conserved quantity with the volume. For the energy equation the conserved quantity within a volume is formulated in terms of phase internal energy; the fluxes of energy are by mobile phase advection and thermal diffusion; energy flux associated with component diffusive flux is ignored; and energy sources are either associated with mass sources or heat sources;

$$\frac{\partial}{\partial t} \left[\sum_{\gamma=l,n,g,h,i,p} (\phi \rho_{\gamma} s_{\gamma} u_{\gamma}) \right] = - \sum_{\gamma=l,n,g} \nabla (\rho_{\gamma} h_{\gamma} \mathbf{v}_{\gamma}) + \nabla (\mathbf{k}_e \nabla T) + \sum_{\gamma=l,n,g} (h_{\gamma} m_{\gamma}) + q \quad (10)$$

Advective fluxes of the mobile phases are computed according to Darcy's law;

$$\mathbf{v}_{\gamma} = - \frac{k_{r\gamma} \mathbf{k}}{\mu_{\gamma}} (\nabla P_{\gamma} + \rho_{\gamma} g \mathbf{z}) \quad (11)$$

Water (w) was assumed to exist in the aqueous (l), gas (g), hydrate (h) and ice (i) phases under equilibrium conditions. The conservation equation for water mass considered water flux via molecular diffusion through the mobile phases:

$$\frac{\partial}{\partial t} \left[\sum_{\gamma=l,g,h,i} (\phi \rho_{\gamma} s_{\gamma} \omega_{\gamma}^w) \right] = - \sum_{\gamma=l,n,g} \nabla (\rho_{\gamma} \omega_{\gamma}^w \mathbf{v}_{\gamma}) - \sum_{\gamma=l,n,g} \nabla (\mathbf{J}_{\gamma}^w) + \sum_{\gamma=l,n,g} (\omega_{\gamma}^w m_{\gamma}) \quad (12)$$

Diffusive fluxes of components through the mobile phases are computed from gradients in molar concentration, considering molecular diffusion, but ignoring hydraulic dispersion;

$$\mathbf{J}_{\gamma}^i = - \phi \rho_{\gamma} s_{\gamma} \frac{M^i}{M_{\gamma}} (\tau_{\gamma} D_{\gamma}^i) \nabla \chi_{\gamma}^i \quad (13)$$

Mobile-CO₂ (mc), -CH₄ (mm), and -N₂ (mn) were assumed to exist in the aqueous (l), nonaqueous-liquid (n), and gas (g) phases under equilibrium conditions. The conservation equation for mobile-CO₂ (mc), -CH₄ (mm), and -N₂ (mn) mass included kinetic exchange of hydrate formers between the mobile and hydrate and gross transport between the mobile and hydrate phase through kinetic hydrate formation;

$$\begin{aligned} \frac{\partial}{\partial t} \left[\sum_{\gamma=l,n,g} (\phi \rho_{\gamma} s_{\gamma} \omega_{\gamma}^i) \right] = & - \sum_{\gamma=l,n,g} \nabla (\rho_{\gamma} \omega_{\gamma}^i \mathbf{v}_{\gamma}) - \sum_{\gamma=l,n,g} \nabla (\mathbf{J}_{\gamma}^i) \\ & + \sum_{\gamma=l,n,g} (\omega_{\gamma}^i m_{\gamma}) - K_e (P_m^i - P_h^i) - K_f (P_m^v - P_h^v); \text{ for } i = mc, mm, \text{ and } mn \end{aligned} \quad (14)$$

Hydrate-CO₂ (hc), -CH₄ (hm), and -N₂ (hn) were assumed to exist only in the hydrate. The conservation equation for hydrate-CO₂ (hc), -CH₄ (hm), and -N₂ (hn) mass included kinetic exchange of hydrate formers between the mobile and hydrate and gross transport between the mobile and hydrate phase through kinetic hydrate formation;

$$\frac{\partial}{\partial t} [\phi \rho_h s_h \omega_h^i] = K_e (P_m^i - P_h^i) + K_f (P_m^v - P_h^v); \text{ for } i = hc, hm, \text{ and } hn \quad (15)$$

Inhibitor (s) is assumed to only exist dissolved in the aqueous phase (l) and precipitated (p), as reflected in its conservation of mass equation;

$$\frac{\partial}{\partial t} \left[\left(\phi \rho_l s_l \omega_l^s \right) + \left(\phi \rho_p s_p \right) \right] = -\nabla \cdot \left(\rho_l \omega_l^s \mathbf{V}_l \right) - \nabla \cdot \left(\mathbf{J}_l^s \right) + \left(\omega_l^w m_l \right) \quad (16)$$

2.3 Constitutive Equations

The constitutive equations relate the primary variables to the secondary variables. The primary variable sets are defined in the subsequent section according to phase conditions, using a variable switching scheme. In general the constitutive equations are nonlinear. The EOS yields phase composition and density, as described above. In this section an overview of the calculation approaches are described for thermodynamic and transport properties of each phase.

2.3.1 Aqueous Viscosity

Aqueous viscosity is determined from the brine viscosity, mole fraction of dissolved formers, and pure viscosities of the dissolved formers, using the formulation of Grunberg and Nissan (Reid et al., 1987). Brine viscosity is determined as a function of pure water viscosity and dissolved salt mass fraction (Phillips et al., 1981.) Pure water viscosity is determined as a function of temperature and pressure from the ASME Steam Table Formulations (Meyer et al., 1993).

2.3.2 Gas Viscosity

Gas viscosity is determined from the mole fraction of gas components and viscosities of the pure gas components, using the combination method of Wilke (Reid et al., 1987). Pure CO₂ gas viscosity is determined as a function of temperature and pure CO₂ gas density using the empirical formulation of Fenghour et al. (1998). Pure CH₄ gas viscosity is determined as a function of temperature and pure CH₄ gas density using the empirical formulation of Hanley et al. (1997). Pure N₂ gas viscosity is determined as a function of temperature and pure N₂ gas density using the empirical formulation of Lemmon et al. (2004).

2.3.3 Nonaqueous-Liquid Viscosity

Nonaqueous-liquid viscosity is determined from the logarithmic mixing rule of Grunberg and Nissan (Reid et al., 1987) from the viscosities of the pure components. Pure CO₂ liquid viscosity is determined as a function of temperature and the product of the nonaqueous-liquid molar density and CO₂ molecular weight, using the empirical formulation of Fenghour et al. (1998). Pure CH₄ liquid viscosity is determined as a function of temperature and the product of the nonaqueous-liquid molar density and CH₄ molecular weight, using the empirical formulation of Hanley et al. (1997). Pure N₂ liquid viscosity is determined as a function of temperature and the product of the nonaqueous-liquid molar density and N₂ molecular weight, using the empirical formulation of Lemmon et al. (2004).

2.3.4 Aqueous Diffusion Coefficients

Diffusion coefficients for CO₂, CH₄, N₂, and salt in the aqueous phase are required. Diffusion of water through the aqueous phase is computed via a molar balance of all aqueous constituents. The diffusion coefficient for CO₂ in the aqueous phase is determined as a function of temperature, pure CO₂ viscosity and aqueous viscosity, using the correlation of Renner (1998). The diffusion coefficients for CH₄ and N₂ in the aqueous phase are determined as a function of temperature and aqueous viscosity from the method of Wilke and Chang (Reid et al., 1987). The salt diffusion coefficient in the aqueous phase is determined as a function of temperature, salt concentration, and aqueous viscosity, using the correlation of Bromley (1973).

2.3.5 Gas Diffusion Coefficients

Diffusion coefficients for CO₂, CH₄, N₂, and water vapor in the gas phase are required. Diffusion coefficients are determined as a function of temperature, pressure and gas composition, by combining binary diffusion coefficients, according to Blanc's law (Reid et al., 1987). Binary-diffusion coefficients are determined from the method of Wilke and Chang (Reid et al., 1987).

2.3.6 Nonaqueous-Liquid Diffusion Coefficients

Diffusion coefficients for CO₂, CH₄, and N₂ nonaqueous-liquid phase are required. Diffusion coefficients are determined as a function of temperature and nonaqueous-liquid viscosity, using the method of Wilke and Chang (Reid et al., 1987).

2.3.7 Aqueous Thermal Conductivity

Aqueous thermal conductivity is computed from the pure-water thermal conductivity and salt concentration as a function of temperature and salt concentration, using the correlation of Ozbek and Phillips (1980). Pure-water thermal conductivity is computed as a function of temperature and pressure using the ASME Steam Table formulations (Meyer, 1993).

2.3.8 Gas Thermal Conductivity

Gas thermal conductivity is determined from the gas composition and pure-component gas thermal conductivities, using the Maxon and Saxena modification to the Waasiljewa mixing rule (Reid et al., 1987). Pure CO₂ gas thermal conductivity is determined as a function of temperature and pure CO₂ gas density using the empirical formulation of Vesovic et al. (1990). Pure CH₄ gas thermal conductivity is determined as a function of temperature and pure CH₄ gas density using the empirical formulation of Hanley et al. (1997). Pure N₂ gas thermal conductivity is determined as a function of temperature and pure N₂ gas density using the empirical formulation of Lemmon et al. (2004).

2.3.9 Nonaqueous-Liquid Thermal Conductivity

Nonaqueous-liquid thermal conductivity is determined from the mixing rule of Li (Reid et al., 1987) from the thermal conductivities of the pure components. Pure CO₂ liquid thermal conductivity is determined as a function of temperature and the product of the nonaqueous-liquid molar density and CO₂ molecular weight, using the empirical formulation of Vesovic et al. (1990). Pure CH₄ liquid thermal conductivity is determined as a function of temperature and the product of the nonaqueous-liquid molar density and CH₄ molecular weight, using the empirical formulation of Hanley et al. (1997). Pure N₂ liquid thermal conductivity is determined as a function of temperature and the product of the nonaqueous-liquid molar density and N₂ molecular weight, using the empirical formulation of Lemmon et al. (2004).

2.3.10 Ice Thermal Conductivity

Thermal conductivity of ice is determined as a function of temperature, using a polynomial fit to the data of Dickerson (1969).

2.3.11 Hydrate Thermal Conductivity

Thermal conductivity of hydrate is determined as a function of temperature only, using a functional form (Waite et al., 2007).

2.3.12 Aqueous Enthalpy and Internal Energy

Aqueous enthalpy is determined the brine enthalpy, mass fraction of aqueous components and pure CO₂, CH₄, and N₂ component enthalpies, using a mass fraction mixing rule combined with the heat of solution. The brine enthalpy is determined from pure liquid water enthalpy and salt concentration, using the mixing formulation of Gudmundsson and Thrainsson (1969). The enthalpy of liquid pure water is determined from the steam table formulations (Meyer et al., 1993). The pure CO₂, CH₄, and N₂ component enthalpies are computed based on the fraction of gas and nonaqueous liquid phases in equilibrium with the aqueous phase. Pure CO₂ enthalpy is determined as a function of temperature and pressure from tabular data (Span and Wagner, 1996). Pure CH₄ enthalpy is determined as a function of temperature and pressure from tabular data (Setzmann and Wagner, 1991). Pure N₂ enthalpy is determined as a function of temperature and pressure from tabular data (Span et al., 2000). Heats of solution for CO₂, CH₄, and N₂ are determined from the partial differential of Henry's constant at constant pressure with respect to temperature. Henry's constant for CO₂ in brine was determined as a function of salt concentration and temperature, using the empirical formulation of Battistelli (1997). Henry's constant for CH₄ and N₂ in brine were determined as a function of temperature using the formulations of Sloan (1997), and corrected for salt using the empirical formulation of Battistelli (1997). Aqueous internal energy is determined directly from the aqueous enthalpy, density, and system pressure.

2.3.13 Gas Enthalpy and Internal Energy

Gas enthalpy and internal energy are determined from the gas composition and pure component gas enthalpies, using mass fraction weighting. Pure CO₂ enthalpy and internal energy is determined as a function of temperature and pressure from tabular data (Span and Wagner, 1996). Pure CH₄ enthalpy and internal energy is determined as a function of temperature and pressure from tabular data (Setzmann and Wagner, 1991). Pure N₂ enthalpy and internal energy is determined as a function of temperature and pressure from tabular data (Span et al., 2000). Pure water vapor enthalpy is determined from the ASME Steam Table Formulations (Meyer, 1993), and pure water vapor internal energy is determined from the water vapor enthalpy, water vapor density and system pressure.

2.3.14 Nonaqueous-Liquid Enthalpy and Internal Energy

Nonaqueous-liquid enthalpy and internal energy are determined from the nonaqueous-liquid composition and pure component liquid enthalpies, using mass fraction weighting. Pure CO₂ enthalpy and internal energy is determined as a function of temperature and pressure from tabular data (Span and Wagner, 1996). Pure CH₄ enthalpy and internal energy is determined as a function of temperature and pressure from tabular data (Setzmann and Wagner, 1991). Pure N₂ enthalpy and internal energy is determined as a function of temperature and pressure from tabular data (Span et al., 2000). Water is assumed not to be a component of the nonaqueous-liquid phase.

2.3.15 Ice Enthalpy and Internal Energy

Ice enthalpy and internal energy are assumed to be equivalent. The ice enthalpy is determined as a function of temperature, using a using polynomial fit of data from ASHRAE (1977) with a reference point of liquid water at 273.15 K.

2.3.16 Hydrate Enthalpy and Internal Energy

Hydrate enthalpy and internal energy are assumed to be equivalent. The hydrate enthalpy is determined from the hydrate composition and pure component gas enthalpies of the hydrate formers (i.e., CO₂, CH₄, and N₂), liquid water enthalpy, and composition weighted heats of dissociation for the hydrate formers. Heats of

dissociation for pure CO₂, CH₄, and N₂ hydrates as a function of temperature are determined from the method of Yoon et al. (2003), and are based on hydrate dissociating into liquid water and gaseous CO₂, CH₄, and N₂.

2.4 Numerical Solution

The governing conservation equations, Eqns. 10 through 16, are solved numerically. The numerical solution is founded on the concept of discretizing both time and space. Temporal discretization is backward Euler, requiring a global solution of all primary variables at new point in time. Spatial discretization uses the integrated finite difference method (Ferraresi, 1989) on a structured computational grid. The integrated finite difference method assumes that state properties are computed at the centroids of the grid volumes and fluxes are computed at the surfaces between grid volumes. The temporal and spatial discretizations convert the governing conservation equations from partial differential to algebraic form. The resulting algebraic equations are nonlinear, requiring a linearization approach to resolve. The iterative Newton-Raphson scheme is used for linearization. The solution scheme requires one primary unknown for each governing conservation equation for each grid cell. The maximum number of unknowns for the STOMP-HYDT-KE simulator per grid cell is nine, when the three hydrate formers (i.e., CO₂, CH₄, and N₂) and inhibitor are active. Each hydrate former has separate solutions for the mobile and hydrate components. The simulator allows the users to eliminate one or two hydrate formers and the inhibitor from the solution set. Therefore the minimum number of unknowns per grid cell is four.

The primary unknowns or variables for all of the active governing equations at each grid cell must 1) define the state of the system, 2) be independent, and for computational efficiency, 3) provide a direct computational path for all of the secondary variables. Primary variables that require iterative solutions to determine secondary variables should be avoided if at all possible. The appearance and disappearance of phases (e.g., gas, nonaqueous-liquid, hydrate, ice) make it impossible to select a single set of primary variables that meet the three criteria listed above. The primary variable switching approach is used in STOMP simulators to avoid violating one of the three primary variable criteria. Primary variable switching involves

Energy	Water	Mobile CO ₂	Mobile CH ₄	Mobile N ₂	Hydrate CO ₂	Hydrate CH ₄	Hydrate N ₂	Salt
Phase Condition #0			$s_h = 0, s_g = 0, s_n = 0, z^c = 0, z^m = 0, z^n = 0$					
T	P_l	P_v^c	P_v^m	P_v^n	m_h^c	m_h^m	m_h^n	ψ_b^s
Phase Condition #1			$s_h = 0, s_g \geq 0, s_n \geq 0, z^c \geq z^m, z^c \geq z^n$					
T	P_l	T	P_l	T	P_l	T	P_l	T
Phase Condition #2			$s_h = 0, s_g \geq 0, s_n \geq 0, z^m \geq z^c, z^m \geq z^n$					
T	P_l	z^c	P_{na}	z^n	m_h^c	m_h^m	m_h^n	ψ_b^s
Phase Condition #3			$s_h = 0, s_g \geq 0, s_n \geq 0, z^n \geq z^c, z^n \geq z^m$					
T	P_l	z^c	z^m	P_{na}	m_h^c	m_h^m	m_h^n	ψ_b^s

Table 1a. Primary Variable Sets and Phase Conditions without Hydrate

Energy	Water	Mobile CO ₂	Mobile CH ₄	Mobile N ₂	Hydrate CO ₂	Hydrate CH ₄	Hydrate N ₂	Salt
Phase Condition #4			$s_h > 0, s_g \geq 0, s_n \geq 0, z^c \geq z^m, z^c \geq z^n, \varphi_e^c \geq \varphi_e^m, \varphi_e^c \geq \varphi_e^n$					
T	P_l	P_{na}	z^m	z^n	s_h	φ_h^m	φ_h^n	ψ_b^s
Phase Condition #5			$s_h > 0, s_g \geq 0, s_n \geq 0, z^m \geq z^c, z^m \geq z^n, \varphi_e^c \geq \varphi_e^m, \varphi_e^c \geq \varphi_e^n$					
T	P_l	z^c	P_{na}	z^n	s_h	φ_h^m	φ_h^n	ψ_b^s
Phase Condition #6			$s_h > 0, s_g \geq 0, s_n \geq 0, z^n \geq z^c, z^n \geq z^m, \varphi_e^c \geq \varphi_e^m, \varphi_e^c \geq \varphi_e^n$					
T	P_l	z^c	z^m	P_{na}	s_h	φ_h^m	φ_h^n	ψ_b^s
Phase Condition #7			$s_h > 0, s_g \geq 0, s_n \geq 0, z^c \geq z^m, z^c \geq z^n, \varphi_e^m \geq \varphi_e^c, \varphi_e^m \geq \varphi_e^n$					
T	P_l	P_{na}	z^m	z^n	φ_h^c	s_h	φ_h^n	ψ_b^s
Phase Condition #8			$s_h > 0, s_g \geq 0, s_n \geq 0, z^m \geq z^c, z^m \geq z^n, \varphi_e^m \geq \varphi_e^c, \varphi_e^m \geq \varphi_e^n$					
T	P_l	z^c	P_{na}	z^n	φ_h^c	s_h	φ_h^n	ψ_b^s
Phase Condition #9			$s_h > 0, s_g \geq 0, s_n \geq 0, z^n \geq z^c, z^n \geq z^m, \varphi_e^m \geq \varphi_e^c, \varphi_e^m \geq \varphi_e^n$					
T	P_l	z^c	z^m	P_{na}	φ_h^c	s_h	φ_h^n	ψ_b^s
Phase Condition #10			$s_h > 0, s_g \geq 0, s_n \geq 0, z^c \geq z^m, z^c \geq z^n, \varphi_e^n \geq \varphi_e^c, \varphi_e^n \geq \varphi_e^m$					
T	P_l	P_{na}	z^m	z^n	φ_h^c	φ_h^m	s_h	ψ_b^s
Phase Condition #11			$s_h > 0, s_g \geq 0, s_n \geq 0, z^m \geq z^c, z^m \geq z^n, \varphi_e^n \geq \varphi_e^c, \varphi_e^n \geq \varphi_e^m$					
T	P_l	z^c	P_{na}	z^n	φ_h^c	φ_h^m	s_h	ψ_b^s
Phase Condition #12			$s_h > 0, s_g \geq 0, s_n \geq 0, z^n \geq z^c, z^n \geq z^m, \varphi_e^n \geq \varphi_e^c, \varphi_e^n \geq \varphi_e^m$					
T	P_l	z^c	z^m	P_{na}	φ_h^c	φ_h^m	s_h	ψ_b^s

Table 1b. Primary Variable Sets and Phase Conditions with Hydrate

changing the primary variable set which changes in thermodynamic states and phase conditions. When the full suite of hydrate formers is active, STOMP-HYDT-KE utilizes 13 different primary variable sets. The 13 sets and correlating thermodynamic states and phase conditions are listed in Table 1. Transitions between phase conditions occur just prior to a new Newton-Raphson iteration. This allows for multiple phase condition transitions within a single time step.

The mobile masses of hydrate formers use one of two variables; either the mole fraction of hydrate formers in the total gas and nonaqueous-liquid phases or the total gas and nonaqueous-liquid pressure. The mobile hydrate former with the highest mole fraction uses the total gas and nonaqueous-liquid pressure, and the two

lower hydrate formers use the mole fraction of hydrate formers in the total gas and nonaqueous-liquid phases. The use of the mole fraction of hydrate formers in the total gas and nonaqueous-liquid phases is particularly attractive as a primary variable, as it directly allows the calculation of the composition and density of the gas and nonaqueous-liquid phases, through the hybrid tabular-cubic equation of state. For no hydrate conditions, Phase Conditions #1 through #3, the total mass of hydrate formers is chosen as the primary variable, which is exactly the quantity being conserved. If the grid cell is within hydrate stability conditions for the composition of mobile hydrate formers then the hydrate formation rate will be positive, resulting in a non-zero value of the total mass of hydrate formers and a transition in phase condition. For hydrate conditions, Phase Conditions #4 through #12, the hydrate masses of hydrate formers use one of two variables; either the mole fraction of hydrate formers in the gas phase in equilibrium with the hydrate or the hydrate saturation. The hydrate former with the highest mole fraction in the hydrate, uses the hydrate saturation as its primary variable, and the two lower hydrate formers use the mole fraction of hydrate formers in the gas phase in equilibrium with the hydrate.

Each time step involves a number of Newton-Raphson iterations, where the initial guess to the primary variables are the converged primary variables at the conclusion of the previous time step. At the start of each iteration, the primary variables are used to determine the phase condition for every active node. The partial derivatives in the Jacobian matrix are computed numerically in STOMP-HYDT-KE, which requires setting an increment for each primary variable. Once the phase conditions are established and the primary variable increments are set, the constitutive equations are solved to determine the secondary variables. The secondary variables are then used to determine conservation equation residuals and residual partial derivatives, which comprise the Jacobian matrix. The linear system solver then returns corrections to the primary variables. Before continuing on to the next iteration, the primary variables are updated with the corrections and a convergence check is conducted. STOMP-HYDT-KE uses a global convergence requirement, which means that convergence requirements must be met for all primary variables in every active node. The metric for convergence is that either the residual falls below a specified fraction of the total conserved quantity in the node, or the correction to the primary variable falls below a specified fraction of a reference value. Converged solutions proceed to a new time step, after reporting any requested results. Unconverged solutions proceed to a new iteration or result in a convergence failure. Convergence failures occur when the number of Newton-Raphson iterations exceed a specified value. When this occurs, the time step is cut by a specified fraction, and the time step is restarted. If the time step falls below a specified value from a sequence of time-step cuts, then the simulation stops.

The algorithmic structure for the core of the STOMP-HYDT-KE simulator is based on four components: 1) initialization, 2) time-stepping loop, 3) Newton-Raphson iteration loop, and 4) closure. During initialization, the input file is read twice. The first input file read is used to determine memory requirement and to allocate memory to the global arrays. The second input read is used to define the problem. After reading the input file the second time, the initial conditions are checked for errors and initial phase conditions are set. With the initial phase conditions and primary variables set, all secondary variables are computed. Next the Jacobian matrix structure is defined, including consideration of bandwidth and active hydrate formers. Before starting a new time step, all surface fluxes are computed.

At the start of a new time step, the time-step quantity is determined, user-requested output is recorded, and old time-step information is stored. The next series of calculations are preparatory for building the Jacobian matrix. Boundary condition properties are computed. Source/sink contributions are determined. Internal surface and boundary surface fluxes are computed. The Jacobian matrix and problem vector are then loaded in conservation equation sequence: 1) thermal energy, 2) water mass, 3) mobile CO₂ mass, 4) mobile CH₄ mass, 5) mobile N₂ mass, 6) hydrate CO₂ mass, 7) hydrate CH₄ mass, 8) hydrate N₂ mass, and 9) salt mass, assuming no-flow adiabatic conditions for all boundary surfaces. Next, the Jacobian matrix and problem vector are modified for boundary conditions applied to boundary surfaces. The Jacobian matrix is then further modified for vertical equilibrium domains and coupled wells. Once constructed, the Jacobian matrix and problem vector are submitted to the linear system solver, which returns the solution vector of primary

variable corrections. The primary variable corrections are then used to update the primary variables and check for convergence.

If convergence is not achieved and the iteration count is less than or equal to the specified limit, then the updated primary variables are used to set the phase condition, assign primary variable increments, and compute the secondary variables. The number of Newton-Raphson iterations is incremented and new Newton-Raphson iteration is started. If convergence is not achieved and the iteration count is greater than the specified limit, then the primary variables and phase conditions are reset to their old-time step values. Secondary variables are computed, the time-step is reduced by a user specified amount, and a new time step is started. If the reduced time-step quantity is below a user specified value, then the simulation halts, creating a restart file and recording user-specified output. If convergence is achieved, the updated primary variables are used to set phase conditions, assign primary variable increments, compute secondary variables, and compute interior and boundary surface fluxes for use in nonreactive and reactive transport. A new time step quantity is determined, user-requested output is recorded, and a new time-step loop is started. The simulation continues in this manner until the user-specified maximum number of time steps or user-specified simulation time limit is reached.

2.5 Initial Conditions

Initial conditions are used to set the starting thermodynamic state of the system at every grid cell. Initial conditions can be specified via the user input or from a restart file. Restart files contain a record of all primary variables and phase condition for every grid cell. Because STOMP-HYDT-KE allows for non-equilibrium conditions between the mobile- and hydrate formers, initial conditions can be specified as being in thermodynamic equilibrium or in a non-equilibrium state. To limit the number of combinations of variables used to define the state of the system, ten initial condition options were developed. Flash calculation routines are used to convert the initial condition specification to one of the 12 phase conditions listed in Table 1. A summary of the twelve initial condition types and the associated flash calculations are listed in Table 2a and Table 2b, without and with nonaqueous-liquid conditions, respectively. The table indicates the Initial Condition number, the distinguishing phase conditions, and the possible resulting Phase Condition numbers. For initial conditions with hydrate present, the hydrate formers in the mobile and hydrate phases can either be in equilibrium or not. The Iterative Solved Variable(s) column indicates those variables that are solved in the flash calculation using a Newton-Raphson iteration scheme. Variables within a set of braces are solved simultaneously. Multiple braces indicate two sequential solves are required for the flash calculation. For Initial Conditions #6 and #7 the specified variables allow for a direct solution of all the needed primary variables for the phase condition. For those initial conditions that can yield multiple phase conditions, the resulting phase condition is determined by the ratio of hydrate formers and whether gas phase is present.

Initial conditions #1, #2, #6, and #7 are used to specify initial states without hydrate. If the specified conditions are within the hydrate stability region for the concentrations of mobile hydrate formers, then the phase condition will transition from to a hydrate phase condition, but with zero initial hydrate saturation. Hydrate formers dissolved in the aqueous phase, without gas or nonaqueous-liquid, will only have the potential to form hydrate, if their equilibrium vapor pressure, as determined by the Henry's law, is greater than the equilibrium vapor pressure for the hydrate. Initial conditions #1 through #5 are used to specify initial states without nonaqueous liquid, as shown in Table 2a. If the specified initial conditions are within the liquid or two phase region of the phase envelope, then an error message is generated, and the simulation stops. Initial conditions #6 through #10 are used to specify initial states with nonaqueous liquid, as shown in Table 2b. Initial conditions #6 and #8 are without gas and only the nonaqueous-liquid saturation is specified. Initial conditions #7, #9, and #10 are with both gas and nonaqueous-liquid. For these initial conditions, the combined gas and nonaqueous-liquid saturations are specified and the flash calculation determines their ratios. Initial conditions #3, #4, #8, and #9 have hydrate, but the hydrate and mobile phases are not

necessarily in equilibrium. Initial conditions #5 and #10 have hydrate and assume equilibrium between the mobile and hydrate phases, which reduces the degrees of freedom in specifying the initial state.

Specified Variables	Iteratively Solved Variables	Phase Condition Variables
Initial Condition #1	$s_h = 0, s_g = 0, s_n = 0$	Phase Conditions #1 - #3
$\left\{ T, P_l, \varphi_m^c, \varphi_m^m, \varphi_m^n, W_l^f \right\}$	$\left\{ \varphi_g^c, \varphi_g^m, \varphi_g^n \right\}$ $\left\{ z^c, z^m, z^n \right\}$	$\left\{ T, P_l, P_{gn}, z^c, z^m, z^n, \right.$ $\left. m_h^c, m_h^m, m_h^n, \psi_b^s \right\}$
Initial Condition #2	$s_h = 0, s_g > 0, s_n = 0$	Phase Conditions #1 - #3
$\left\{ T, P_g, s_g, \varphi_m^c, \varphi_m^m, \varphi_m^n \right\}$	$\left\{ \varphi_g^c, \varphi_g^m, \varphi_g^n \right\}$ $\left\{ z^c, z^m, z^n \right\}$	$\left\{ T, P_l, P_{gn}, z^c, z^m, z^n, \right.$ $\left. m_h^c, m_h^m, m_h^n, \psi_b^s \right\}$
Initial Condition #3	$s_h > 0, s_g = 0, s_n = 0, \text{nonequil.}$	Phase Conditions #4 - #12
$\left\{ T, P_l, \varphi_m^c, \varphi_m^m, \varphi_m^n, W_l^f \right.$ $\left. \varphi_h^c, \varphi_h^m, \varphi_h^n, s_h \right\}$	$\left\{ \varphi_g^c, \varphi_g^m, \varphi_g^n \right\}$ $\left\{ z^c, z^m, z^n \right\}$ $\left\{ \varphi_e^c, \varphi_e^m, \varphi_e^n \right\}$	$\left\{ T, P_l, P_{gn}, z^c, z^m, z^n, \right.$ $\left. s_h, \varphi_e^c, \varphi_e^m, \varphi_e^n, \psi_b^s \right\}$
Initial Condition #4	$s_h > 0, s_g > 0, s_n = 0, \text{nonequil.}$	Phase Conditions #4 - #12
$\left\{ T, P_g, s_g, \varphi_m^c, \varphi_m^m, \varphi_m^n, \right.$ $\left. \varphi_h^c, \varphi_h^m, \varphi_h^n, s_h \right\}$	$\left\{ \varphi_g^c, \varphi_g^m, \varphi_g^n \right\}$ $\left\{ \varphi_e^c, \varphi_e^m, \varphi_e^n \right\}$	$\left\{ T, P_l, P_{gn}, z^c, z^m, z^n, \right.$ $\left. s_h, \varphi_e^c, \varphi_e^m, \varphi_e^n, \psi_b^s \right\}$
Initial Condition #5	$s_h > 0, s_g > 0, s_n = 0, \text{equil.}$	Phase Conditions #4 - #12
$\left\{ T, s_g, \varphi_h^c, \varphi_h^m, \varphi_h^n, s_h \right\}$	$\left\{ \varphi_e^c, \varphi_e^m, \varphi_e^n \right\}$	$\left\{ T, P_l, P_{gn}, z^c, z^m, z^n, \right.$ $\left. s_h, \varphi_e^c, \varphi_e^m, \varphi_e^n, \psi_b^s \right\}$

Table 2a. Initial Condition, Flash Condition, and Phase Condition Chart without Nonaqueous-Liquid Conditions

Specified Variables	Iteratively Solved Variables	Phase Condition Variables
Initial Condition #6	$s_h = 0, s_g = 0, s_n > 0$	Phase Conditions #1 - #3
$\left\{ T, P_n, s_n, \varphi_m^c, \varphi_m^m, \varphi_m^n \right\}$	$\left\{ \varphi_n^c, \varphi_n^m, \varphi_n^n \right\}$	$\left\{ T, P_l, P_{gn}, z^c, z^m, z^n, \right. \\ \left. m_h^c, m_h^m, m_h^n, \psi_b^s \right\}$
Initial Condition #7	$s_h = 0, s_g > 0, s_n > 0$	Phase Conditions #1 - #3
$\left\{ T, P_{gn}, s_{gn}, \varphi_m^c, \varphi_m^m, \varphi_m^n \right\}$	$\left\{ z^c, z^m, z^n \right\}$	$\left\{ T, P_l, P_{gn}, z^c, z^m, z^n, \right. \\ \left. m_h^c, m_h^m, m_h^n, \psi_b^s \right\}$
Initial Condition #8	$s_h > 0, s_g = 0, s_n > 0, \textit{nonequil.}$	Phase Conditions #4 - #12
$\left\{ T, P_n, s_n, \varphi_m^c, \varphi_m^m, \varphi_m^n \right. \\ \left. \varphi_h^c, \varphi_h^m, \varphi_h^n, s_h \right\}$	$\left\{ \varphi_n^c, \varphi_n^m, \varphi_n^n \right\}$ $\left\{ \varphi_e^c, \varphi_e^m, \varphi_e^n \right\}$	$\left\{ T, P_l, P_{gn}, z^c, z^m, z^n, \right. \\ \left. s_h, \varphi_e^c, \varphi_e^m, \varphi_e^n, \psi_b^s \right\}$
Initial Condition #9	$s_h > 0, s_g > 0, s_n > 0, \textit{nonequil.}$	Phase Conditions #4 - #12
$\left\{ T, P_{gn}, s_{gn}, \varphi_m^c, \varphi_m^m, \varphi_m^n, \right. \\ \left. \varphi_h^c, \varphi_h^m, \varphi_h^n, s_h \right\}$	$\left\{ z^c, z^m, z^n \right\}$ $\left\{ \varphi_e^c, \varphi_e^m, \varphi_e^n \right\}$	$\left\{ T, P_l, P_{gn}, z^c, z^m, z^n, \right. \\ \left. s_h, \varphi_e^c, \varphi_e^m, \varphi_e^n, \psi_b^s \right\}$
Initial Condition #10	$s_h > 0, s_g > 0, s_n > 0, \textit{equil.}$	Phase Conditions #4 - #12
$\left\{ T, s_{gn}, \varphi_h^c, \varphi_h^m, \varphi_h^n, s_h \right\}$	$\left\{ \varphi_e^c, \varphi_e^m, \varphi_e^n \right\}$ $\left\{ z^c, z^m, z^n \right\}$	$\left\{ T, P_l, P_{gn}, z^c, z^m, z^n, \right. \\ \left. s_h, \varphi_e^c, \varphi_e^m, \varphi_e^n, \psi_b^s \right\}$

Table 2b. Initial Condition, Flash Condition, and Phase Condition Chart with Nonaqueous-Liquid Conditions

3.0 Demonstration Problems

Three levels of problems were used to demonstrate the STOMP-HYDT-KE simulator. Verification problems were used to demonstrate specific features of the simulator, such as phase transitions, initial conditions, boundary conditions or sources. Verification problems were designed to verify that the simulator is executing properly and have known solutions or end-points. For complex multifluid systems a common verification problem is one that is initialized with gradients across the computational domain and then the simulation executes to equilibrium conditions over time. Benchmark problems generally are more complex than verification problems. Benchmark problems are often used to compare different simulators, but could be problems with analytical solutions. Validation problems can range from simple to complex, but have experimental results against which to compare the simulation. Demonstration of a numerical simulator against a series of validation problems provides growing assurance that the simulator is modeling processes and executing properly, but does not validate the code.

3.1 Verification Problems

3.1.1 Transition to Equilibrium without Hydrates: TTE1

This problem used a two-node grid to test the transition from saturated to unsaturated conditions for the mobile fluids. Initial conditions in the two nodes are listed in Table 3. Node 1 was fully aqueous saturated, but at a lower pressure than Node 2, which is partially aqueous saturated. Node 1 was initialized using Initial Condition #1 (see Table 2a), and Node 2 using Initial Condition #2 (see Table 2a). The problem starts with a 1-second time step and stops after 1000 years, executing in 103 time steps with a time growth factor of 1.25. No convergence failures occurred during the simulation, using a Newton-Raphson iteration of 16. The transient to equilibrium in terms of temperature, pressure and saturation are shown in Figure 9. All three parameters transition smoothly to equilibrium conditions after $2e+4$ s. The transient to equilibrium in terms of gas mass fractions of the hydrate former components, as shown in Figure 10, occurs in two stages. The first stage, between 0 and $2e+4$ s, is dominated by the redistribution of fluids, and the second stage between $2e+4$ and $2e+6$ s, is controlled by the diffusion of phase components. Thermal equilibrium occurred during the fluid redistribution period. The input file for this problem is shown below the solution figures.

Node	Initial Condition	T ($^{\circ}C$)	P ($psia$)	ϕ_m^c	ϕ_m^m	ϕ_m^n	s_g	W_l^f
1	#1	20.0	1900.0	0.1	0.8	0.1	0.0	0.9
2	#2	30.0	2100.0	0.8	0.1	0.1	0.8	1.0

Table 3. Initial Conditions for the Transition to Equilibrium without Hydrates Problem: TTE1

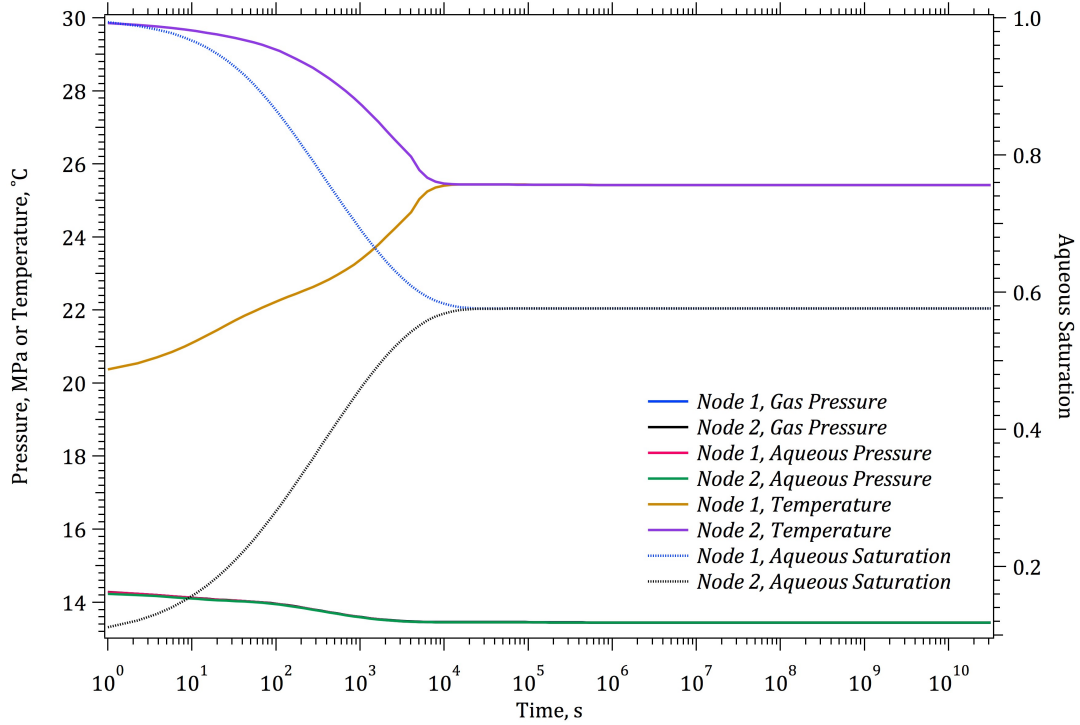


Figure 9. Transition to Equilibrium (TTE1) for Gas Pressure, Aqueous Pressure, Temperature, and Aqueous Saturation

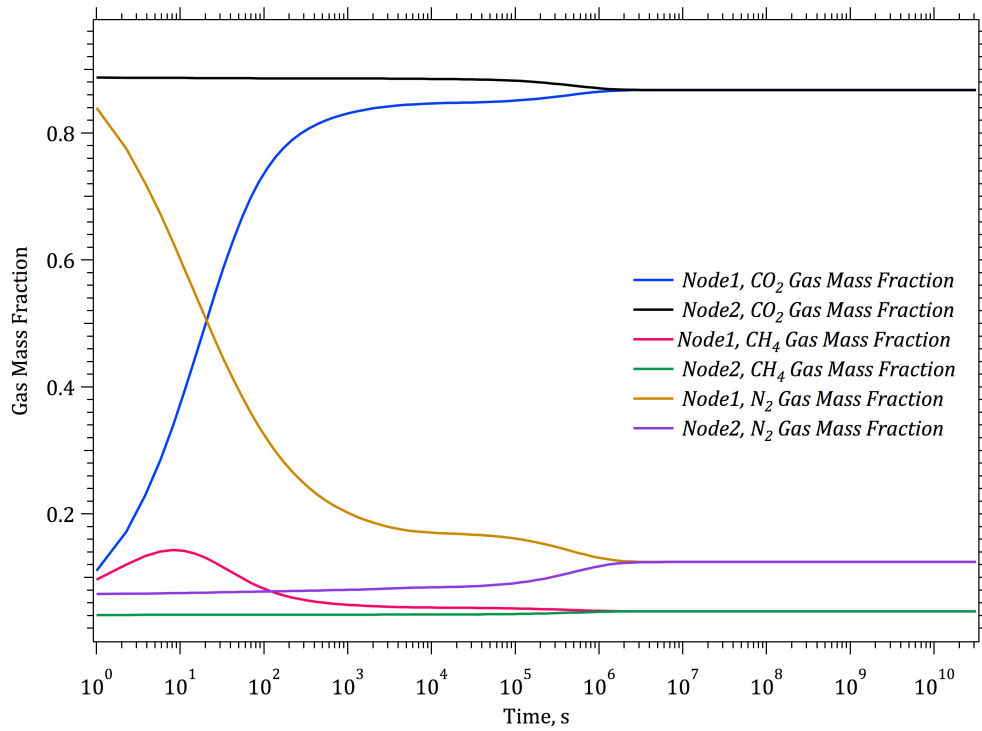


Figure 10. Transition to Equilibrium (TTE1) for Gas Mass Fractions of Hydrate Formers

Input File for Transition to Equilibrium without Hydrates: TTE1

~Simulation Title Card

1,
Verification TTE1,
Mark White,
Pacific Northwest National Laboratory,
06 November 2012,
13:23 PST,
3,
2-node transition to equilibrium without hydrates
Node 1: initial saturated, lower temperature, lower pressure, lower CO2 concentration
Node 2: initial unsaturated, higher temperature, higher pressure, higher CO2
concentration

~Solution Control Card

Normal,
HYDT-KE w/NaCl w/Isobrine,
1,
0,yr,1000,yr,1,sec,1000,yr,1.25,16,1.e-06,
1000,
Variable Aqueous Diffusion,
Variable Gas Diffusion,
Variable Nonaqueous Liquid Diffusion,
#exchange,formation,dissociation,
8.e-6,kmol/s m³,1.e-2,kmol/s m³,1.e-2,kmol/s m³,2.5,
0,

~Grid Card

Cartesian,
2,1,1,
0,cm,2@10,cm,
0,cm,10,cm,
0,cm,10,cm,

~Rock/Soil Zonation Card

1,
Core,1,2,1,1,1,1,

~Mechanical Properties Card

Core,2.60,g/cm³,0.22,0.22,compressibility,6.25e-10,1/Pa,,,Millington and Quirk,,,

~Hydraulic Properties Card

Core,0.5,darcy,0.5,darcy,0.5,darcy,

~Saturation Function Card

72.0,dynes/cm,24.0,dynes/cm,,,26.7,dynes/cm,
Core,van Genuchten w/Webb,2.04,1/m,2.857,0.1,,72.0,dynes/cm,0.1,

~Aqueous Relative Permeability Card

Core,Mualem,,

~Gas Relative Permeability Card

Core,Mualem,,

~Nonaqueous Liquid Relative Permeability Card

Core,Mualem,,

~Thermal Properties Card

Core,Parallel,2.86,W/m K,2.86,W/m K,2.86,W/m K,700,J/kg K,

~Salt Transport Card

Core,0.0,ft,0.0,ft,

~Initial Conditions Card

12,
#Saturated-Unsaturated Two-Node Transient to Equilibrium
#IC1 (sh = 0, sn = 0, sg = 0, nonequilibrium)
Temperature,20.0,C,,,,,,,,1,1,1,1,1,1,
Pressure,1900.0,psi,,,,,,,,1,1,1,1,1,1,
Mobile CO2 Mole Fraction of Formers,0.1,,,,,,,,1,1,1,1,1,1,
Mobile N2 Mole Fraction of Formers,0.8,,,,,,,,1,1,1,1,1,1,
Aqueous Relative Saturation of Formers,0.9,,,,,,,,1,1,1,1,1,1,
IC1,1,1,1,1,1,
#IC2 (sh = 0, sn = 0, sg > 0, nonequilibrium)
Temperature,30.0,C,,,,,,,,2,2,1,1,1,1,
Pressure,2100.0,psi,,,,,,,,2,2,1,1,1,1,
Gas Saturation,0.9,,,,,,,,2,2,1,1,1,1,
Mobile CO2 Mole Fraction of Formers,0.8,,,,,,,,2,2,1,1,1,1,
Mobile N2 Mole Fraction of Formers,0.1,,,,,,,,2,2,1,1,1,1,
IC2,2,2,1,1,1,1,

~Output Control Card

2,
1,1,1,
2,1,1,
1,1,s,m,6,6,6,
16,
Phase Condition,,
Gas Pressure,MPa,
Aqueous Pressure,MPa,
Gas CO2 Mole Fraction of Formers,,
Gas CH4 Mole Fraction of Formers,,
Gas N2 Mole Fraction of Formers,,
Temperature,c,
Aqueous Saturation,,
Gas Saturation,,
Hydrate Saturation,,
Hydrate CO2 Mass Fraction,,
Hydrate CH4 Mass Fraction,,
Hydrate N2 Mass Fraction,,
CO2 Gas Mass Fraction,,
CH4 Gas Mass Fraction,,
Integrated CO2 Mass,kg,
0,
15,
Gas Pressure,MPa,
Aqueous Pressure,MPa,
Temperature,c,
Aqueous Saturation,,
Nonaqueous Liquid Saturation,,
Gas Saturation,,
Hydrate Saturation,,
Hydrate CO2 Mass Fraction,,
Hydrate CH4 Mass Fraction,,
CO2 Aqueous Mass Fraction,,
CH4 Aqueous Mass Fraction,,
CO2 Nonaqueous Liquid Mass Fraction,,
CH4 Nonaqueous Liquid Mass Fraction,,
CO2 Gas Mass Fraction,,
CH4 Gas Mass Fraction,,

3.1.2 Transition to Equilibrium from Hydrate and Mobile Phase Non-equilibria: TTE2

This problem used a two-node grid to test the transition from a state with the hydrate and mobile phases not being in thermodynamic equilibrium in either node, and the two nodes having difference in initial pressure and hydrate saturation. Initial conditions for this problem are listed in Table 4. Both nodes used the Initial Condition #4 to specify the initial states (see Table 2a). Node 1 is initialized with a pressure that is within the hydrate stability pressure of 9.43 MPa for the specified hydrate composition and a small amount of hydrate. Node 2 is initialized with a pressure that is below the hydrate stability pressure and a moderate amount of hydrate. The problem starts with a 0.1-second time step and stops after 1000 years, executing in 103 time steps with a time-growth factor of 1.25. No convergence failures occurred during the simulation, using a Newton-Raphson iteration of 16. The transient nature of the simulation with respect to guest molecule exchange and hydrate formation/dissociation is controlled through four kinetic parameters: 1) hydrate guest-molecule exchange rate constant, 8×10^{-6} kmol/s m³; 2) hydrate formation rate constant, 1×10^{-2} kmol/s m³; 3) hydrate dissociation rate constant, 1×10^{-2} kmol/s m³; and 4) hydrate formation rate aqueous saturation exponent, 2.5.

The transient to equilibrium in terms of temperature, pressure, and phase saturations is shown in Figure 11 and in terms of hydrate former concentrations in Figure 12. Within the first second the gas pressures equilibrate, dropping below the hydrate stability pressure in both nodes. This drop in pressure leads to dissociation of the hydrate and a reduction in temperature in both nodes. After 4×10^4 seconds, all the hydrate in Node 1 has dissociated into gas and water, which initiates a recovery in the gas pressure. The hydrate in Node 2 stabilizes after 10^7 seconds, resulting in pressure and temperature plateaus. The mobile and hydrate phase concentrations of CH₄, CO₂, and N₂ remain out of equilibrium until 2×10^7 seconds. Equilibrium occurs through the exchange of the hydrate formers between the mobile phase and hydrate during the period from 10^3 and 10^7 seconds. During the exchange process the hydrate composition changes and shifts the equilibrium point. As a result hydrate dissociation occurs with a resulting further drop in temperature and increase in gas pressure. Once the mobile and hydrate phases are in equilibria, temperature, pressure, and phase compositions stabilize after 10^7 seconds. The kinetics of the hydrate dissociation and exchange of the guest molecules was controlled by the kinetic rate constants for these processes that were specified in the input file. For this problem the value of the dissociation rate and exchange rate parameters are not critical as the principal concern is the path to equilibrium and the ultimate equilibrium point. The input file for this problem is shown below the solution figures.

Node	Initial Condition	T (°C)	P (MPa)	S_g	ϕ_m^c	ϕ_m^m	S_h	ϕ_h^c	ϕ_h^m
1	#4	10.0	10.0	0.25	0.20	0.05	0.05	0.20	0.75
2	#4	10.0	9.0	0.25	0.20	0.05	0.50	0.20	0.75

Table 4. Initial Conditions for the Transition to Equilibrium from Hydrate and Mobile Phase Non-equilibria: TTE2

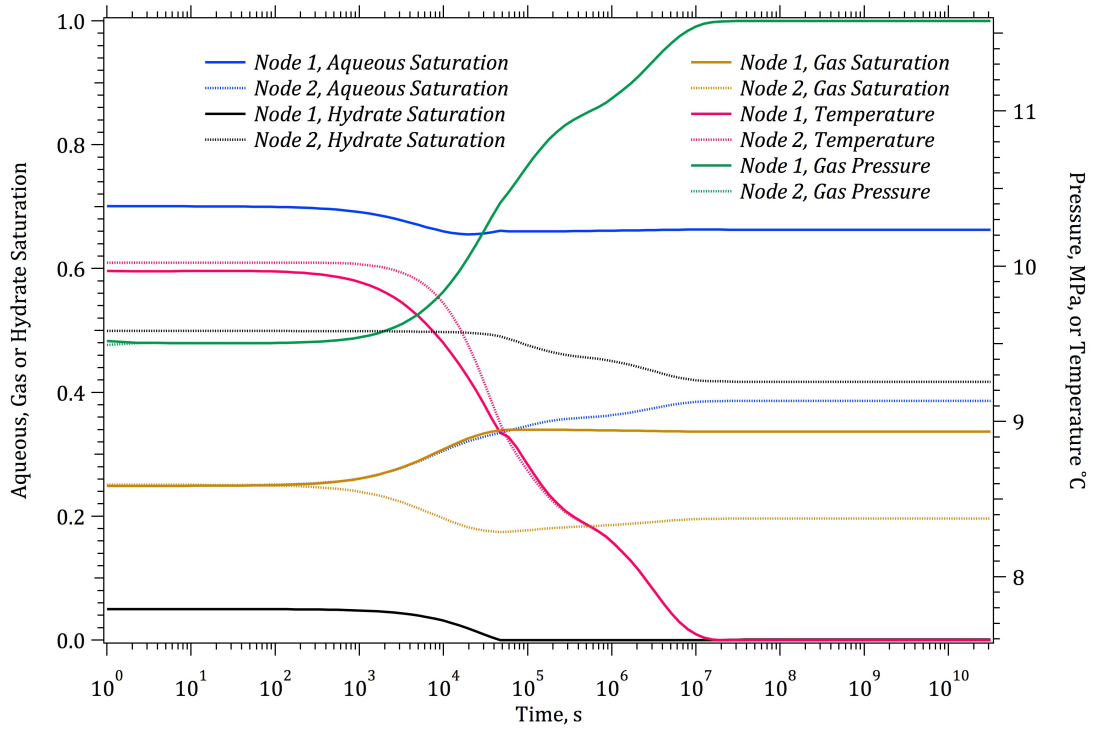


Figure 11. Transition to Equilibrium (TTE2) for Gas Pressure, Aqueous Pressure, Temperature, and Aqueous Saturation

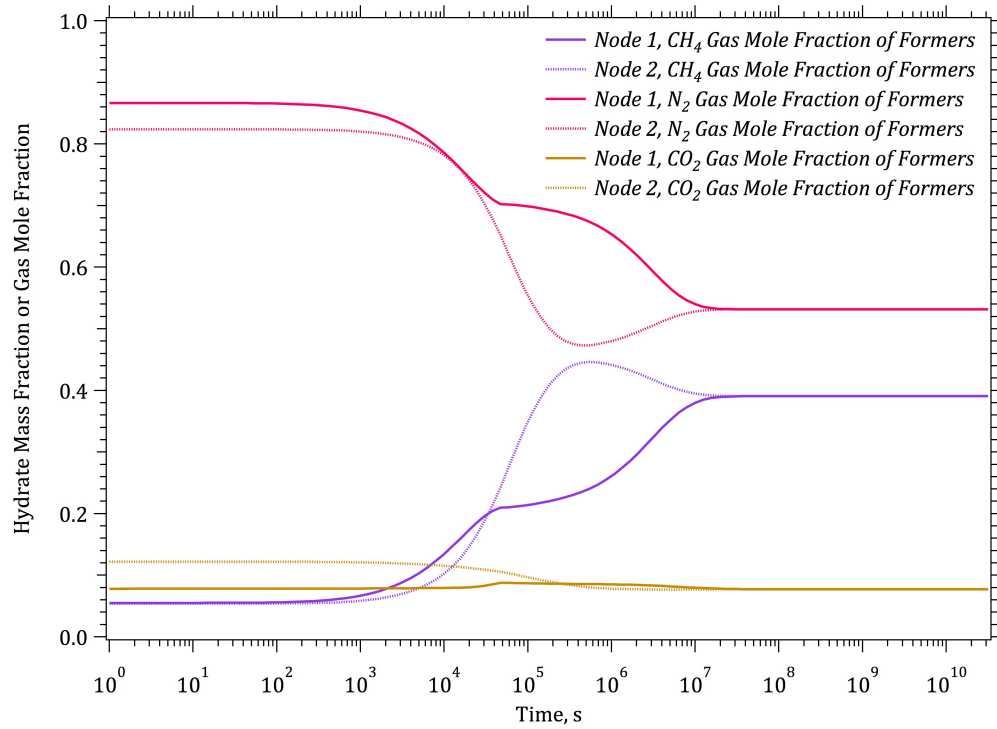


Figure 12. Transition to Equilibrium (TTE1) for Gas Mass Fractions of Hydrate Formers

Input File for Transition to Equilibrium without Hydrates: TTE2

~Simulation Title Card

1,
Verification TTE2,
Mark White,
Pacific Northwest National Laboratory,
06 November 2012,
13:23 PST,
6,
2-node transition to equilibrium with hydrates
initial mobile CO2 concentration > hydrate CO2 concentration
initial equal temperature and saturation conditions
initial equal hydrate and gas saturations
Node 1: initial higher pressure
Node 2: initial lower pressure

~Solution Control Card

Normal,
HYDT-KE w/NaCl w/Isobrine,
1,
0,yr,1000,yr,1.0,sec,1000,yr,1.25,16,1.e-06,
10000,
Variable Aqueous Diffusion,
Variable Gas Diffusion,
Variable Nonaqueous Liquid Diffusion,
#exchange,formation,dissociation,
8.e-6,kmol/s m³,1.e-2,kmol/s m³,1.e-2,kmol/s m³,2.5,
0,

~Grid Card

Cartesian,
2,1,1,
0,cm,2@10,cm,
0,cm,10,cm,
0,cm,10,cm,

~Rock/Soil Zonation Card

1,
Core,1,2,1,1,1,1,

~Mechanical Properties Card

Core,2.60,g/cm³,0.22,0.22,compressibility,6.25e-10,1/Pa,,,Millington and Quirk,,,

~Hydraulic Properties Card

Core,0.5,darcy,0.5,darcy,0.5,darcy,

~Saturation Function Card

72.0,dynes/cm,24.0,dynes/cm,,,26.7,dynes/cm,
Core,van Genuchten w/Webb,2.04,1/m,2.857,0.1,,72.0,dynes/cm,0.1,

~Aqueous Relative Permeability Card

Core,Mualem,,

~Gas Relative Permeability Card

Core,Mualem,,

~Nonaqueous Liquid Relative Permeability Card

Core,Mualem,,

~Thermal Properties Card

Core,Parallel,2.86,W/m K,2.86,W/m K,2.86,W/m K,700,J/kg K,

~Salt Transport Card

Core,0.0,ft,0.0,ft,

~Initial Conditions Card

11,
#IC4 (sh > 0, sn = 0, sg > 0, nonequilibrium)
Temperature,10.0,C,,,,,,,,1,2,1,1,1,1,
Pressure,10.0,MPa,,,,,,,,1,1,1,1,1,1,
Pressure,9.0,MPa,,,,,,,,2,2,1,1,1,1,
Gas Saturation,0.25,,,,,,,,1,2,1,1,1,1,
Mobile N2 Mole Fraction of Formers,0.75,,,,,,,,1,2,1,1,1,1,
Mobile CH4 Mole Fraction of Formers,0.05,,,,,,,,1,2,1,1,1,1,
Hydrate Saturation,0.05,,,,,,,,1,1,1,1,1,1,
Hydrate Saturation,0.5,,,,,,,,2,2,1,1,1,1,
Hydrate N2 Mole Fraction of Formers,0.05,,,,,,,,1,2,1,1,1,1,
Hydrate CH4 Mole Fraction of Formers,0.75,,,,,,,,1,2,1,1,1,1,
IC4,1,2,1,1,1,1,

~Output Control Card

2,
1,1,1,
2,1,1,
1,1,s,m,6,6,6,
16,
Phase Condition,,
Gas Pressure,MPa,
Aqueous Pressure,MPa,
Gas CO2 Mole Fraction of Formers,,
Gas CH4 Mole Fraction of Formers,,
Gas N2 Mole Fraction of Formers,,
Temperature,c,
Aqueous Saturation,,
Gas Saturation,,
Hydrate Saturation,,
Hydrate CO2 Mass Fraction,,
Hydrate CH4 Mass Fraction,,
Hydrate N2 Mass Fraction,,
CO2 Gas Mass Fraction,,
CH4 Gas Mass Fraction,,
Integrated CO2 Mass,kg,
0,
15,
Gas Pressure,MPa,
Aqueous Pressure,MPa,
Temperature,c,
Aqueous Saturation,,
Nonaqueous Liquid Saturation,,
Gas Saturation,,
Hydrate Saturation,,
Hydrate CO2 Mass Fraction,,
Hydrate CH4 Mass Fraction,,
CO2 Aqueous Mass Fraction,,
CH4 Aqueous Mass Fraction,,
CO2 Nonaqueous Liquid Mass Fraction,,
CH4 Nonaqueous Liquid Mass Fraction,,
CO2 Gas Mass Fraction,,
CH4 Gas Mass Fraction,,

3.1.3 Transition to Equilibrium from Hydrate and Mobile Phase Equilibria: TTE3

This problem used a two-node grid to test the transition from two different hydrate and mobile phase equilibria states. The problem is initialized using the Initial Condition #5 (see Table 2a) in both nodes, but with different levels of hydrate saturation and concentrations of hydrate formers. Initial conditions are listed in Table 5. This problem additionally test the capabilities of the simulator for executing in the iso-N₂ mode, under which mass conservation equations for mobile and hydrate N₂ are not solved. Identical solutions to the problem were obtained with the conservation equations for N₂ being active or inactive. The zero-N₂ concentration condition is an important test for the modified bicubic spline interpolation scheme. Without the inclusion of the zero-N₂ diagonal in the interpolation scheme, the problem would not executed properly, yielding non-zero N₂ concentrations. The problem starts with a 0.01-second time step and stops after 1000 years, executing in 123 time steps with a time-growth factor of 1.25. No convergence failures occurred during the simulation, using a Newton-Raphson iteration of 16. The transient nature of the simulation with respect to guest molecule exchange and hydrate formation/dissociation is controlled through four kinetic parameters: 1) hydrate guest-molecule exchange rate constant, 8×10^{-6} kmol/s m³; 2) hydrate formation rate constant, 1×10^{-2} kmol/s m³; 3) hydrate dissociation rate constant, 1×10^{-2} kmol/s m³; and 4) hydrate formation rate aqueous saturation exponent, 2.5.

Within the 2×10^{-1} seconds the gas pressures in Node 1 and 2 equilibrate. With the pressure in Node 2 being below the hydrate stability point, the hydrate slightly dissociates, leading to a drop in the temperature. The system then remains somewhat stable up to 10² seconds, at which point difference in phase compositions drive the system. In this problem Node 1 contains a CO₂-CH₄ hydrate in equal proportions at a saturation of 0.25 and Node 2 contains a CO₂-CH₄ hydrate slightly richer in CH₄ at a saturation of 0.5. An exchange of hydrate formers between the hydrate and mobile phases and across nodes leads to dissociation of hydrate in Node 2 and formation of hydrate in Node 1. There is a corresponding drop in temperature in Node 2 and increase in temperature in Node1. An interesting result from this simulation is the lack of equilibrium in the final hydrate saturations. The governing flow and transport equations drive components concentrations, temperature and pressure toward equilibrium conditions, however, there is not an equivalent driving force for hydrate saturation. As a result the final hydrate saturations are slightly higher in Node 2 than in Node 1, which additionally yields a difference in final gas saturations and a very slight difference in final aqueous saturations. The kinetics of the hydrate dissociation and exchange of the guest molecules was controlled by the kinetic rate constants for these processes that were specified in the input file. For this problem the value of the dissociation rate and exchange rate parameters are not critical as the principal concern is the path to equilibrium and the ultimate equilibrium point. The input file for this problem is shown below the solution figures.

Node	Initial Condition	T (°C)	s_g	s_h	φ_h^c	φ_h^m	φ_h^n	P_{eq} (MPa)
1	#5	4.0	0.25	0.25	0.50	0.5	0.0	2.8129
2	#5	4.0	0.25	0.50	0.40	0.6	0.0	3.0995

Table 5. Initial Conditions for the Transition to Equilibrium from Hydrate and Mobile Phase Equilibria: TTE3

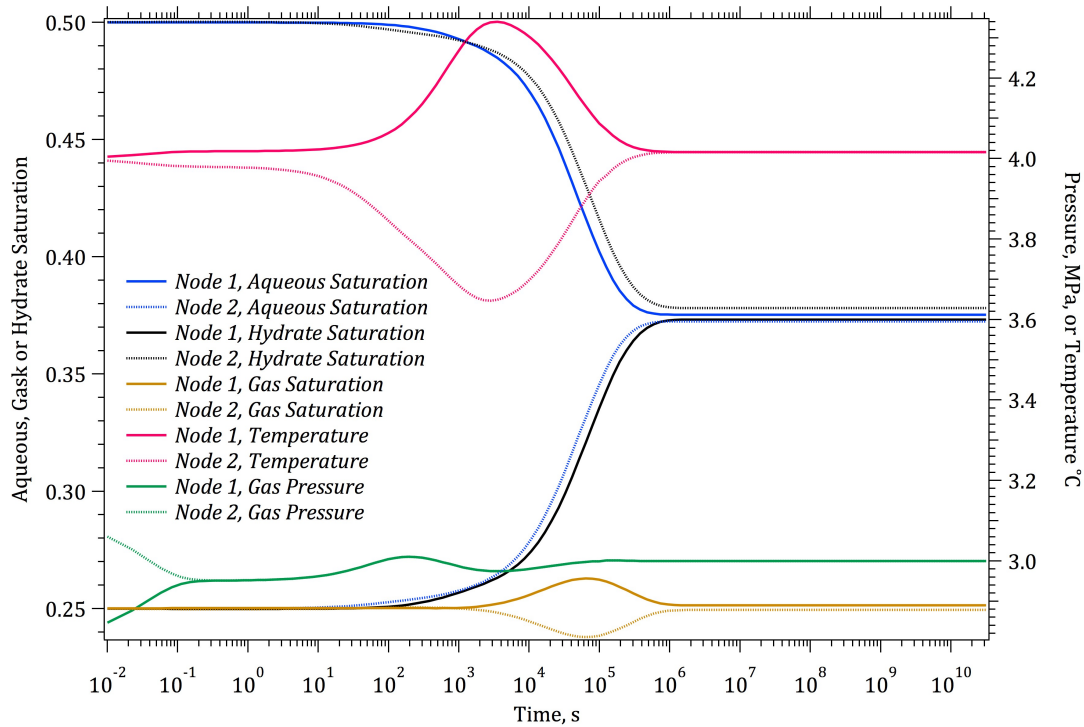


Figure 13. Transition to Equilibrium (TTE3) for Aqueous Saturation, Hydrate Saturation, Gas Saturation, Temperature, and Gas Pressure

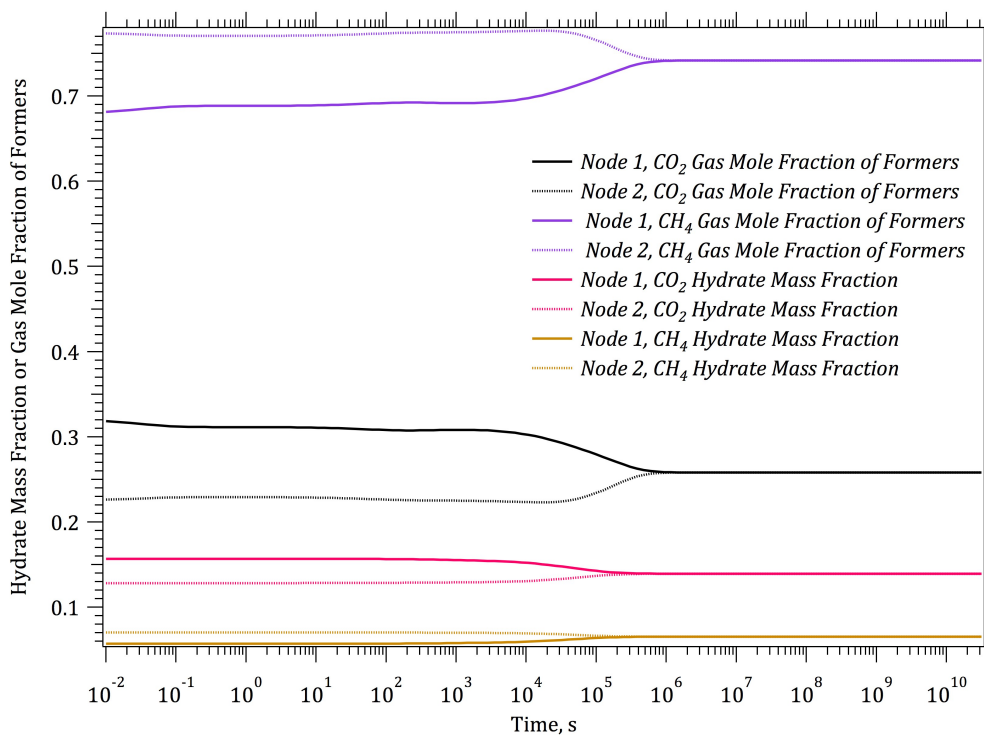


Figure 14. Transition to Equilibrium (TTE3) for Hydrate Mass Fractions and Gas Mole Fraction of Formers

Input File for Transition to Equilibrium without Hydrates: TTE3

~Simulation Title Card

1,
Verification TTE3,
Mark White,
Pacific Northwest National Laboratory,
09 November 2012,
13:59 PST,
6,
2-node transition to equilibrium with hydrates
iso-N2 conditions
initial hydrate and mobile phases in equilibrium
initial gradient in hydrate composition of formers
initial gradient in hydrate saturation
initial constant temperature

~Solution Control Card

Normal,
#HYDT-KE w/NaCl w/Isobrine,
HYDT-KE w/NaCl w/Isobrine w/Iso-N2,
1,
0,yr,1000,yr,0.01,sec,1000,yr,1.25,16,1.e-06,
1000,
Variable Aqueous Diffusion,
Variable Gas Diffusion,
Variable Nonaqueous Liquid Diffusion,
#exchange,formation,dissociation,
8.e-6,kmol/s m³,1.e-2,kmol/s m³,1.e-2,kmol/s m³,2.5,
0,

~Grid Card

Cartesian,
2,1,1,
0,cm,2@10,cm,
0,cm,10,cm,
0,cm,10,cm,

~Rock/Soil Zonation Card

1,
Core,1,2,1,1,1,1,

~Mechanical Properties Card

Core,2.60,g/cm³,0.22,0.22,compressibility,6.25e-10,1/Pa,,,Millington and Quirk,,,

~Hydraulic Properties Card

Core,0.5,darcy,0.5,darcy,0.5,darcy,

~Saturation Function Card

72.0,dynes/cm,24.0,dynes/cm,,,26.7,dynes/cm,
Core,van Genuchten w/Webb,2.04,1/m,2.857,0.1,,72.0,dynes/cm,0.1,

~Aqueous Relative Permeability Card

Core,Mualem,,

~Gas Relative Permeability Card

Core,Mualem,,

~Nonaqueous Liquid Relative Permeability Card

Core,Mualem,,

~Thermal Properties Card

Core,Parallel,2.86,W/m K,2.86,W/m K,2.86,W/m K,700,J/kg K,

~Salt Transport Card

Core,0.0,ft,0.0,ft,

~Initial Conditions Card

12,

#IC5 (sh > 0, sn = 0, sg > 0, equilibrium)

Temperature,4.0,C,,,,,,,,1,1,1,1,1,1,

Gas Saturation,0.25,,,,,,,,1,1,1,1,1,1,

Hydrate Saturation,0.25,,,,,,,,1,1,1,1,1,1,

Hydrate N2 Mole Fraction of Formers,0.0,,,,,,,,1,1,1,1,1,1,

Hydrate CH4 Mole Fraction of Formers,0.5,,,,,,,,1,1,1,1,1,1,

IC5,1,1,1,1,1,1,

#IC5 (sh > 0, sn = 0, sg > 0, equilibrium)

Temperature,4.0,C,,,,,,,,2,2,1,1,1,1,

Gas Saturation,0.25,,,,,,,,2,2,1,1,1,1,

Hydrate Saturation,0.5,,,,,,,,2,2,1,1,1,1,

Hydrate N2 Mole Fraction of Formers,0.0,,,,,,,,2,2,1,1,1,1,

Hydrate CH4 Mole Fraction of Formers,0.6,,,,,,,,2,2,1,1,1,1,

IC5,2,2,1,1,1,1,

~Output Control Card

2,

1,1,1,

2,1,1,

1,1,s,m,6,6,6,

16,

Phase Condition,,

Gas Pressure,MPa,

Aqueous Pressure,MPa,

Gas CO2 Mole Fraction of Formers,,

Gas CH4 Mole Fraction of Formers,,

Gas N2 Mole Fraction of Formers,,

Temperature,c,

Aqueous Saturation,,

Gas Saturation,,

Hydrate Saturation,,

Hydrate CO2 Mass Fraction,,

Hydrate CH4 Mass Fraction,,

Hydrate N2 Mass Fraction,,

CO2 Gas Mass Fraction,,

CH4 Gas Mass Fraction,,

Integrated CO2 Mass,kg,

0,

15,

Gas Pressure,MPa,

Aqueous Pressure,MPa,

Temperature,c,

Aqueous Saturation,,

Nonaqueous Liquid Saturation,,

Gas Saturation,,

Hydrate Saturation,,

Hydrate CO2 Mass Fraction,,

Hydrate CH4 Mass Fraction,,

CO2 Aqueous Mass Fraction,,

CH4 Aqueous Mass Fraction,,

CO2 Nonaqueous Liquid Mass Fraction,,

CH4 Nonaqueous Liquid Mass Fraction,,

CO2 Gas Mass Fraction,,

CH4 Gas Mass Fraction,,

3.1.4 Transition to Equilibrium from Hydrate and Mobile Phase Equilibria: TTE4

This problem used a two-node grid to test the transition from two different hydrate and mobile phase equilibria states. The problem is initialized using the Initial Condition #5 (see Table 2a) in both nodes, but with different levels of hydrate saturation and concentrations of hydrate formers. Initial conditions are listed in Table 6. This problem additionally test the capabilities of the simulator for executing in the iso-CH₄ mode, under which mass conservation equations for mobile and hydrate CH₄ are not solved. Identical solutions to the problem were obtained with the conservation equations for CH₄ being active or inactive. The problem starts with a 0.01-second time step and stops after 1000 years, executing in 123 time steps with a time-growth factor of 1.25. No convergence failures occurred during the simulation, using a Newton-Raphson iteration of 16. The transient nature of the simulation with respect to guest molecule exchange and hydrate formation/dissociation is controlled through four kinetic parameters: 1) hydrate guest-molecule exchange rate constant, 8×10^{-6} kmol/s m³; 2) hydrate formation rate constant, 1×10^{-2} kmol/s m³; 3) hydrate dissociation rate constant, 1×10^{-2} kmol/s m³; and 4) hydrate formation rate aqueous saturation exponent, 2.5.

Although there are only small differences in the N₂ mole fraction of formers in the hydrate between the two nodes, there is a large difference in equilibrium pressures and thus initial gas pressures. Within 10⁻¹ seconds the gas pressures equilibrate and the gas concentrations of CH₄ and N₂ change toward equilibrium conditions. During this period there were also very slight changes in the hydrate saturation in each node. Conditions stabilize somewhat between 10⁻¹ and 10³ seconds, but then an exchange of CH₄ and N₂ between the mobile and hydrate phases yields a new equilibrium point after 5×10^6 seconds. There is a net decrease of hydrate in Node 1, as its hydrate composition decreases in N₂ concentration. Conversely there is a net increase of hydrate in Node 2, as its hydrate composition increases in N₂ concentration. An interesting result from this simulation is the lack of equilibrium in the final hydrate saturations. The governing flow and transport equations drive components concentrations, temperature and pressure toward equilibrium conditions, however, there is not an equivalent driving force for hydrate saturation. The kinetics of the hydrate dissociation and exchange of the guest molecules was controlled by the kinetic rate constants for these processes that were specified in the input file. For this problem the value of the dissociation rate and exchange rate parameters are not critical as the principal concern is the path to equilibrium and the ultimate equilibrium point. The input file for this problem is shown below the solution figures.

Node	Initial Condition	T (°C)	s_g	s_h	ϕ_h^c	ϕ_h^m	ϕ_h^n	P_{eq} (MPa)
1	#5	4.0	0.25	0.25	0.50	0.0	0.5	29.946
2	#5	4.0	0.25	0.50	0.40	0.0	0.6	13.900

Table 6. Initial Conditions for the Transition to Equilibrium from Hydrate and Mobile Phase Equilibria: TTE4

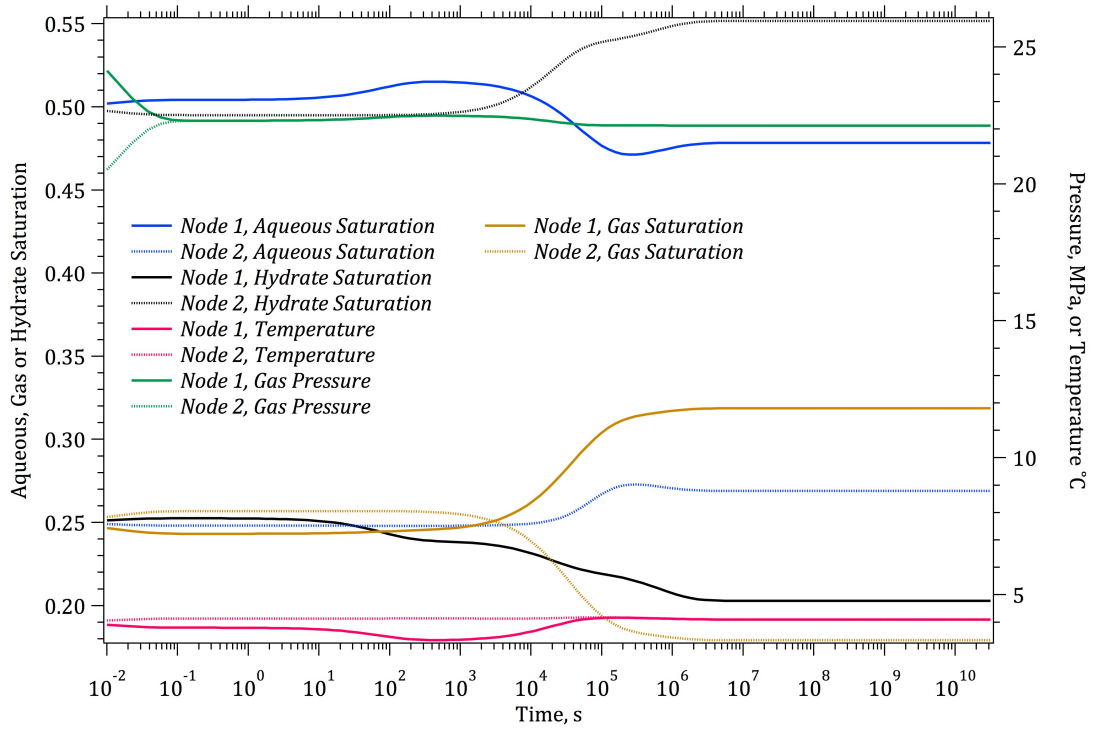


Figure 15. Transition to Equilibrium (TTE3) for Aqueous Saturation, Hydrate Saturation, Gas Saturation, Temperature, and Gas Pressure

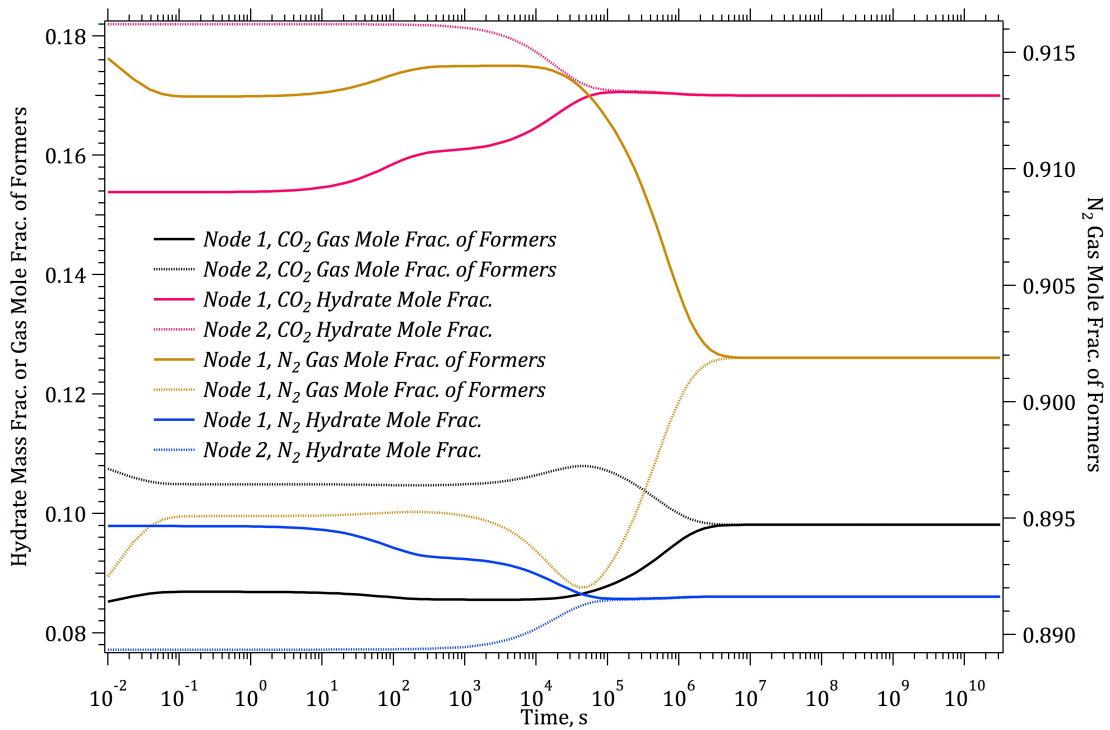


Figure 16. Transition to Equilibrium (TTE3) for Hydrate Mass Fractions and Gas Mole Fraction of Formers

Input File for Transition to Equilibrium without Hydrates: TTE4

~Simulation Title Card

1,
Verification TTE4,
Mark White,
Pacific Northwest National Laboratory,
09 November 2012,
13:59 PST,
6,
2-node transition to equilibrium with hydrates
iso-CH4 conditions
initial hydrate and mobile phases in equilibrium
initial gradient in hydrate composition of formers
initial gradient in hydrate saturation
initial constant temperature

~Solution Control Card

Normal,
HYDT-KE w/NaCl w/Isobrine,
#HYDT-KE w/NaCl w/Isobrine w/Iso-CH4,
1,
0,yr,1000,yr,0.01,sec,1000,yr,1.25,16,1.e-06,
1000,
Variable Aqueous Diffusion,
Variable Gas Diffusion,
Variable Nonaqueous Liquid Diffusion,
#exchange,formation,dissociation,
8.e-6,kmol/s m³,1.e-2,kmol/s m³,1.e-2,kmol/s m³,2.5,
0,

~Grid Card

Cartesian,
2,1,1,
0,cm,2@10,cm,
0,cm,10,cm,
0,cm,10,cm,

~Rock/Soil Zonation Card

1,
Core,1,2,1,1,1,1,

~Mechanical Properties Card

Core,2.60,g/cm³,0.22,0.22,compressibility,6.25e-10,1/Pa,,,Millington and Quirk,,,

~Hydraulic Properties Card

Core,0.5,darcy,0.5,darcy,0.5,darcy,

~Saturation Function Card

72.0,dynes/cm,24.0,dynes/cm,,,26.7,dynes/cm,
Core,van Genuchten w/Webb,2.04,1/m,2.857,0.1,,72.0,dynes/cm,0.1,

~Aqueous Relative Permeability Card

Core,Mualem,,

~Gas Relative Permeability Card

Core,Mualem,,

~Nonaqueous Liquid Relative Permeability Card

Core,Mualem,,

~Thermal Properties Card

Core,Parallel,2.86,W/m K,2.86,W/m K,2.86,W/m K,700,J/kg K,

~Salt Transport Card
Core,0.0,ft,0.0,ft,

~Initial Conditions Card

12,
#IC5 (sh > 0, sn = 0, sg > 0, equilibrium)
Temperature,4.0,C,,,,,,,,1,1,1,1,1,1,
Gas Saturation,0.25,,,,,,,,1,1,1,1,1,1,
Hydrate Saturation,0.25,,,,,,,,1,1,1,1,1,1,
Hydrate CH4 Mole Fraction of Formers,0.0,,,,,,,,1,1,1,1,1,1,
Hydrate N2 Mole Fraction of Formers,0.5,,,,,,,,1,1,1,1,1,1,
IC5,1,1,1,1,1,1,
#IC5 (sh > 0, sn = 0, sg > 0, equilibrium)
Temperature,4.0,C,,,,,,,,2,2,1,1,1,1,
Gas Saturation,0.25,,,,,,,,2,2,1,1,1,1,
Hydrate Saturation,0.5,,,,,,,,2,2,1,1,1,1,
Hydrate CH4 Mole Fraction of Formers,0.0,,,,,,,,2,2,1,1,1,1,
Hydrate N2 Mole Fraction of Formers,0.4,,,,,,,,2,2,1,1,1,1,
IC5,2,2,1,1,1,1,

~Output Control Card

2,
1,1,1,
2,1,1,
1,1,s,m,6,6,6,
16,
Phase Condition,,
Gas Pressure,MPa,
Aqueous Pressure,MPa,
Gas CO2 Mole Fraction of Formers,,
Gas CH4 Mole Fraction of Formers,,
Gas N2 Mole Fraction of Formers,,
Temperature,c,
Aqueous Saturation,,
Gas Saturation,,
Hydrate Saturation,,
Hydrate CO2 Mass Fraction,,
Hydrate CH4 Mass Fraction,,
Hydrate N2 Mass Fraction,,
CO2 Gas Mass Fraction,,
CH4 Gas Mass Fraction,,
Integrated CO2 Mass,kg,
0,
15,
Gas Pressure,MPa,
Aqueous Pressure,MPa,
Temperature,c,
Aqueous Saturation,,
Nonaqueous Liquid Saturation,,
Gas Saturation,,
Hydrate Saturation,,
Hydrate CO2 Mass Fraction,,
Hydrate CH4 Mass Fraction,,
CO2 Aqueous Mass Fraction,,
CH4 Aqueous Mass Fraction,,
CO2 Nonaqueous Liquid Mass Fraction,,
CH4 Nonaqueous Liquid Mass Fraction,,
CO2 Gas Mass Fraction,,
CH4 Gas Mass Fraction,,

3.2 Benchmark Problems

3.2.1 Mixed CO₂ and N₂ Gas Flow through a CH₄ Hydrate Bearing Column

This problem considers the flow of a 1:1 mole fraction ratio of CO₂:N₂ gas into a 1-m horizontal column containing a CH₄-hydrate bearing sediment. The column was discretized into 100 nodes, each 1 cm in length. The column was assumed to have uniform initial conditions, as shown in Table 7. An equi-molar mixture of CO₂ and N₂ gas is injected at the inlet boundary at a volumetric flux rate of 1.69e-04 m/s. The outlet boundary is maintained at the initial pressure condition. The simulation is executed for 1 hour. Simulation results are shown as profiles across the column at selected points in time (i.e., 0 s, 10 s, 50 s, 100 s, 500 s, 1000 s, and 3600 s). Hydrate saturation profiles are shown in Figure 17. With N₂ in the influent mixture, hydrate saturations across the column remain at or below the initial level of 0.5, except for late in the simulation when secondary hydrate forms near the inlet. Hydrate composition profiles in terms of mass fractions are shown in Figures 18 through 20 for CO₂, CH₄, and N₂, respectively. Initially the column is filled with pure CH₄ hydrate, yielding an initial CH₄ mass fraction of hydrate of 0.129 and an initial water mass fraction of hydrate of 0.871. Over time the CO₂ and N₂ exchange with the CH₄ in the hydrate yielding the CH₄ profiles shown in Figure 19. At the end of the simulation the CO₂ and N₂ hydrate mass fractions are 0.237 and 0.026, respectively, indicating that the hydrate is predominately comprised of CO₂ as the guest molecule.

The simulation uses a Neumann boundary condition (i.e., flux) for the gas inlet and a Dirichlet boundary condition (i.e., gas pressure) for the gas outlet boundary. Closed boundaries are specified for the aqueous phase, and the constant temperatures of 4°C at the inlet and outlet boundaries are specified. Aqueous saturations respond to the dissociation/formation of hydrate, as shown in Figure 21; where at the end of the simulation aqueous saturations are low at the inlet and high at the outlet. Gas saturations remain fairly constant through the simulation, as shown in Figure 22. The fixed temperature on the outlet allows for heat transfer back into the column, as shown in Figure 23, resulting hydrate dissociation as the hydrate composition changes from pure CH₄ to a CH₄-CO₂-N₂ mixed hydrate. An alternative approach to this simulation would be to impose an outflow type boundary for energy at the outlet, which would allow the outlet temperature to float.

Nodes	Initial Condition	T (°C)	s_g	s_h	ϕ_h^c	ϕ_h^m	ϕ_h^n	P_{eq} (MPa)
1-100	#5	4.0	0.25	0.5	0.0	0.0	1.0	3.841

Table 7. Initial Conditions for the Mixed CO₂ and N₂ Gas Flow through a CH₄ Hydrate Bearing Column Problem

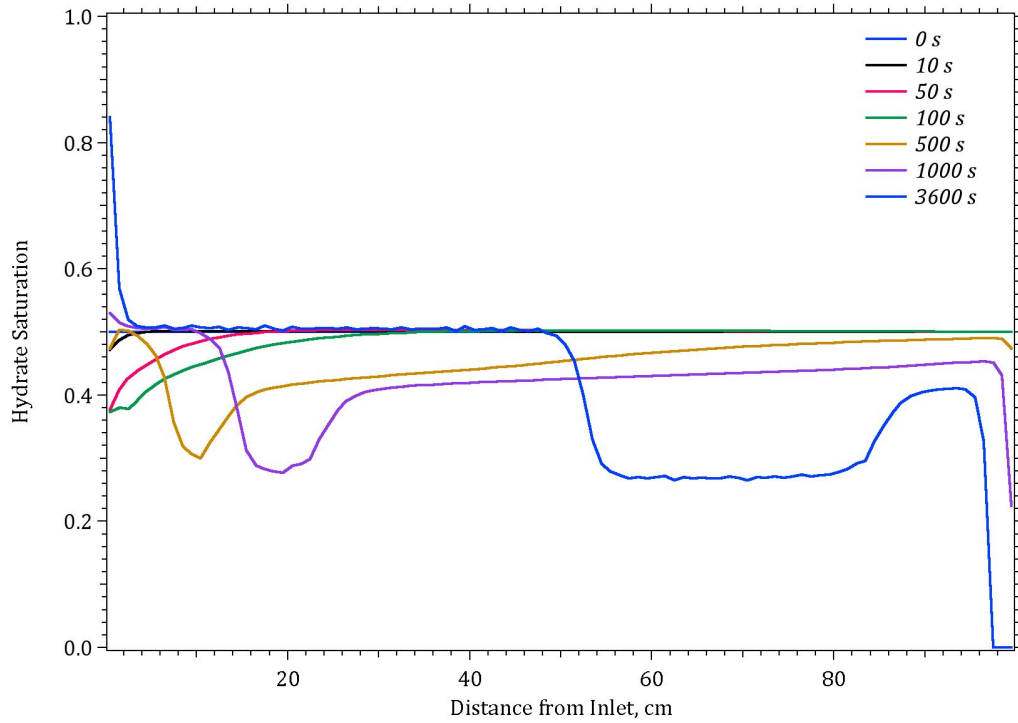


Figure 17. Profiles of Hydrate Saturation at 0, 10, 50, 100, 500, 1000, and 3600 s.

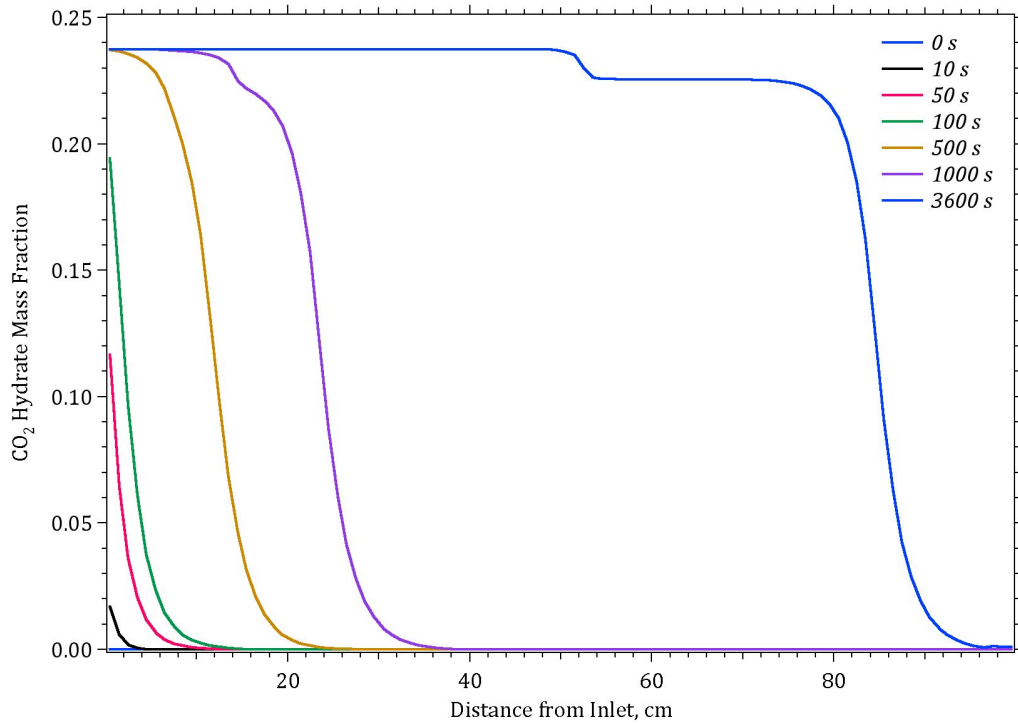


Figure 18. Profiles of CO₂ Hydrate Mass Fraction at 0, 10, 50, 100, 500, 1000, and 3600 s.

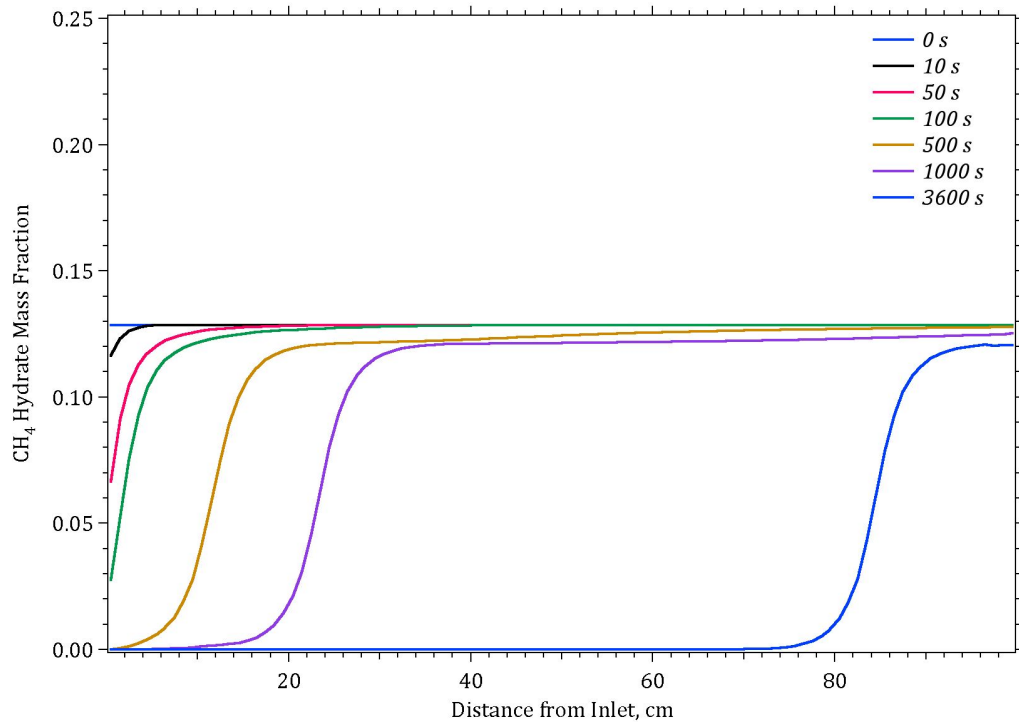


Figure 19. Profiles of CH₄ Hydrate Mass Fraction at 0, 10, 50, 100, 500, 1000, and 3600 s.

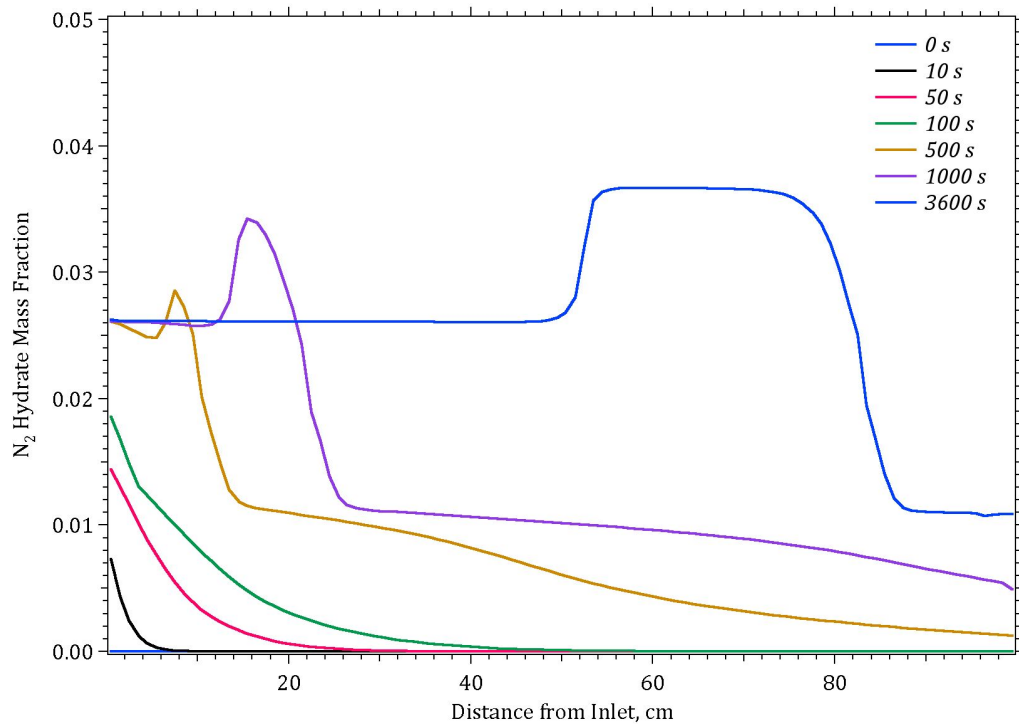


Figure 20. Profiles of N₂ Hydrate Mass Fraction at 0, 10, 50, 100, 500, 1000, and 3600 s.

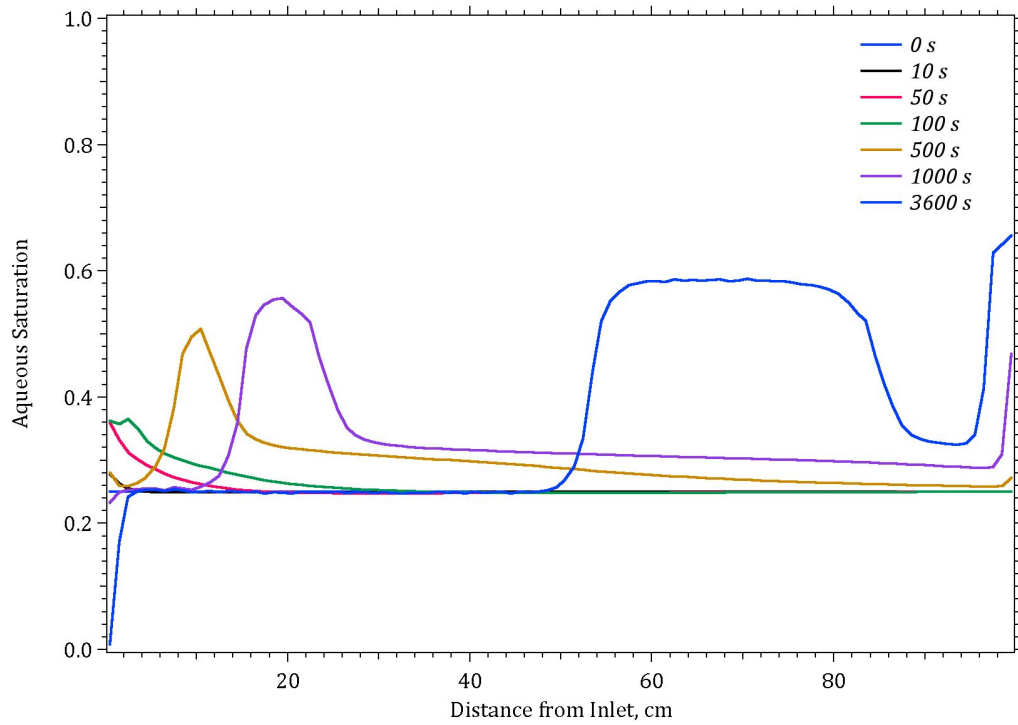


Figure 21. Profiles of Aqueous Saturation at 0, 10, 50, 100, 500, 1000, and 3600 s.

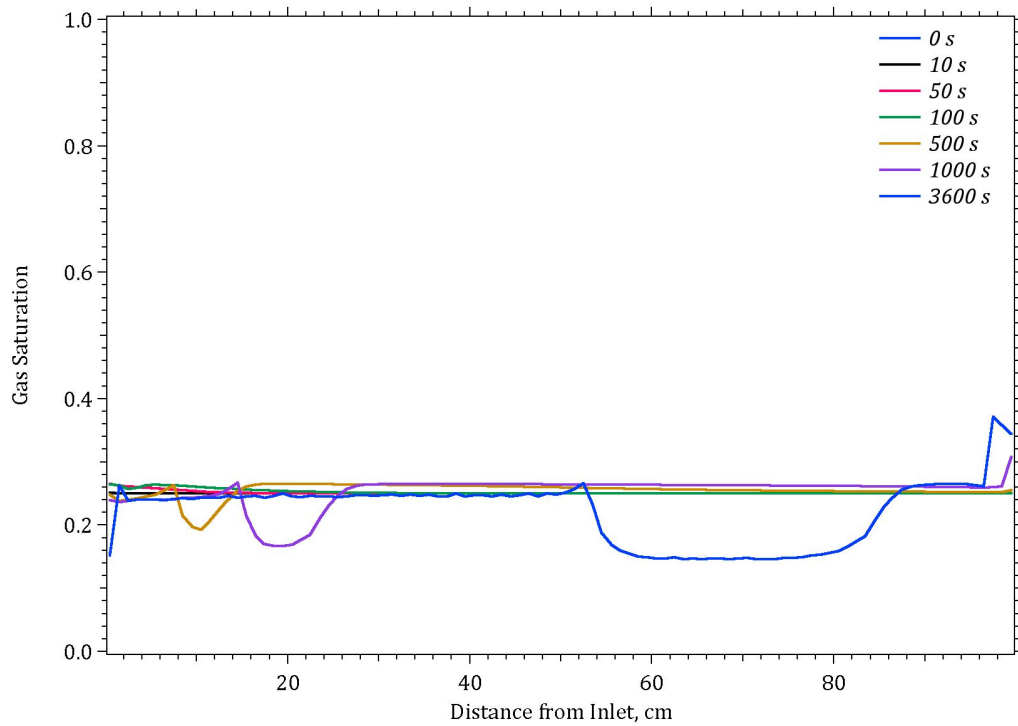


Figure 22. Profiles of Gas Saturation at 0, 10, 50, 100, 500, 1000, and 3600 s.

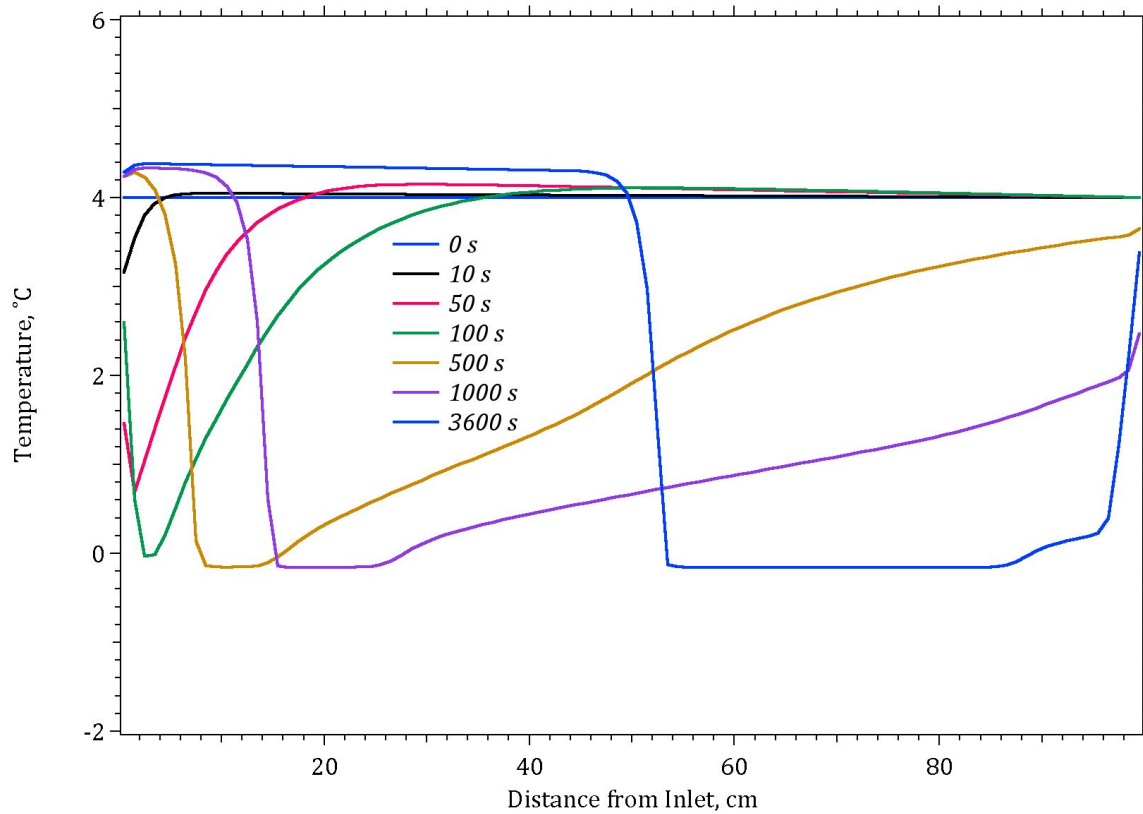


Figure 23. Profiles of Temperature at 0, 10, 50, 100, 500, 1000, and 3600 s.

3.3 Validation Problems

3.3.1 KIGAM 2006 Experiment

A series of experiments were conducted on a vertical soil column that involved the creation of methane hydrates, the exchange of nitrogen and carbon dioxide as hydrate guest molecules and then the dissociation of mixed hydrates. All experiments were conducted at KIGAM in Daejeon, Korea, using the experimental apparatus shown in Figure 24. Whereas the exchange components of the experiments are the central focus of these numerical investigations, all stages of the conducted experiments were used to derive need numerical simulation parameters: 1) soil packing, 2) water flooding, 3) gas flooding, 4) methane hydrate formation, 5) exchange pressurization, 6) exchange processes, and 7) hydrate dissociation.

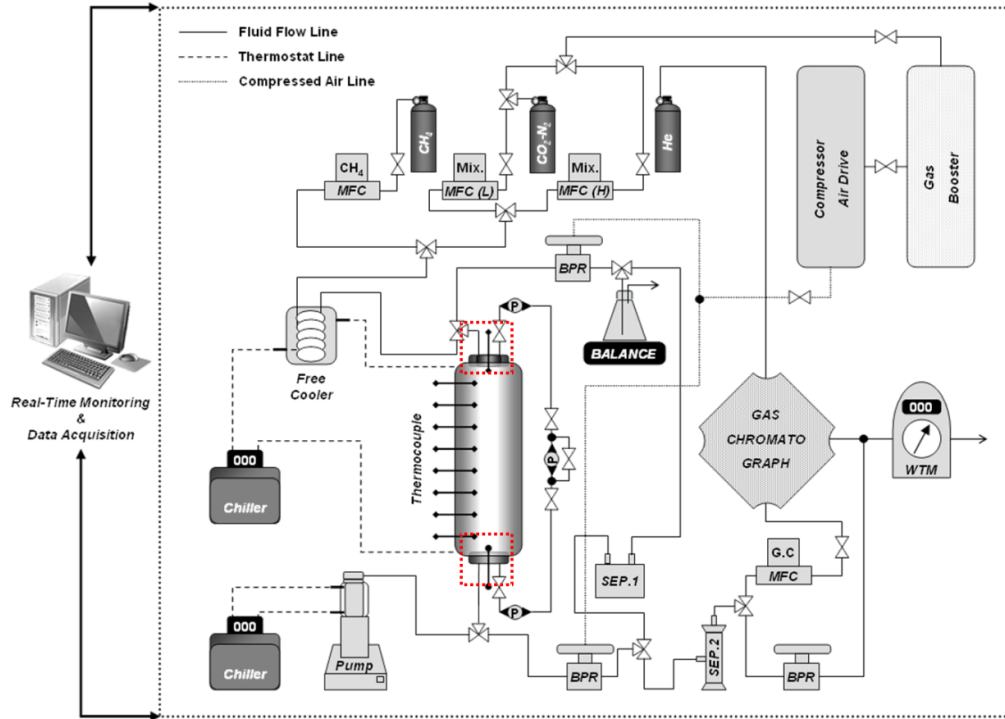


Figure 24. Experimental Apparatus

The KIGAM experiments were conducted using a vertical cylindrical column, packed with a quartz sediment. The cylinder dimensions and computed volume are shown in Table 9. The soil volume was computed from its weight and grain density; and the soil bulk density was computed from the soil weight and cylinder volume, as shown in Table 9. The soil porosity was determined from the net mass of water injected to create saturated conditions and the density of water at experimental conditions (i.e., 19.6°C, 1 atm). Water injection experiments were additionally used to determine the soil intrinsic permeability, as shown in Table 9. The percent silt- and sand-sized particles were determined from the soil grain size distribution, shown in Figure 25. No clay-sized particles were indicated by the grain size distribution data. The clay-sized percent, shown in Table 9, was computed as a fitting parameter for the pedotransfer function for porosity, as described in the Simulation Parameters section.

The STOMP-HYDT-KE simulator requires functions that describe the relationships between capillary pressure and saturation (e.g., van Genuchten (1980), Brooks and Corey (1964)); and saturation and relative permeability. Parameters (i.e., soil hydraulic characteristics) needed for these functions were not measured directly during the experiment. Pedotransfer functions of Wösten et al. (2001) were used to compute the needed soil hydraulic characteristics from the available soil data, which included the bulk density, porosity, and grain-size distributions. Four pedotransfer functions were used to estimate the soil hydraulic characteristics. The pedotransfer function for porosity was first used in an inverse manner to derive a fitted clay percent:

$$\begin{aligned} \phi = & 0.7919 + 0.001691 \text{ clay} - 0.0001664 \text{ silt} - 0.29619 \rho_b - 0.000001491 \text{ silt}^2 \\ & + \frac{0.02427}{\text{clay}} + \frac{0.01113}{\text{silt}} + 0.01472 \ln(\text{silt}) - 0.000619 \rho_b \text{ clay} \end{aligned} \quad (17)$$

Cylinder Inner Diameter	5.5 cm
Cylinder Length	46.0 cm
Cylinder Volume	1092.9 cm ³
Soil Weight	1898.6 g
Soil Grain Density	2.633 gm/cm ³
Soil Volume	721.1 cm ³
Saturated Water Weight	364.76 g
Soil Bulk Density	1.737 gm/cm ³
Water Density	0.9976 gm/cm ³
Saturated Water Volume	365.64 cm ³
Soil Porosity	0.3346
Intrinsic Permeability	202 mD
% Clay (<2 μ m) (computed from Eqn. 18)	1.65%
% Silt (2-50 μ m)	21.79%
% Sand (50-200 μ m)	70.58%

Table 8. Experimental Apparatus and Petrophysical Properties

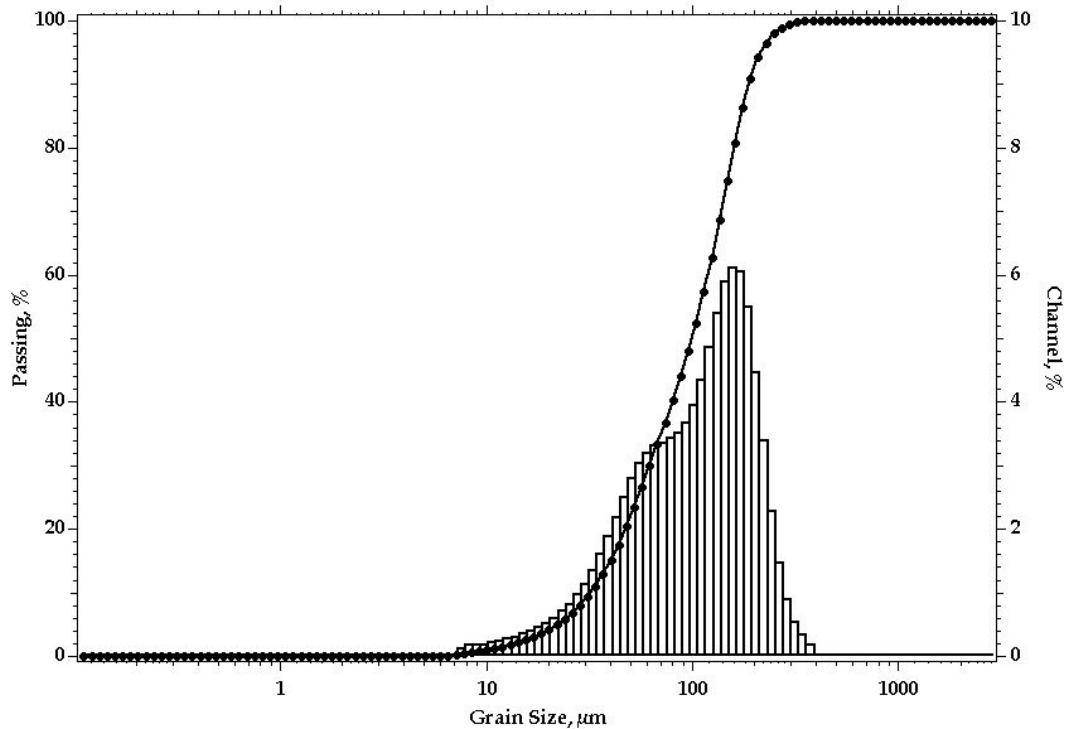


Figure 25. Soil Grain Size Distribution

With a value of 1.65% for percent clay the van Genuchten α parameter was determined from the Wösten (2001) pedotransfer function:

$$\alpha = \exp \left[\begin{array}{l} -14.96 + 0.03808 \text{ clay} + 0.0351 \text{ silt} + 15.29 \rho_b - 0.192 - 4.671 \rho_b^2 \\ -0.000781 \text{ clay}^2 + 0.0663 \ln(\text{silt}) - 0.04546 \rho_b \text{ silt} \end{array} \right] \quad (18)$$

and the van Genuchten n parameters was determined from the Wösten (2001) pedotransfer function:

$$n = -25.23 - 0.02913 \text{ clay} + 0.0074 \text{ silt} + 45.5 \rho_b - 7.24 \rho_b^2 + 0.0003658 \text{ clay}^2 - \frac{12.81}{\rho_b} - \frac{0.1524}{\text{silt}} - 0.2876 \ln(\text{silt}) - 44.6 \ln(\rho_b) - 0.02264 \rho_b \text{ clay} \quad (19)$$

As a check the Wösten (2001) pedotransfer function for saturated hydraulic conductivity was computed:

$$K_{sat} = 8.685 + 0.06825 \text{ silt} + 0.2986 \text{ clay} - 0.967 \rho_b^2 - 0.000484 \text{ clay}^2 - 0.000322 \text{ silt}^2 + \frac{0.001}{\text{silt}} - 0.643 \ln(\text{silt}) - 0.01398 \rho_b \text{ clay} \quad (20)$$

which is equivalent to an intrinsic permeability of 50.4 mD; a reasonable comparison to the measured value of 202 mD. The resulting hydraulic characteristics are summarized in Table 9. A critical missing component of the hydraulic characteristics are the functions and parameters that describe the relationships between phase saturation and phase relative permeability. The STOMP-HYDT-KE offers several options for declaring these functions. The water flood experiments were used to establish the intrinsic permeability of the experimental soil, and the gas-flood experiments were used to establish functions and parameters for aqueous and gas relative permeability.

Porosity	0.3346
% Clay (<2 μ m) (computed from Eqn. 18)	1.65%
van Genuchten a	0.0341 1/cm
van Genuchten n	1.422
van Genuchten/Mualem m	0.2968
PTF Intrinsic Permeability	50.4 mD
Experimental Intrinsic Permeability	202 mD

Table 9. Soil Hydraulic Characteristics

3.3.1.1 Gas Flooding

The gas-flooding stage involved injecting water-saturated methane gas into the experimental soil column, which was initially saturated with water. Methane gas was injected into the top of the column at 11 °C. The total produced water reported in the experiment was 226.4 g, from the initial water mass of 364.8 g, yielding an average water saturation of 0.386. In addition to this observation, the maximum gas flow rate measured was 1600 scfm (1.1456 g/min). To model this stage of the experiment the experimental column was discretized into 100 nodes with a uniform vertical spacing of 0.46 cm. A system pressure of 0 psig was assumed. No injection pressures were reported for this stage of the experiment. Two approaches were taken to model the gas flooding stage: 1) constant pressure injection and 2) constant rate injection. For the

constant pressure simulations there were two experimental observations that were used to develop models for the gas and aqueous relative permeability functions: 1) the total produced water and 2) the maximum gas flow rate. The constant pressure simulations were conducted using an inlet pressure of 42.05 psia (0.289 MPa) and an outlet pressure of 14.7 psia (0.101 MPa).

As an initial attempt the Mualem aqueous and gas relative permeability functions were applied to this problem:

$$k_{rl} = (\bar{s}_l)^{1/2} \left(1 - \left(1 - (\bar{s}_l)^{1/m} \right)^m \right)^2; \bar{s}_l = \frac{s_l - s_{lr}}{1 - s_{lr}} \quad (22)$$

$$k_{rg} = (\bar{s}_g)^{1/2} \left(1 - \left(\bar{s}_t \right)^{1/m} \right)^2; \bar{s}_g = \frac{s_{lr}}{1 - s_{lr}}; \bar{s}_t = \frac{s_t - s_{lr}}{1 - s_{lr}} \quad (23)$$

This yielded a total produced water amount substantially lower than the experimental observation. This indicates that the Mualem relative permeability functions yield phase relative permeabilities that are too low. In the second attempt the Mualem functions were replaced with the modified Corey functions:

$$k_{rl} = a_l (\bar{s}_l)^{b_l}; \bar{s}_l = \frac{s_l - s_{lr}}{1 - s_{lr}} \quad (24)$$

$$k_{rg} = a_g (\bar{s}_g)^{b_g}; \bar{s}_g = \frac{s_g - s_{gr}}{1 - s_{lr}} \quad (25)$$

After several iterations with the constant pressure simulations it was determined that using $a_l = 1.0$, $b_l = 3.0$, $s_{lr} = 0.3$, $a_g = 1.0$, $b_g = 3.0$, and $s_{gr} = 0.3$, yielded a produced water amount of 226.2 g, roughly equivalent to that observed in the experiment. To check the sensitivity of the results to whether the simulation was executed in a constant pressure or constant flow rate mode, the simulation was repeated using a constant injection flow rate. To avoid over pressurizing the column a flow rate of 160 sccm was used until gas reached the bottom of the column and then the flow rate was increased to 1600 sccm. Both the constant pressure and constant flow rate simulations were executed for 1000 min. Plots of produced water for both simulations are shown in Figure 26. This plot shows the produced water observation is somewhat insensitive to the simulation scenario. Plots of the CH₄ mass flow rate leaving the column bottom are shown in Figure 27. The two injection scenarios represent the bounding limits for matching the reported observation of a maximum gas flow rate of 1600 sccm. In the constant-pressure scenario the maximum gas flow rate occurs at the end of the simulation, with decreasing aqueous saturation and increasing gas relative permeability. As dry CH₄ is injected reductions in aqueous saturation later in the simulation period are due to water carried out in the gas phase. In the constant injection rate scenario the gas rate is fixed at the maximum after gas breakthrough occurs. The pressure and aqueous saturation profiles at the end of the two gas-flood simulations are shown in Figure 28. These plots demonstrate the similarity in the two bounding scenarios at the end of the simulation. The steep transition in the aqueous saturation curve is due to the high exponent in the relative permeability functions. The gas-flood experiments provide one set of relative permeability parameters that fit the observations, but are not unique. Additional experimental data are needed to complete the parameterization of these functions.

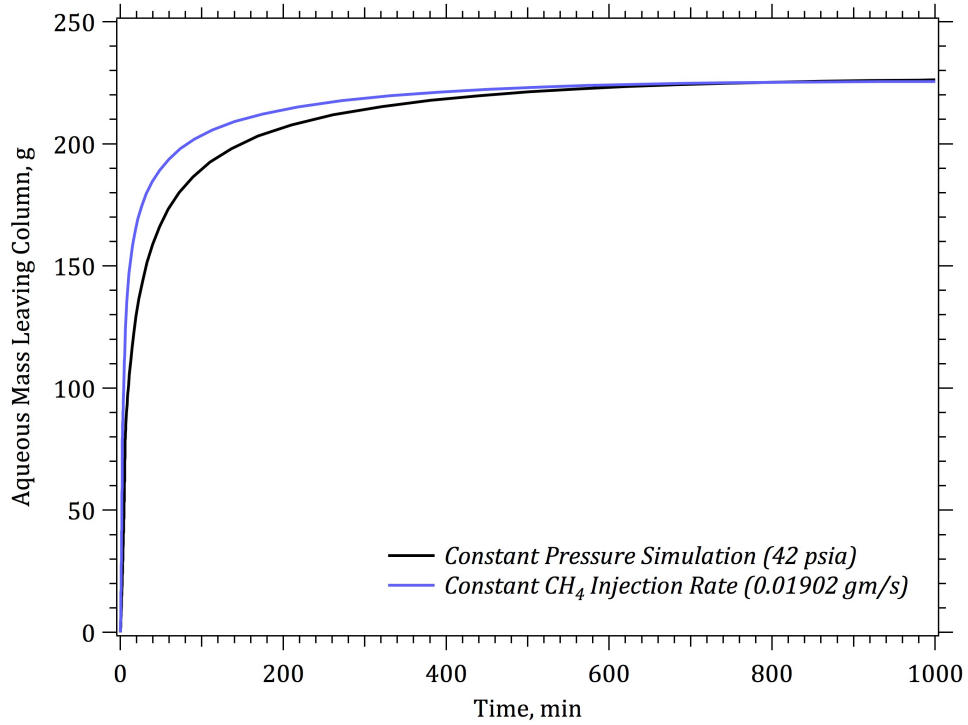


Figure 26. Drained Water Mass versus Time during the Gas Flooding Simulation for the Constant Pressure and Constant Flow Rate Scenarios

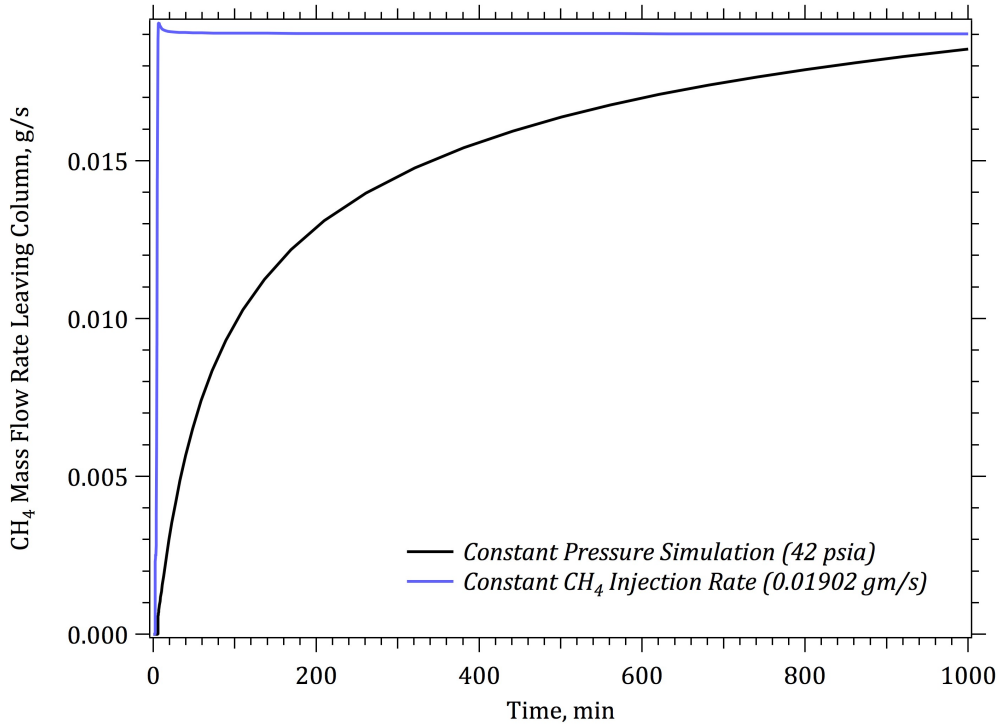


Figure 27. Gas Mass Flow Rate versus Time during the Gas Flooding Simulation for the Constant Pressure and Constant Flow Rate Scenarios

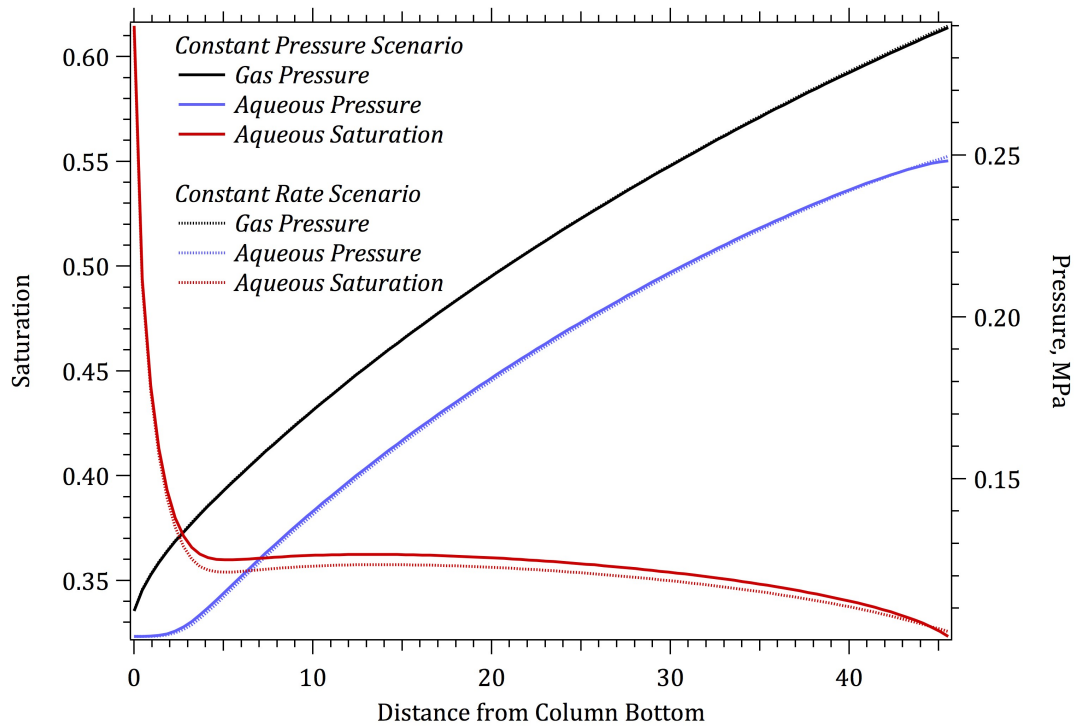


Figure 28. Pressure and Saturation Profiles versus Column Height at the End of the Gas Flooding Simulation for the Constant Pressure and Constant Flow Rate Scenarios

3.3.1.2 Hydrate Formation

The hydrate-formation stage of the experiment was numerically modeled using five simulations: 1) first pressurization and methane injection, 2) first sealed temperature reduction, 3) second pressurization and methane injection, 4) second sealed temperature reduction, and 5) third pressurization and methane injection. During the first pressurization and methane injection, methane was injected at the top of the column at a constant rate of 0.025 g/s for 600 s for a total injection of 14.962 gm (20896.42 scc). The pressure increase during this injection period was below the hydrate stability pressure at 11 °C, thus no hydrate was formed. The distribution of temperature, gas pressure and aqueous pressure at the end of the 600-s injection period is shown in Figure 36. The second simulation of the hydrate formation stage involved numerically modeling a sealed column and reducing the water jacket temperature to 1 °C. This was simulated with constant temperature and no-flow boundary conditions around the computational domain, using the final state of the first pressurization simulation for initial conditions. The constant-temperature boundary condition simulated the water jacket and the no-flow boundary conditions simulated the sealed column. A simulation period of 12 hr was selected. As the simulation progresses the temperature drops in the column, reducing the equilibrium pressure of the hydrate and increasing the hydrate formation driving force and rate. The rate of hydrate formation is controlled by the hydrate formation rate constant, which was set to 1.e-2 kmol/s, with an aqueous saturation exponent of 2.5. As hydrate forms, methane is consumed from the gas phase, lowering the gas phase pressure until the gas phase is in equilibrium with the hydrate at 1 °C at 2.88 MPa (403 psig). The temperature response leads that of pressure as shown in Figure 37, with the rate of pressure decay being a function of the hydrate formation rate, as shown in Figure 38. Hydrate formation consumes water from the aqueous phase and CH₄ from the gas phase. At the end of the simulation 10.45 gm of the 14.962 gm of total CH₄ have been incorporated into hydrate, as shown in Figure 39, requiring 71.38 gm of the 130.19 gm of total water. The hydration number for the resulting hydrate is 6.083, which indicates not all of the SI cages are occupied, compared with the ideal hydration number of 5.75 for the sI structure.

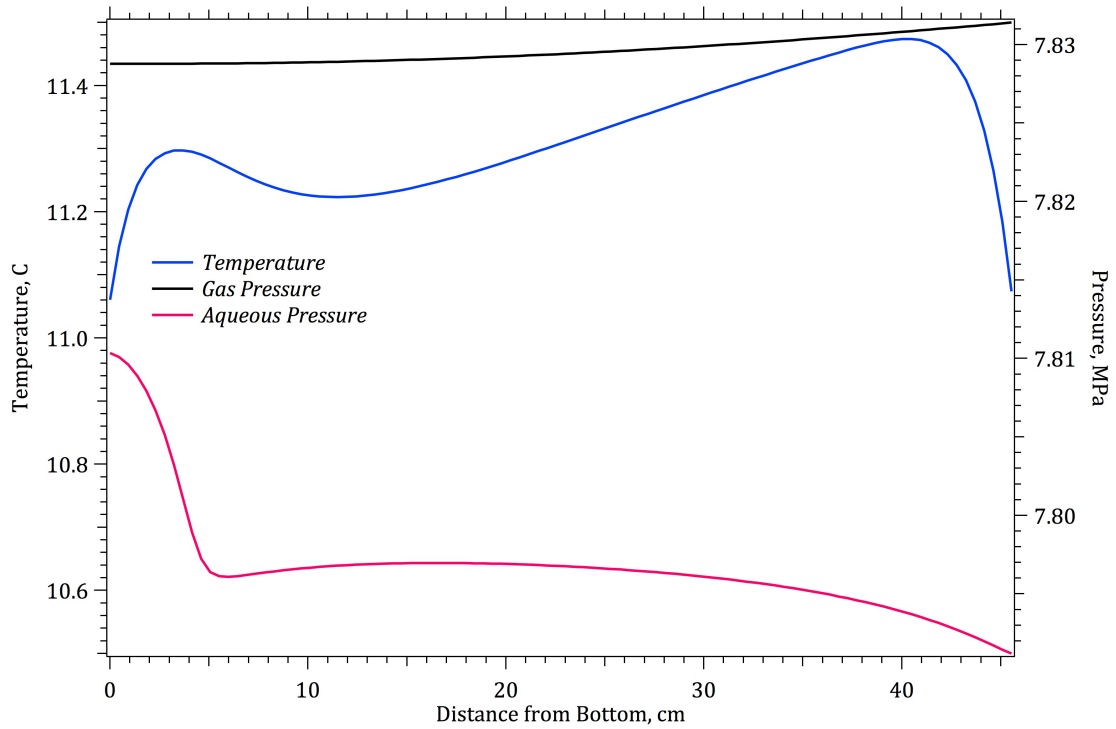


Figure 29. Temperature and Pressure Profiles versus Column Height at the End of the First Pressurization Simulation of the Hydrate Formation Stage

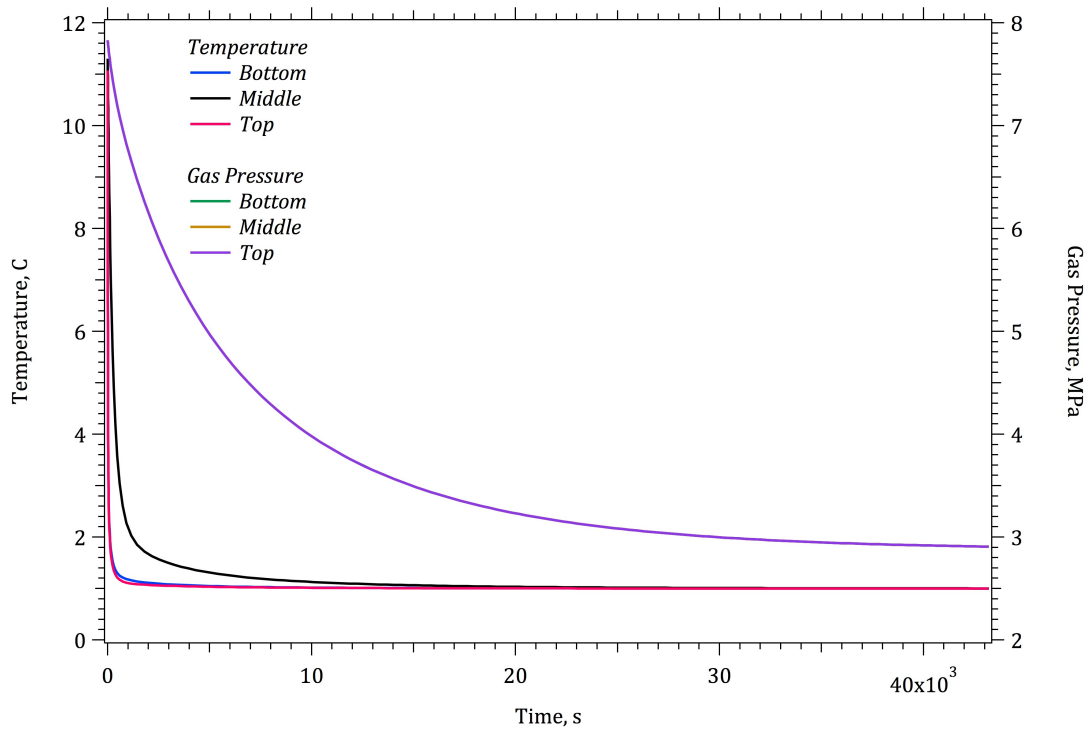


Figure 30. Temperature and Pressure versus Time during the Temperature Reduction to 1°C Simulation of the Hydrate Formation Stage

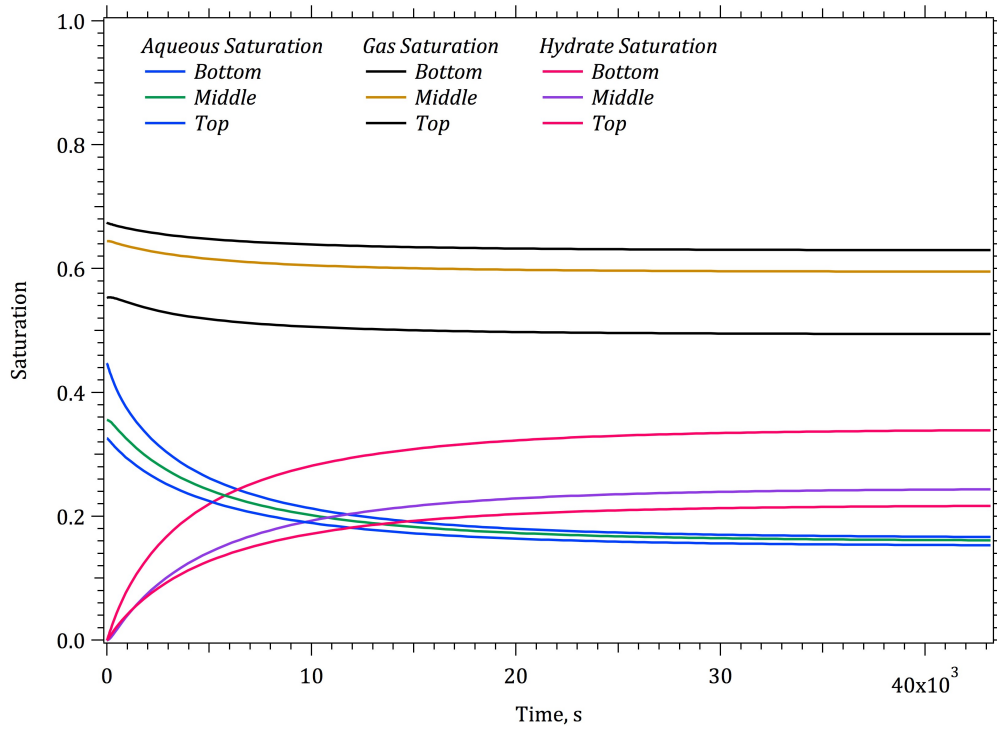


Figure 31. Aqueous, Gas, and Hydrate Saturation versus Time during the Temperature Reduction to 1°C Simulation of the Hydrate Formation Stage

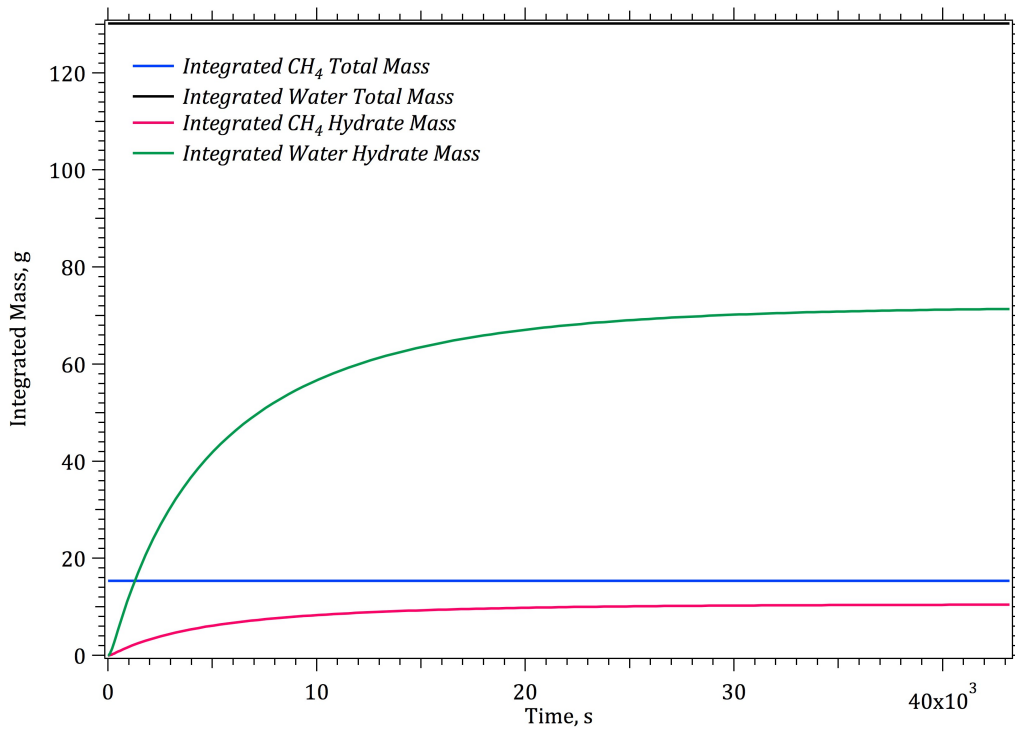


Figure 32. Integrated CH₄ and Water Mass versus Time during the Temperature Reduction to 1°C Simulation of the Hydrate Formation Stage

The third simulation of the hydrate formation stage involved a second pressurization and injection of CH₄. This simulation started with the final conditions from the first sealed temperature reduction simulation as the initial conditions. Methane was injected at the top of the column at 1 °C and a constant rate of 0.025 g/s for 600 s for a total injection of 16.647 gm (23250.47 scc). The lateral and column bottom boundaries were assigned to be constant temperature (1 °C) and closed to fluid flow. Unlike the first pressurization and injection stage, the conditions inside the column are within the hydrate stability region for pure CH₄ hydrate, which leads to a slight production of hydrate during the injection. Compression of the gases during the injection yields small increases in temperature, with the greatest increases being at the middle of the column due to the reduced area for heat transfer compared with the column ends. Temperatures are reduced to 1 °C via a second sealed temperature reduction simulation, which comprises the fourth simulation. The final simulation of the hydrate formation stage involves pressurizing the column to 1400 psig (9.754 MPa). In the experiment it was reported that 11,727 scc (8.397 g) were injected during this pressurization stage. Only 3,102 scc (2.221 g) of CH₄ were computed via the numerical simulation to be injected during the final pressurization stage. The overall CH₄ mass injected during the experiment was 55,873.95 scc (40.0 g), compared with 48,000 scc (34.37 g) from the numerical simulation.

3.3.1.3 Swapping Production

The swapping-production stage of the experiment involved injecting a 8:2 by volume mixture of CO₂:N₂ at a constant flow rate of 480 scc/min over three cycles. The first cycle involved an injection period of 789.48 min. The second cycle involved a soaking time of 120 min, followed with an injection period of 45.50 min. The third cycle involved a soaking time of 120 min, followed with an injection period of 33.13 min. The density of CO₂ at standard conditions is 1.977 kg/m³ and the density of N₂ at standard conditions is 1.251 kg/m³, which equates to a mass injection rate of 0.759 g/min of CO₂ and 0.120 g/min of N₂ at the 8:2 volume mixture. Mass was injected into the upper most node in the simulation using a nonaqueous-liquid mass rate source. For this type of source, STOMP-HYDT-KE requires the user to specify the injection mass rate and component mole fractions. When converted the mass injection rate was 0.879 g/min at 1.0 C, the CO₂ mole fraction was 0.801 and the N₂ mole fraction was 0.199. Neither water nor CH₄ were injected. The swapping-production stage was simulated with three simulations, one for each cycle. The restart file from the final hydrate formation simulation was used to initialize the simulation for the first cycle. The restart file from the first cycle was used to initialize the second cycle, and similarly for the initialization of the third cycle. The bottom boundary was set to 1 °C and a pressure of 9.754 MPa (1414.7 psia) for both the aqueous and nonaqueous phases. Fluid flow was only allowed to occur out the bottom boundary and diffusion across the bottom boundary was ignored. The side and top boundaries were assumed to be closed to fluid flow, and were maintained at 1 °C. At a pressure of 9.754 MPa (1414.7 psia) and a temperature of 1 °C, and molar ratio of 0.801:0.199 of CO₂:N₂ the injectant is a gas-liquid mixture, in a volumetric ratio of 0.432:0.568 of gas:nonaqueous liquid. The gas phase has a molar ratio of 0.660:0.340 of CO₂:N₂ and the nonaqueous liquid has a molar ratio of 0.845:0.155 of CO₂:N₂. All simulations used a hydrate formation/dissociation kinetic rate of 1.e-2 kmol/s m³, and a guest-molecule exchange kinetic rate of 8.e-6 kmol/s m³.

3.3.1.3.1 First Cycle

Experimental results from the first cycle were that 23,500.83 scc (16.82 g) of total CH₄ was produced from the column, of which 2,151.48 scc (1.54 g) was derived from hydrate. In comparison numerical simulation results from the first cycle were that 27,943 scc (20.00 g) of total CH₄ was produced from the column, of which 2,123.7 scc (1.52 g) was derived from hydrate. Details of the numerical simulation are shown in the time history plots. Initially the column is filled with primarily CH₄ gas, hydrate, and a smaller fraction of aqueous. As the CO₂-N₂ mixture enters the column the upper portion of the column transitions to being filled with hydrate, gas, nonaqueous liquid and a smaller fraction of aqueous, as shown in Figure 40. Transition to a gas-nonaqueous liquid system occurs as the composition increases in CO₂ concentration. The leading edge of this transition generally contains gas in the region above the upper phase envelope, greater than the critical temperature, but less than the cricondentherm temperature. After 140 minutes, see Figure

40, the column reaches near steady conditions, with the arrival of the nonaqueous liquid at the column bottom. The decrease in the nonaqueous liquid saturation from the top to the bottom of the column is due to the increasing CH₄ concentration in the nonaqueous fluids, being liberated from the hydrate. The distribution of the hydrate formers (i.e., CO₂, CH₄, and N₂) at three positions in the column during the simulation period are shown in the time history plots, shown in Figures 41 through 43. Initially the only hydrate former in the column is CH₄. With the injection of CO₂ and N₂ the fluid in the column transitions from gas to liquid and gas conditions. CH₄ in the gas is driven out the column, but also dissolves into the nonaqueous-liquid, which additionally migrates through the column. The concentration of formers in the hydrate is controlled by the exchange process, which is driven by higher concentrations of CO₂ and N₂ in the gas and nonaqueous-liquid. CH₄ which exchanges with CO₂ and N₂ contributes to the concentrations of CH₄ in the gas and nonaqueous-liquid. In the gas-liquid regions of the column; CO₂ and CH₄ have higher concentrations in the nonaqueous-liquid than gas, and N₂ the opposite. The hydrate sees a net increase due to the shift in hydrate equilibria as the hydrate transitions from a pure CH₄ hydrate to a hydrate of mixed formers. At the end of the simulation the CH₄ mass fraction of formers in the hydrate is 0.68 and the CO₂:N₂ ratio in the hydrate is 4.66:1.

Change in the total mass (differential total mass) of hydrate formers within the column and change in the hydrate mass (differential hydrate mass) of hydrate formers within the column is shown in Figure 44. The differential total masses of hydrate formers reach a plateau once the initial CH₄ in the gas exits the column, at about 140 min. After that time, only slight increases in CO₂ and N₂ and slight decreases in CH₄ occur. These slight differences are due to the kinetically controlled exchange of hydrate formers between the mobile and hydrate phases, as more clearly indicated in the plots of differential hydrate mass. The plots of differential

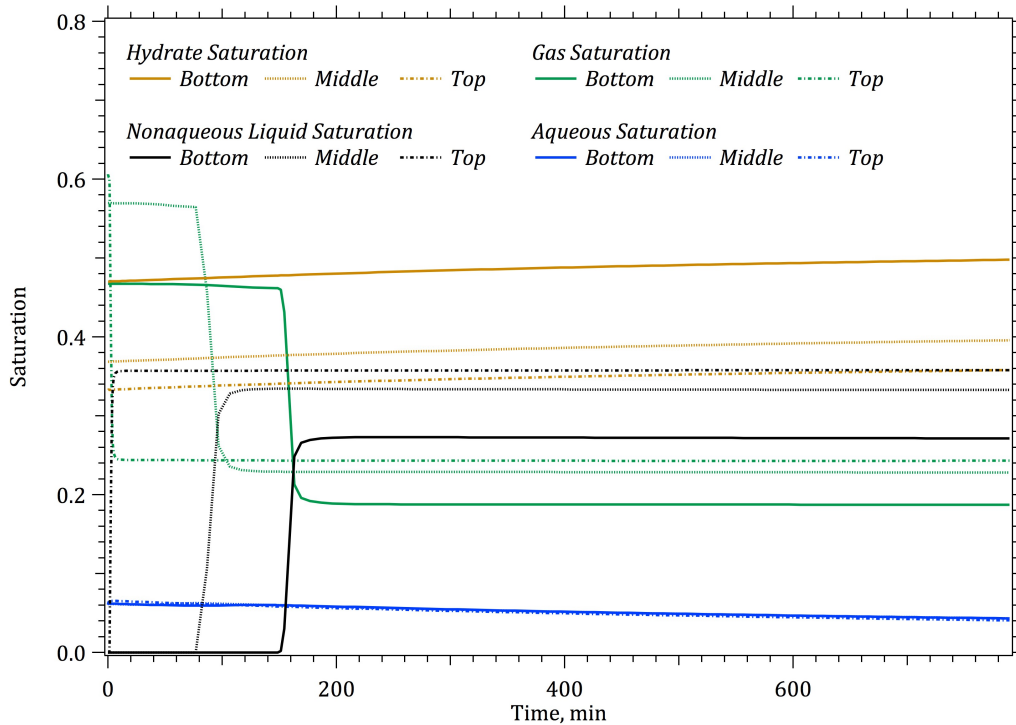


Figure 33. Hydrate, Gas, Nonaqueous-Liquid, and Aqueous Saturation versus Time at the Column Top, Middle and Bottom for Cycle 1 of the Swapping at Constant Flow Rate Simulation

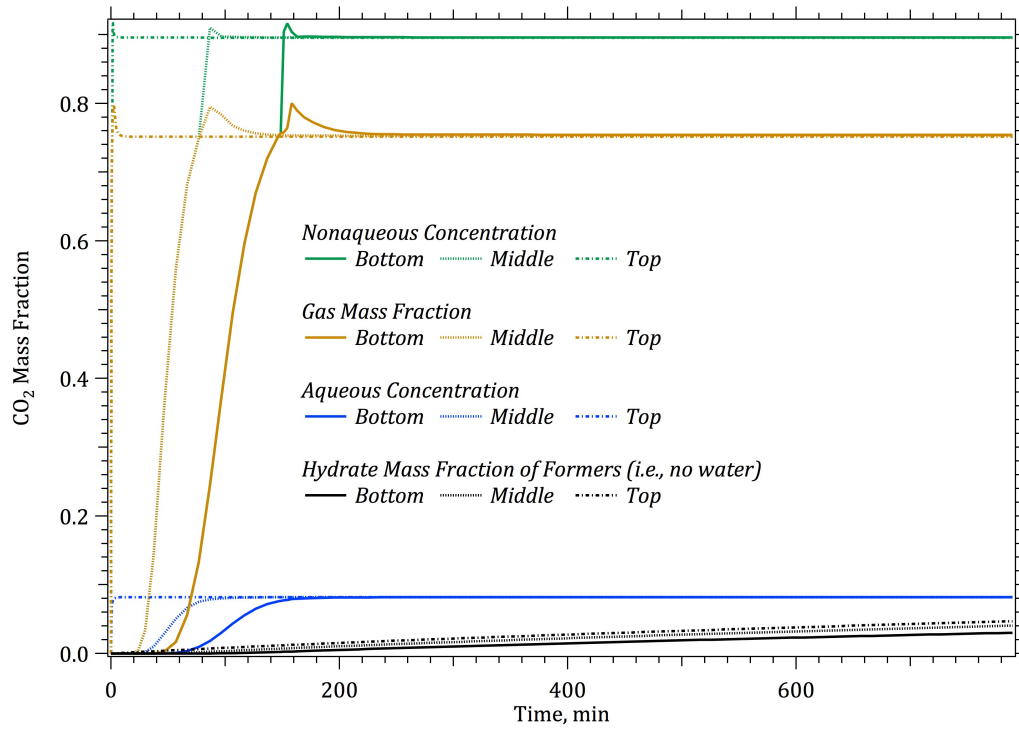


Figure 34. CO₂ Mass Fraction in Hydrate, Gas, Nonaqueous-Liquid and Aqueous versus Time at the Column Top, Middle and Bottom for Cycle 1 of the Swapping at Constant Flow Rate Simulation

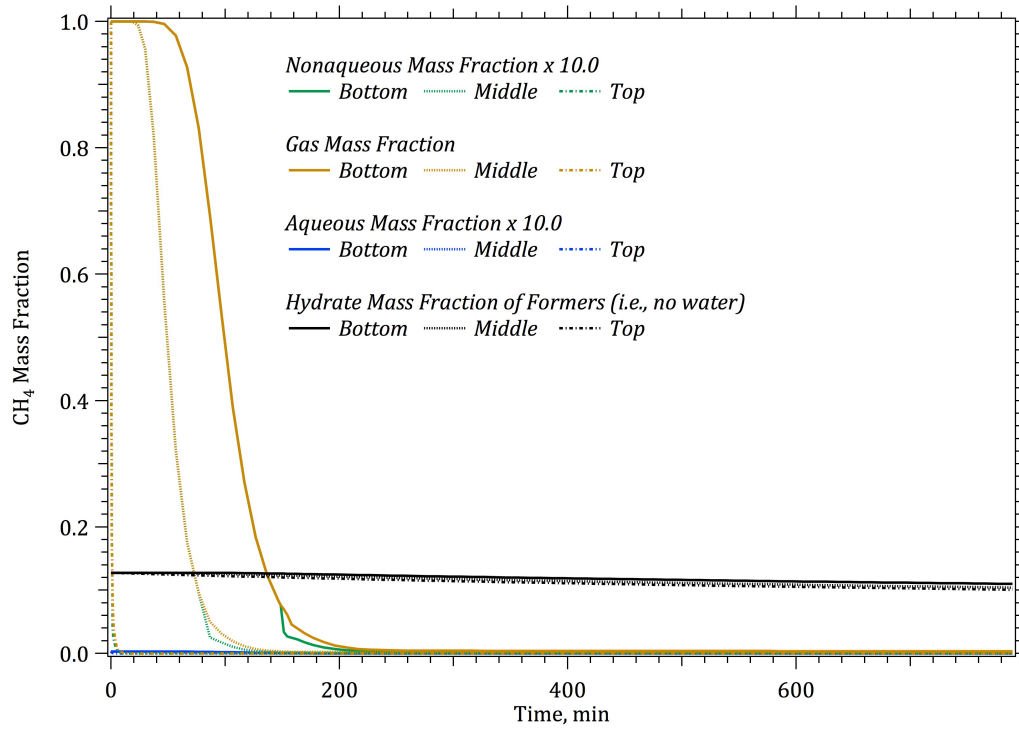


Figure 35. CH₄ Mass Fraction in Hydrate, Gas, Nonaqueous-Liquid and Aqueous versus Time at the Column Top, Middle and Bottom for Cycle 1 of the Swapping at Constant Flow Rate Simulation

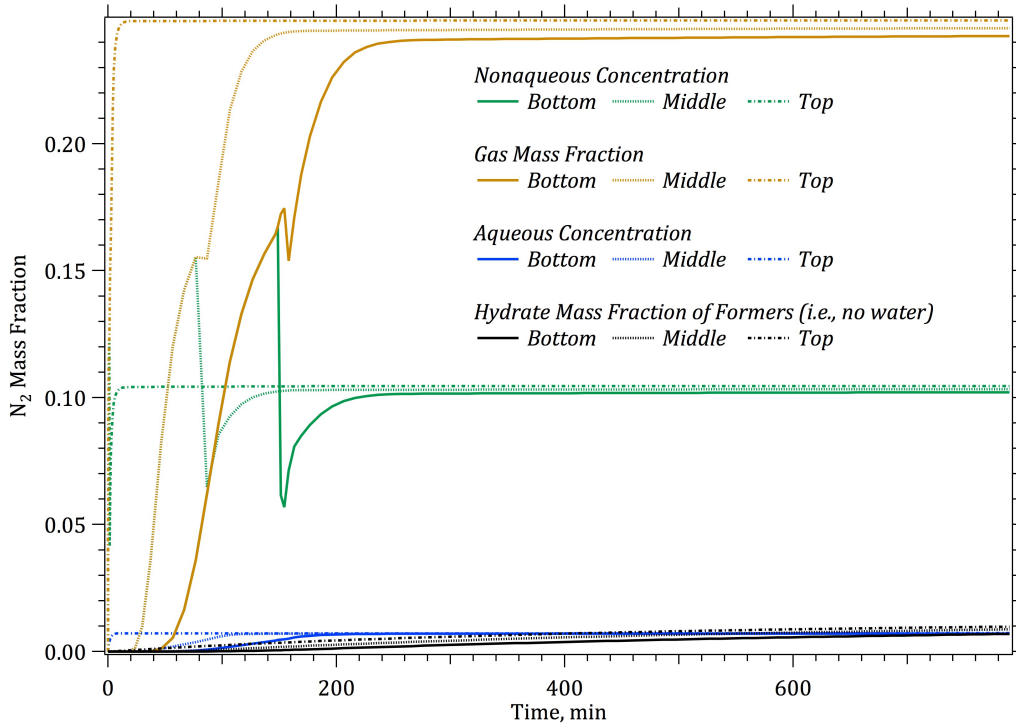


Figure 36. N₂ Mass Fraction in Hydrate, Gas, Nonaqueous-Liquid and Aqueous versus Time at the Column Top, Middle and Bottom for Cycle 1 of the Swapping at Constant Flow Rate Simulation

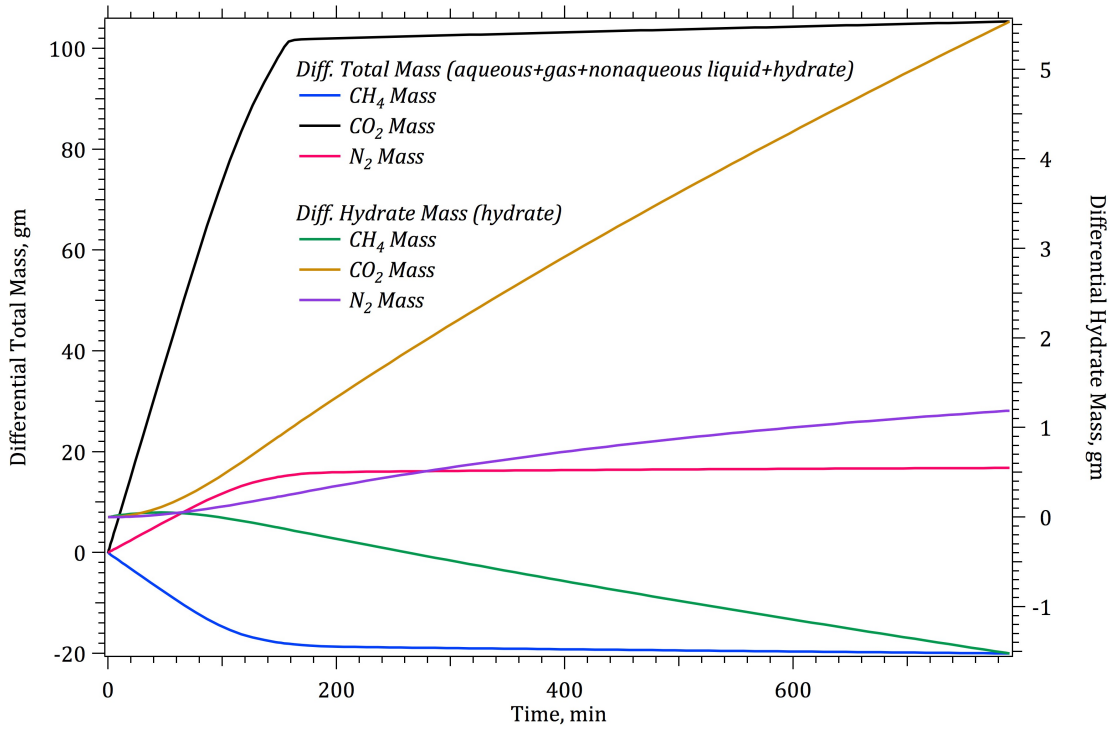


Figure 37. Differential Total and Hydrate CO₂, CH₄, and N₂ Mass versus Time at the Column Top, Middle and Bottom for Cycle 1 of the Swapping at Constant Flow Rate Simulation

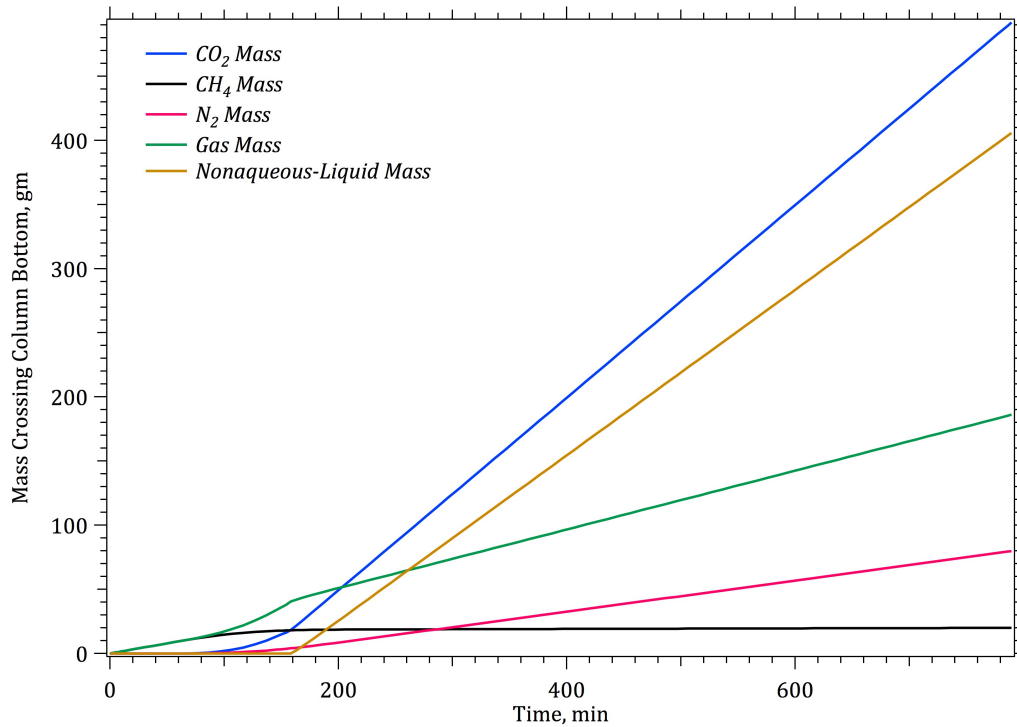


Figure 38. CO₂, CH₄, N₂, Gas, and Nonaqueous-Liquid Mass Crossing the Bottom Surface versus Time for Cycle 1 of the Swapping at Constant Flow Rate Simulation

hydrate mass show a short transition period, then a longer period after 80 min. of constant rate of exchange of the hydrate guest molecules, with the hydrate progressively gaining CO₂ and N₂ and losing CH₄. Plots of the mass of formers crossing the column bottom, shown in Figure 45, are consistent with the response within the column. Gaseous CH₄ is initially swept from the column at a rapid rate, followed by a much slower rate once the hydrate exchange process controls the release of CH₄. CO₂ and N₂ breakthrough occur around 155 min., after which the amount of CO₂ and N₂ leaving the column is nearly identical to the injection rate, except for the small amount that exchanges with the hydrate CH₄.

3.3.1.3.2 Second Cycle

Experimental results from the second cycle were that 1427.8 scc (1.024 g) of total CH₄ was produced from the column. In comparison numerical simulation results were that 247.4 scc (0.171 g) of total CH₄ was produced from the column. Details of the numerical simulation are shown in the time history plots. The second cycle numerical simulation is initiated using the end point from the first cycle simulation. The second cycle starts with a soaking period of 120 min., where the column is modeled as being closed on the ends with constant temperature boundaries. During the soaking period the gas and nonaqueous liquid redistribute, as shown in Figure 46, due to their density differences. After the soaking period the CO₂-N₂ mixture is injected at the column top, and constant pressure conditions are maintained at the column bottom. The distribution of the hydrate formers changes slightly during the soaking period, as shown in Figures 47 through 49. The exchange of the hydrate formers between the mobile phases and hydrate is most evident in the increase of CH₄ concentrations in the mobile phases, as shown in Figures 48 and 49. After the soaking period the CH₄ that has migrated into the mobile phases, is again swept from the column with the injected mixture of CO₂ and N₂, but the injection period is not sufficiently long enough to sweep all of the produced CH₄ from the column. The total amount of CH₄ exchanged after the soaking period was 317 scc (0.2275 g), as shown in Figure 50, which is less than the 247.4 scc (0.1771 g) of CH₄ leaving the column. Of the total mass leaving the column bottom, the gas to nonaqueous liquid ratio is 1:2.34, as shown in Figure 51.

3.3.1.3.3 Third Cycle

Experimental results from the third cycle were that 102.4 scc (0.073 g) of total CH₄ was produced from the column. In comparison numerical simulation results were that 258.5 scc (0.185 g) of total CH₄ was produced from the column. Details of the numerical simulation are shown in the time history plots, as shown in Figures 52 through 57. The characteristics of the third cycle simulation are very similar to that of the second cycle. The 120-min. soaking period allows for a redistribution of gas and nonaqueous liquid, and there is an exchange of CO₂ and N₂ with CH₄ in the hydrate during this period. With injection of CO₂ and N₂ the exchanged CH₄ is swept out of the column. At the end of the third cycle the hydrate remains predominately CH₄, with 13.65 g of CH₄, 7.46 g of CO₂, and 1.39 g of N₂. The experimental results compare well with the simulation results for the first cycle, as this first cycle is principally involves flushing the mobile CH₄ with the injected CO₂ and N₂. In the second and third cycles the experimental results show decay in produced CH₄ with each cycle. The numerical simulation shows a more consistent amount of produced CH₄ with each cycle. The numerical simulation exchange model is founded on a linear exchange rate model with an overall exchange rate constant. The experimental results suggest there may be a more complex mechanism involved.

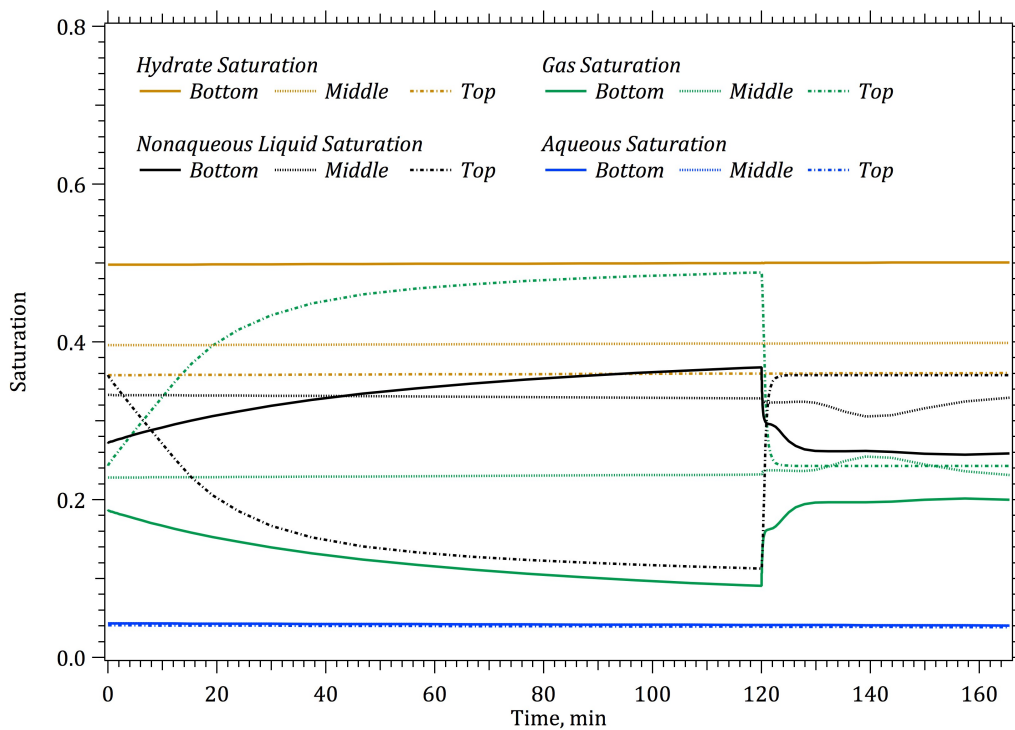


Figure 39. Hydrate, Gas, Nonaqueous-Liquid, and Aqueous Saturation versus Time at the Column Top, Middle and Bottom for Cycle 2 of the Swapping at Constant Flow Rate Simulation

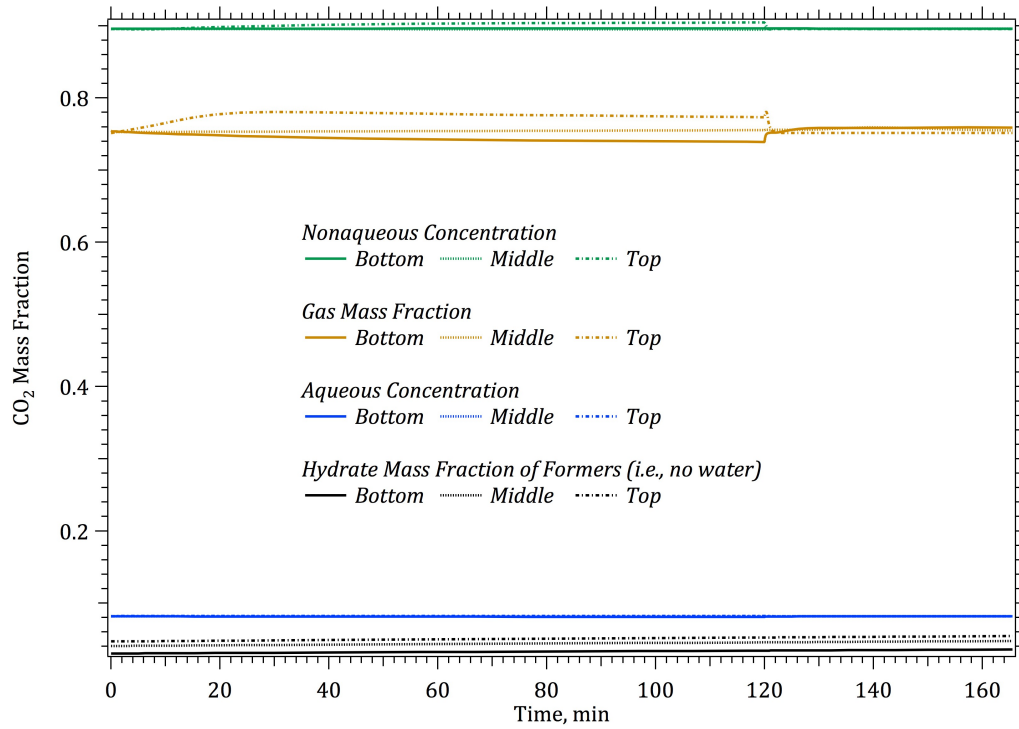


Figure 40. CO₂ Mass Fraction in Hydrate, Gas, Nonaqueous-Liquid and Aqueous versus Time at the Column Top, Middle and Bottom for Cycle 2 of the Swapping at Constant Flow Rate Simulation

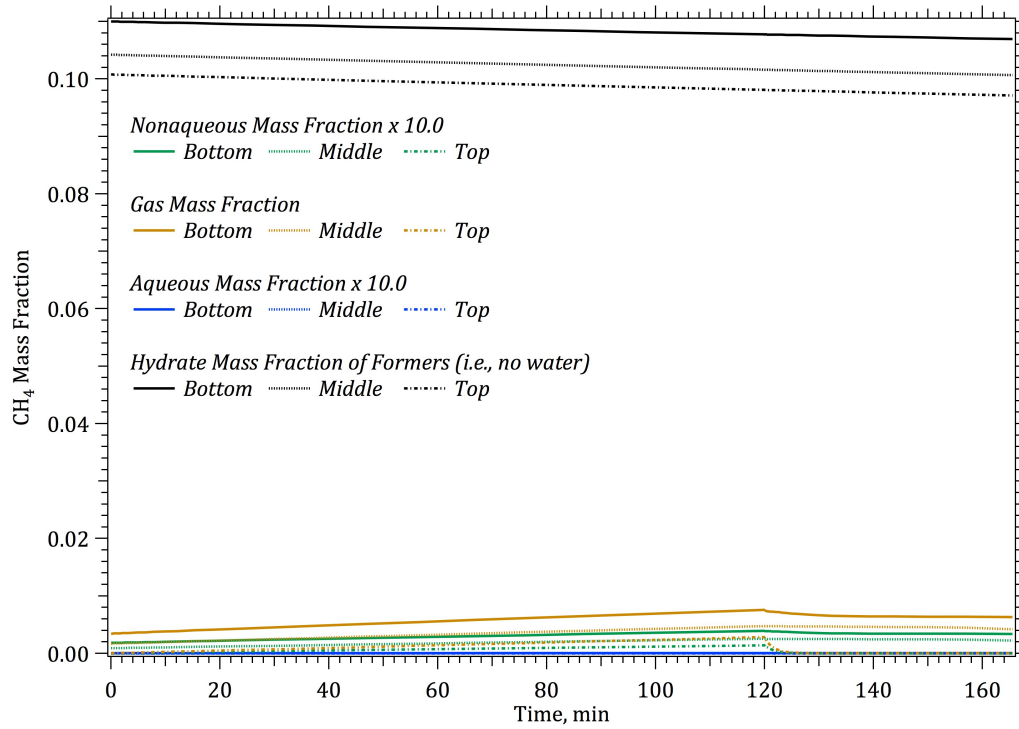


Figure 41. CH₄ Mass Fraction in Hydrate, Gas, Nonaqueous-Liquid and Aqueous versus Time at the Column Top, Middle and Bottom for Cycle 2 of the Swapping at Constant Flow Rate Simulation

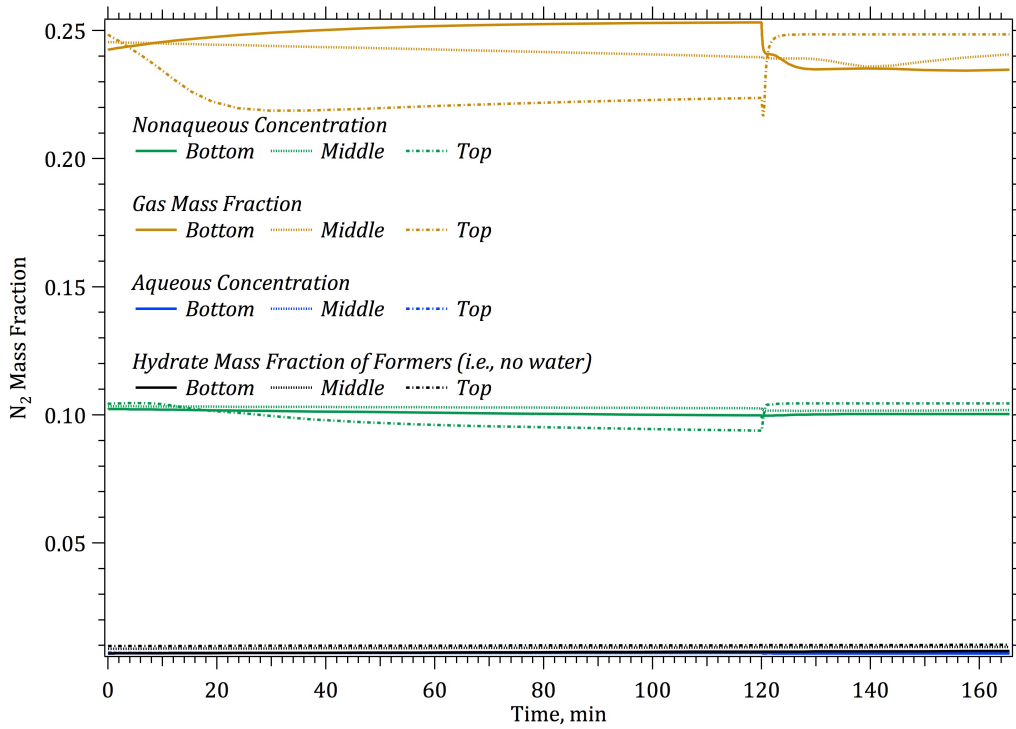


Figure 42. N_2 Mass Fraction in Hydrate, Gas, Nonaqueous-Liquid and Aqueous versus Time at the Column Top, Middle and Bottom for Cycle 2 of the Swapping at Constant Flow Rate Simulation

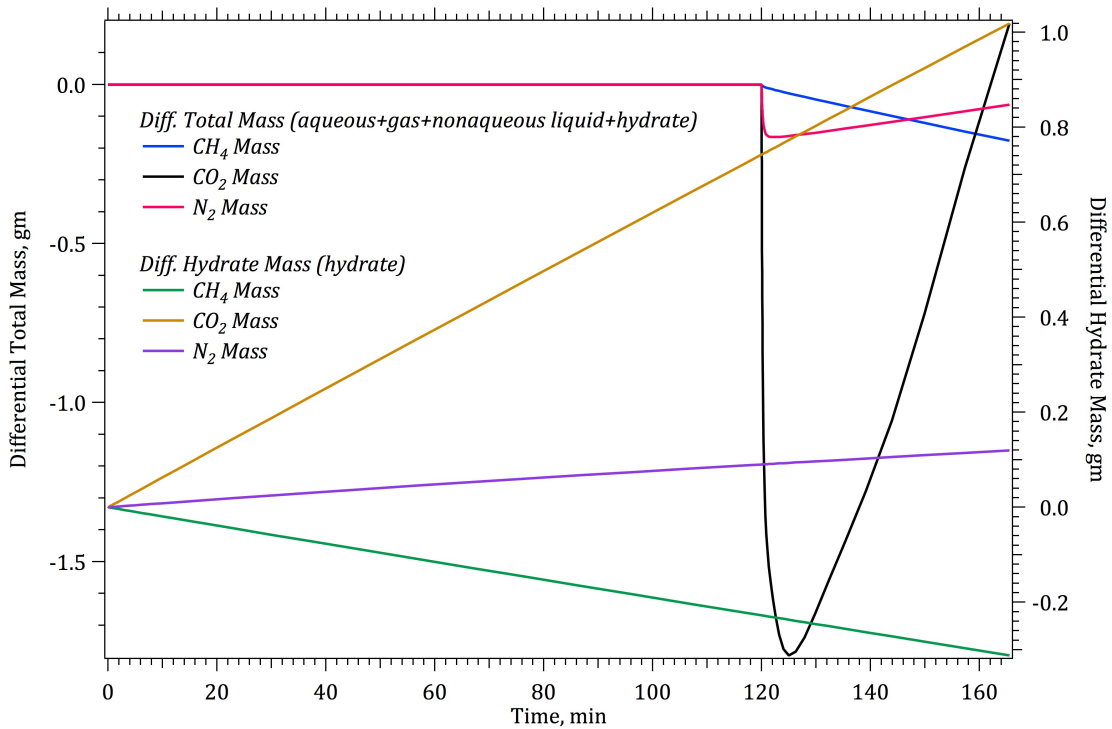


Figure 43. Differential Total and Hydrate CO_2 , CH_4 , and N_2 Mass versus Time at the Column Top, Middle and Bottom for Cycle 2 of the Swapping at Constant Flow Rate Simulation

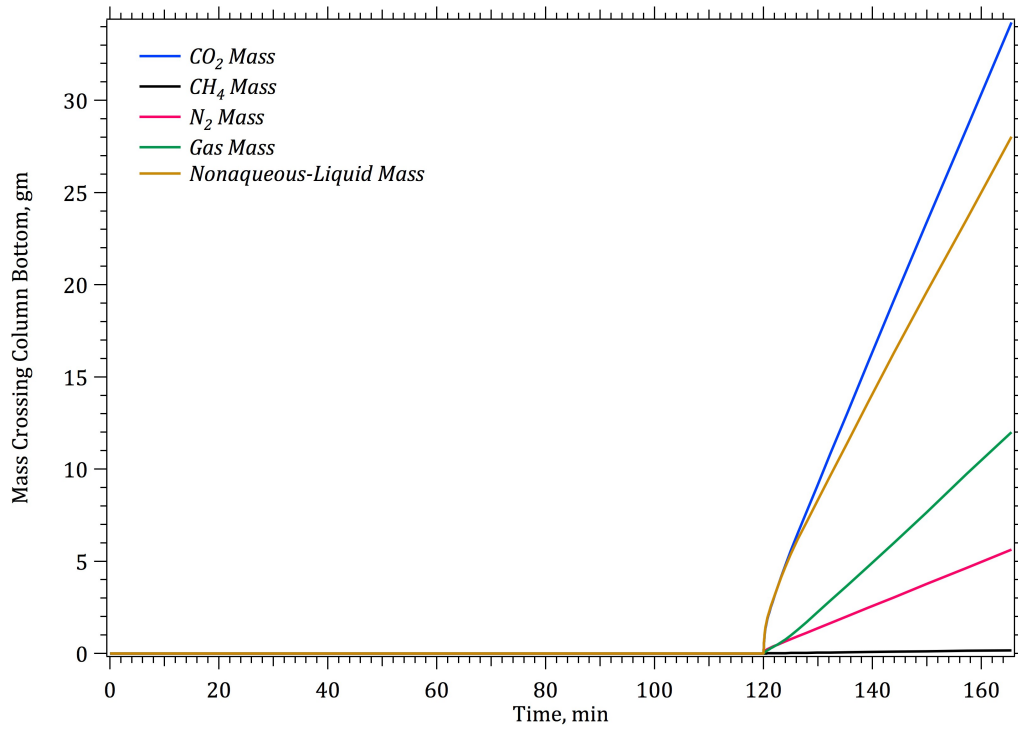


Figure 44. CO₂, CH₄, N₂, Gas, and Nonaqueous-Liquid Mass Crossing the Bottom Surface versus Time for Cycle 2 of the Swapping at Constant Flow Rate Simulation

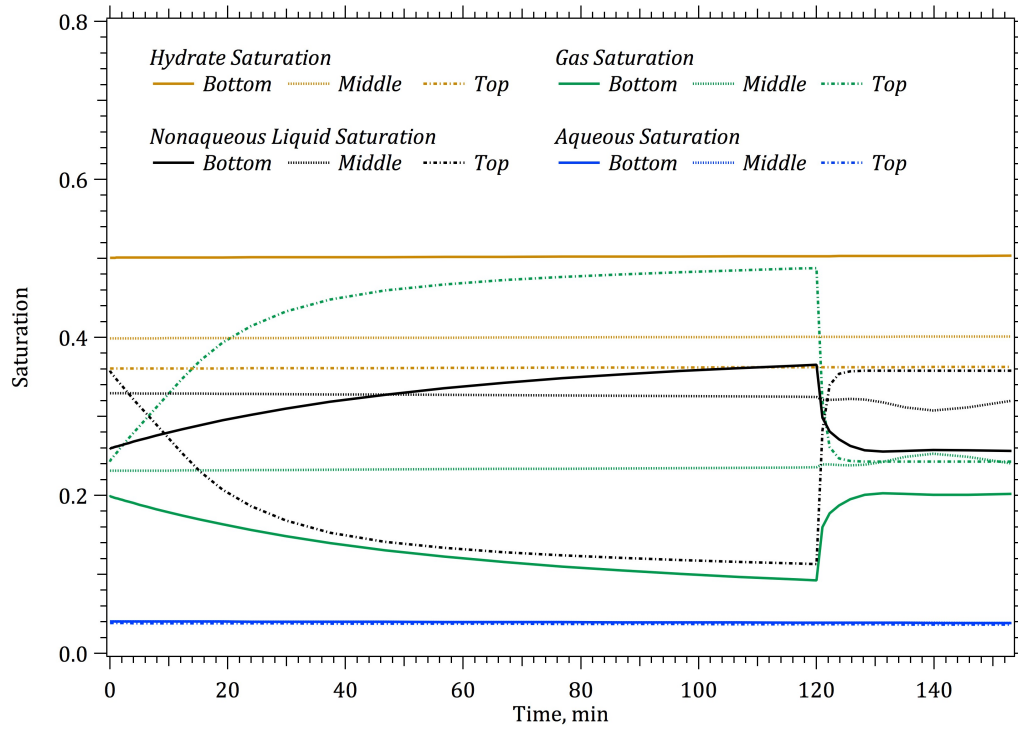


Figure 45. Hydrate, Gas, Nonaqueous-Liquid, and Aqueous Saturation versus Time at the Column Top, Middle and Bottom for Cycle 3 of the Swapping at Constant Flow Rate Simulation

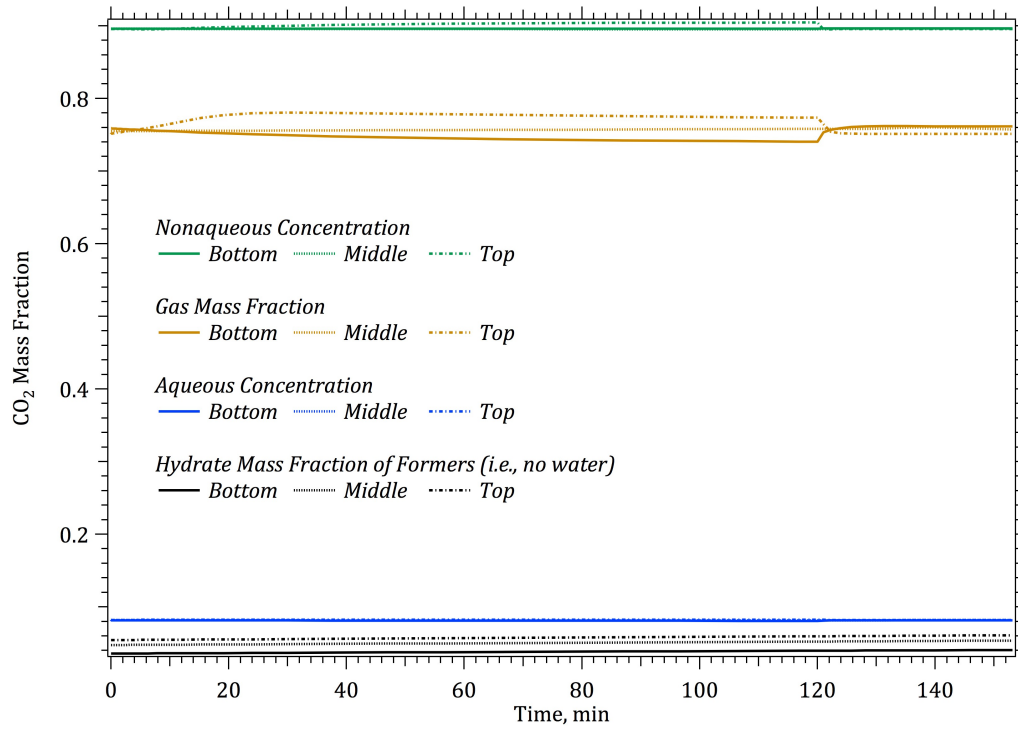


Figure 46. CO₂ Mass Fraction in Hydrate, Gas, Nonaqueous-Liquid and Aqueous versus Time at the Column Top, Middle and Bottom for Cycle 3 of the Swapping at Constant Flow Rate Simulation

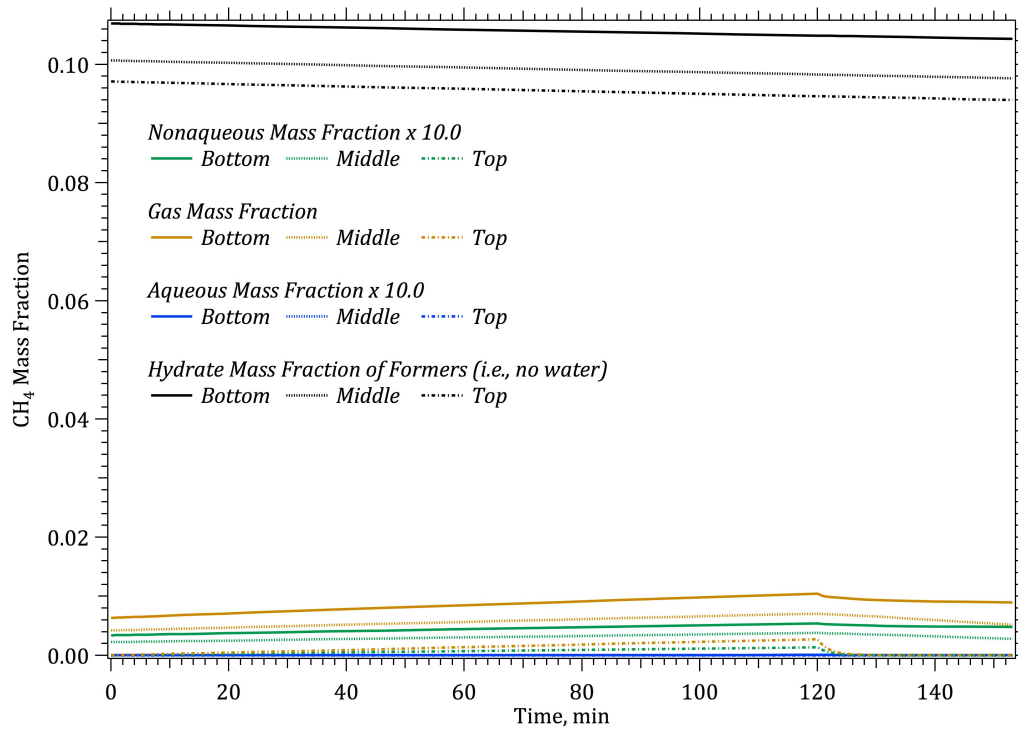


Figure 47. CH₄ Mass Fraction in Hydrate, Gas, Nonaqueous-Liquid and Aqueous versus Time at the Column Top, Middle and Bottom for Cycle 3 of the Swapping at Constant Flow Rate Simulation

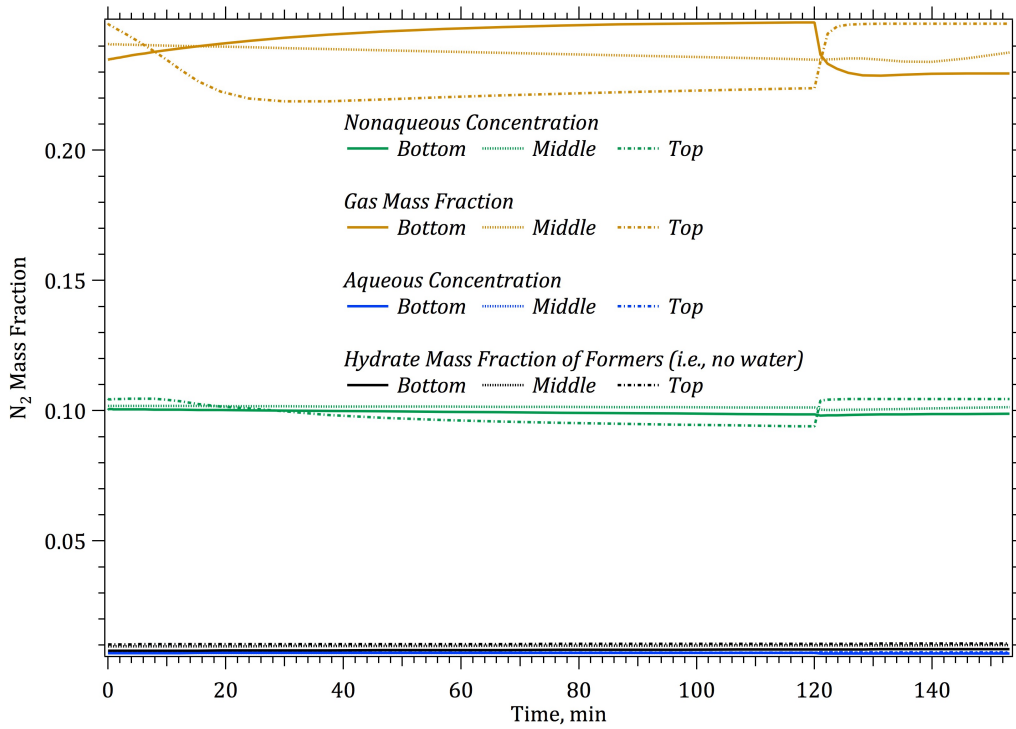


Figure 48. N₂ Mass Fraction in Hydrate, Gas, Nonaqueous-Liquid and Aqueous versus Time at the Column Top, Middle and Bottom for Cycle 3 of the Swapping at Constant Flow Rate Simulation

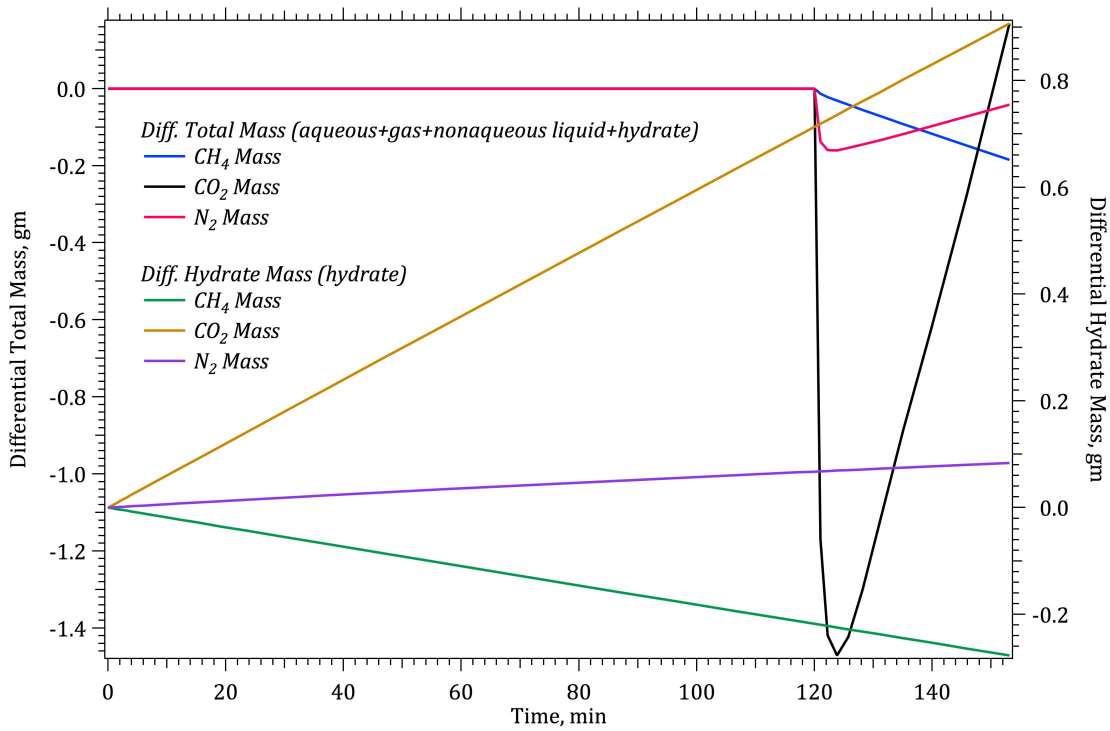


Figure 49. Differential Total and Hydrate CO₂, CH₄, and N₂ Mass versus Time at the Column Top, Middle and Bottom for Cycle 3 of the Swapping at Constant Flow Rate Simulation

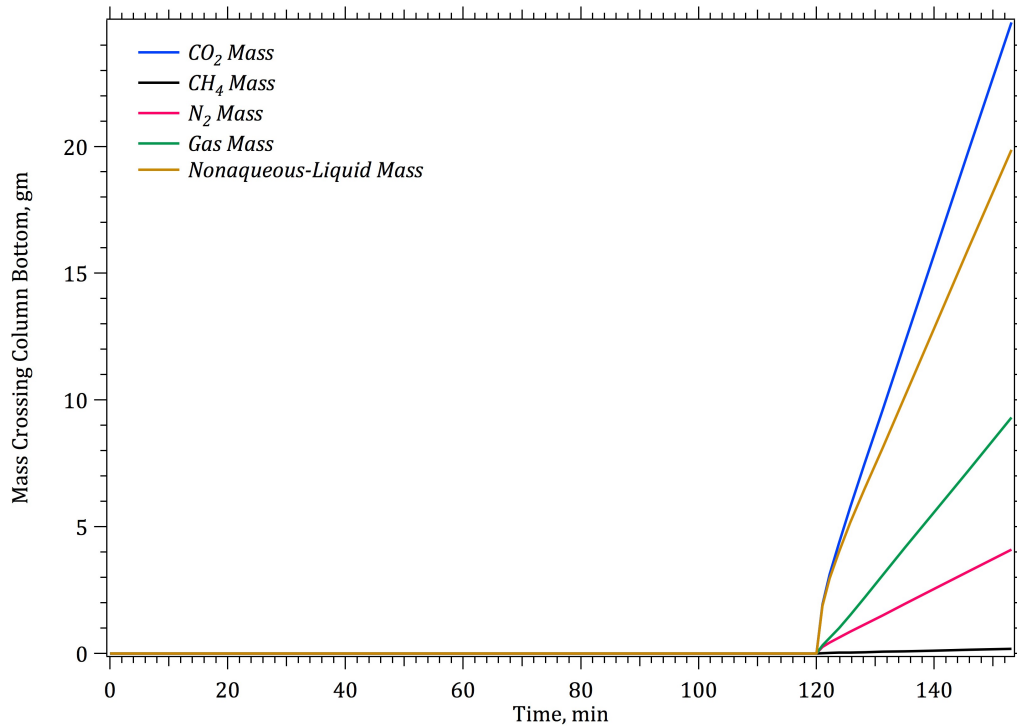


Figure 50. CO₂, CH₄, N₂, Gas, and Nonaqueous-Liquid Mass Crossing the Bottom Surface versus Time for Cycle 3 of the Swapping at Constant Flow Rate Simulation

3.3.1.4 Input Files

Input File for Gas Flooding at Constant Pressure

```

~Simulation Title Card
1,
Gas Flooding,
Mark White and Won Suk Lee,
PNNL and KIGAM,
25 February 2013,
08:39 PST,
1,
Gas flooding at constant pressure.

~Solution Control Card
Normal,
HYDT-KE w/NaCl w/Isobrine,
1,
0.0,hr,1000.0,min,0.1,sec,1.0,hr,1.25,16,1.e-06,
10000,
Variable Aqueous Diffusion,
Variable Gas Diffusion,
Variable Nonaqueous Liquid Diffusion,
1.e-4,kmol/s m^3,1.e-2,kmol/s m^3,1.e-2,kmol/s m^3,2.5,
0,

~Grid Card
Cartesian,
1,1,100,
0,cm,4.874248,cm,

```

0,cm,4.874248,cm,
0,cm,100@0.46,cm,

~Rock/Soil Zonation Card
1,
Sand,1,1,1,1,1,100,

~Mechanical Properties Card
Sand,2.633,g/cm³,0.3346,0.3346,compressibility,1.e-12,1/Pa,,,Millington and Quirk,,,

~Hydraulic Properties Card
Sand,0.202,darcy,0.202,darcy,0.202,darcy,

~Saturation Function Card
72.0,dynes/cm,24.0,dynes/cm,,,26.7,dynes/cm,
Sand, van Genuchten w/Webb,0.0341,1/cm,1.422,0.0,,72.0,dynes/cm,0.0,

~Aqueous Relative Permeability Card
Sand,Free Corey,1.0,3.0,0.3,0.0,

~Gas Relative Permeability Card
Sand,Free Corey,1.0,3.0,0.3,0.0,

~Nonaqueous Liquid Relative Permeability Card
Sand,Free Corey,1.0,3.0,0.3,0.0,

~Thermal Properties Card
Sand,Parallel,2.86,W/m K,2.86,W/m K,2.86,W/m K,700,J/kg K,

~Salt Transport Card
Sand,0.0,ft,0.0,ft,

~Initial Conditions Card
6,
#IC1 (sh = 0, sn = 0, sg = 0, nonequilibrium)
Temperature,11.0,C,,,,,1,1,1,1,1,100,
Aqueous Pressure,14.7,psi,,,,,1,1,1,1,1,100,
Mobile CH4 Mole Fraction of Formers,0.0,,,,,1,1,1,1,1,100,
Mobile N2 Mole Fraction of Formers,0.0,,,,,1,1,1,1,1,100,
Aqueous Relative Saturation of Formers,0.0,,,,,1,1,1,1,1,100,
IC1,1,1,1,1,1,100,,

~Boundary Conditions Card
2,
Top,Dirichlet Energy,Zero Flux Aqueous,Dirichlet Nonaqueous,
1,1,1,1,100,100,1,
0,hr,11.0,C,42.0,psi,0.0,1.0,1.0,
Bottom,Dirichlet Energy,Dirichlet-Outflow Aqueous,Dirichlet-Outflow Nonaqueous,
1,1,1,1,1,1,1,
0,hr,11.0,C,14.7,psi,14.7,psi,

~Output Control Card
11,
1,1,1,
1,1,10,
1,1,20,
1,1,30,
1,1,40,
1,1,50,
1,1,60,
1,1,70,
1,1,80,
1,1,90,
1,1,100,
1,1,min,cm,6,6,6,

13,
 Phase Condition,,
 Temperature,C,
 Gas Pressure,MPa,
 Aqueous Pressure,MPa,
 Aqueous Density,kg/m^3,
 Gas Density,kg/m^3,
 CH4 Aqueous Mass Fraction,,
 CH4 Gas Mass Fraction,,
 Aqueous Saturation,,
 Gas Saturation,,
 Hydrate Saturation,,
 Integrated CH4 Mass,gm,
 Integrated H2O Mass,gm,
 0,
 9,
 Temperature,C,
 Gas Pressure,MPa,
 Aqueous Pressure,MPa,
 Aqueous Density,kg/m^3,
 Gas Density,kg/m^3,
 CH4 Aqueous Mass Fraction,,
 CH4 Gas Mass Fraction,,
 Aqueous Saturation,,
 Gas Saturation,,

 ~Surface Flux Card
 2,
 Total CH4 Mass Flux,gm/s,gm,Bottom,1,1,1,1,1,1,
 Aqueous Mass Flux,gm/s,gm,Bottom,1,1,1,1,1,1,

Input File for Gas Flooding at Constant Rate

~Simulation Title Card
 1,
 Gas Flooding,
 Mark White and Won Suk Lee,
 PNNL and KIGAM,
 25 February 2013,
 08:05 PST,
 1,
 Gas flooding at constant rate.

~Solution Control Card
 Normal,
 HYDT-KE w/NaCl w/Isobrine,
 1,
 0.0,hr,1000.0,min,0.1,sec,1.0,hr,1.25,16,1.e-06,
 10000,
 Variable Aqueous Diffusion,
 Variable Gas Diffusion,
 Variable Nonaqueous Liquid Diffusion,
 1.e-4,kmol/s m^3,1.e-2,kmol/s m^3,1.e-2,kmol/s m^3,2.5,
 0,

~Grid Card
 Cartesian,
 1,1,100,
 0,cm,4.874248,cm,
 0,cm,4.874248,cm,
 0,cm,100@0.46,cm,

~Rock/Soil Zonation Card

```

1,
Sand,1,1,1,1,1,100,

~Mechanical Properties Card
Sand,2.633,g/cm^3,0.3346,0.3346,compressibility,1.e-12,1/Pa,,,Millington and Quirk,,,

~Hydraulic Properties Card
Sand,0.202,darcy,0.202,darcy,0.202,darcy,

~Saturation Function Card
72.0,dynes/cm,24.0,dynes/cm,,,26.7,dynes/cm,
Sand,van Genuchten w/Webb,0.0341,1/cm,1.422,0.0,,72.0,dynes/cm,0.0,

~Aqueous Relative Permeability Card
Sand,Free Corey,1.0,3.0,0.3,0.0,

~Gas Relative Permeability Card
Sand,Free Corey,1.0,3.0,0.3,0.0,

~Nonaqueous Liquid Relative Permeability Card
Sand,Free Corey,1.0,3.0,0.3,0.0,

~Thermal Properties Card
Sand,Parallel,2.86,W/m K,2.86,W/m K,2.86,W/m K,700,J/kg K,

~Salt Transport Card
Sand,0.0,ft,0.0,ft,

~Initial Conditions Card
6,
#IC1 (sh = 0, sn = 0, sg = 0, nonequilibrium )
Temperature,11.0,C,,,,,,1,1,1,1,1,100,
Aqueous Pressure,14.7,psi,,,,,,1,1,1,1,1,100,
Mobile CH4 Mole Fraction of Formers,0.0,,,,,,1,1,1,1,1,100,
Mobile N2 Mole Fraction of Formers,0.0,,,,,,1,1,1,1,1,100,
Aqueous Relative Saturation of Formers,0.0,,,,,,1,1,1,1,1,100,
IC1,1,1,1,1,1,100,,

~Boundary Conditions Card
1,
Bottom,Dirichlet Energy,Dirichlet-Outflow Aqueous,Dirichlet-Outflow Nonaqueous,
1,1,1,1,1,1,1,
0,hr,11.0,C,14.7,psi,14.7,psi,

~Source Card
1,
Nonaqueous Fluid Mass Source,1,1,1,1,100,100,4,
0,min,0.11472,gm/min,11.0,C,0.0,1.0,1.0,
3,min,0.11472,gm/min,11.0,C,0.0,1.0,1.0,
5,min,1.1472,gm/min,11.0,C,0.0,1.0,1.0,
1000,min,1.1472,gm/min,11.0,C,0.0,1.0,1.0,

~Output Control Card
11,
1,1,1,
1,1,10,
1,1,20,
1,1,30,
1,1,40,
1,1,50,
1,1,60,
1,1,70,
1,1,80,
1,1,90,
1,1,100,

```

1,1,min,cm,6,6,6,
 13,
 Phase Condition,,
 Temperature,C,
 Gas Pressure,MPa,
 Aqueous Pressure,MPa,
 Aqueous Density,kg/m³,
 Gas Density,kg/m³,
 CH4 Aqueous Mass Fraction,,
 CH4 Gas Mass Fraction,,
 Aqueous Saturation,,
 Gas Saturation,,
 Hydrate Saturation,,
 Integrated CH4 Mass,gm,
 Integrated H2O Mass,gm,
 0,
 9,
 Temperature,C,
 Gas Pressure,MPa,
 Aqueous Pressure,MPa,
 Aqueous Density,kg/m³,
 Gas Density,kg/m³,
 CH4 Aqueous Mass Fraction,,
 CH4 Gas Mass Fraction,,
 Aqueous Saturation,,
 Gas Saturation,,

 ~Surface Flux Card
 2,
 Total CH4 Mass Flux,gm/s,gm,Bottom,1,1,1,1,1,1,
 Aqueous Mass Flux,gm/s,gm,Bottom,1,1,1,1,1,1,

Input File for Hydrate Formation #1 (First Pressurization and Methane Injection)

~Simulation Title Card
 1,
 Hydrate Formation #1,
 Mark White and Won Suk Lee,
 PNNL and KIGAM,
 26 February 2013,
 11:02 PST,
 3,
 Pressurization with the injection of 20896.42 scc of methane
 or 15 gm, using a standard pressure and temperature density
 of 0.717 kg/m³, starting with the conditions after the
 gas flooding simulation.

~Solution Control Card
 Restart,
 HYDT-KE w/NaCl w/Isobrine,
 1,
 0.0,sec,600,sec,0.01,sec,100,sec,1.25,16,1.e-06,
 10000,
 Variable Aqueous Diffusion,
 Variable Gas Diffusion,
 Variable Nonaqueous Liquid Diffusion,
 8.e-6,kmol/s m³,1.e-2,kmol/s m³,1.e-2,kmol/s m³,2.5,
 0,

~Grid Card
 Cartesian,
 1,1,100,
 0,cm,4.874248,cm,
 0,cm,4.874248,cm,

0,cm,100@0.46,cm,

~Rock/Soil Zonation Card

1,
Sand,1,1,1,1,1,100,

~Mechanical Properties Card

Sand,2.633,g/cm³,0.3346,0.3346,compressibility,1.e-12,1/Pa,,,Millington and Quirk,,,

~Hydraulic Properties Card

Sand,0.202,darcy,0.202,darcy,0.202,darcy,

~Saturation Function Card

72.0,dynes/cm,24.0,dynes/cm,,,26.7,dynes/cm,
Sand, van Genuchten w/Webb,0.0341,1/cm,1.422,0.0,,72.0,dynes/cm,0.0,

~Aqueous Relative Permeability Card

Sand,Free Corey,1.0,3.0,0.3,0.0,

~Gas Relative Permeability Card

Sand,Free Corey,1.0,3.0,0.3,0.0,

~Nonaqueous Liquid Relative Permeability Card

Sand,Free Corey,1.0,3.0,0.3,0.0,

~Thermal Properties Card

Sand,Parallel,2.86,W/m K,2.86,W/m K,2.86,W/m K,700,J/kg K,

~Salt Transport Card

Sand,0.0,ft,0.0,ft,

~Source Card

1,
Nonaqueous Fluid Mass Source,1,1,1,1,100,100,1,
0,min,0.025,gm/s,11.0,C,0.0,1.0,1.0,

~Boundary Conditions Card

6,
Top,Dirichlet Energy,Zero Flux Aqueous,Zero Flux Nonaqueous,
1,1,1,1,100,100,1,
0,hr,11.0,C,
Bottom,Dirichlet Energy,Zero Flux Aqueous,Zero Flux Nonaqueous,
1,1,1,1,1,1,1,
0,hr,11.0,C,
East,Dirichlet Energy,Zero Flux Aqueous,Zero Flux Nonaqueous,
1,1,1,1,1,100,1,
0,hr,11.0,C,
West,Dirichlet Energy,Zero Flux Aqueous,Zero Flux Nonaqueous,
1,1,1,1,1,100,1,
0,hr,11.0,C,
North,Dirichlet Energy,Zero Flux Aqueous,Zero Flux Nonaqueous,
1,1,1,1,1,100,1,
0,hr,11.0,C,
South,Dirichlet Energy,Zero Flux Aqueous,Zero Flux Nonaqueous,
1,1,1,1,1,100,1,
0,hr,11.0,C,

~Output Control Card

11,
1,1,1,
1,1,10,
1,1,20,
1,1,30,
1,1,40,
1,1,50,

1,1,60,
 1,1,70,
 1,1,80,
 1,1,90,
 1,1,100,
 1,1,s,cm,6,6,6,
 16,
 Temperature,C,
 Gas Pressure,MPa,
 Aqueous Pressure,MPa,
 Aqueous Density,kg/m³,
 Gas Density,kg/m³,
 Hydrate Density,kg/m³,
 CH4 Aqueous Mass Fraction,,
 CH4 Gas Mass Fraction,,
 CH4 Hydrate Mass Fraction,,
 Aqueous Saturation,,
 Gas Saturation,,
 Hydrate Saturation,,
 Integrated CH4 Mass,gm,
 Integrated H2O Mass,gm,
 Integrated Hydrate CH4 Mass,gm,
 Integrated Hydrate H2O Mass,gm,
 0,
 12,
 Temperature,C,
 Gas Pressure,MPa,
 Aqueous Pressure,MPa,
 Aqueous Density,kg/m³,
 Gas Density,kg/m³,
 Hydrate Density,kg/m³,
 CH4 Aqueous Mass Fraction,,
 CH4 Gas Mass Fraction,,
 CH4 Hydrate Mass Fraction,,
 Aqueous Saturation,,
 Gas Saturation,,
 Hydrate Saturation,,

Input File for Hydrate Formation #2 (First Sealed Temperature Reduction)

~Simulation Title Card

1,
 Hydrate Formation #2,
 Mark White and Won Suk Lee,
 PNNL and KIGAM,
 26 February 2013,
 10:44 PST,
 2,
 Temperature reduction to 1 C, starting with the conditions
 after the hydrate formation #1 simulation.

~Solution Control Card

Restart,
 HYDT-KE w/NaCl w/Isobrine,
 1,
 0,sec,12,hr,0.01,sec,0.1,hr,1.25,16,1.e-06,
 10000,
 Variable Aqueous Diffusion,
 Variable Gas Diffusion,
 Variable Nonaqueous Liquid Diffusion,
 8.e-6,kmol/s m³,1.e-2,kmol/s m³,1.e-2,kmol/s m³,2.5,
 0,

~Grid Card

Cartesian,
 1,1,100,
 0,cm,4.874248,cm,
 0,cm,4.874248,cm,
 0,cm,100@0.46,cm,

~Rock/Soil Zonation Card
 1,
 Sand,1,1,1,1,1,100,

~Mechanical Properties Card
 Sand,2.633,g/cm³,0.3346,0.3346,compressibility,1.e-12,1/Pa,,,Millington and Quirk,,,

~Hydraulic Properties Card
 Sand,0.202,darcy,0.202,darcy,0.202,darcy,

~Saturation Function Card
 72.0,dynes/cm,24.0,dynes/cm,,,26.7,dynes/cm,
 Sand,van Genuchten w/Webb,0.0341,1/cm,1.422,0.0,,72.0,dynes/cm,0.0,

~Aqueous Relative Permeability Card
 Sand,Free Corey,1.0,3.0,0.3,0.0,

~Gas Relative Permeability Card
 Sand,Free Corey,1.0,3.0,0.3,0.0,

~Nonaqueous Liquid Relative Permeability Card
 Sand,Free Corey,1.0,3.0,0.3,0.0,

~Thermal Properties Card
 Sand,Parallel,2.86,W/m K,2.86,W/m K,2.86,W/m K,700,J/kg K,

~Salt Transport Card
 Sand,0.0,ft,0.0,ft,

~Boundary Conditions Card
 6,
 Top,Dirichlet Energy,Zero Flux Aqueous,Zero Flux Nonaqueous,
 1,1,1,1,100,100,1,
 0,hr,1.0,C,
 Bottom,Dirichlet Energy,Zero Flux Aqueous,Zero Flux Nonaqueous,
 1,1,1,1,1,1,1,
 0,hr,1.0,C,
 East,Dirichlet Energy,Zero Flux Aqueous,Zero Flux Nonaqueous,
 1,1,1,1,1,100,1,
 0,hr,1.0,C,
 West,Dirichlet Energy,Zero Flux Aqueous,Zero Flux Nonaqueous,
 1,1,1,1,1,100,1,
 0,hr,1.0,C,
 North,Dirichlet Energy,Zero Flux Aqueous,Zero Flux Nonaqueous,
 1,1,1,1,1,100,1,
 0,hr,1.0,C,
 South,Dirichlet Energy,Zero Flux Aqueous,Zero Flux Nonaqueous,
 1,1,1,1,1,100,1,
 0,hr,1.0,C,

~Output Control Card
 11,
 1,1,1,
 1,1,10,
 1,1,20,
 1,1,30,
 1,1,40,
 1,1,50,
 1,1,60,

1,1,70,
 1,1,80,
 1,1,90,
 1,1,100,
 1,1,s,cm,6,6,6,
 16,
 Temperature,C,
 Gas Pressure,MPa,
 Aqueous Pressure,MPa,
 Aqueous Density,kg/m³,
 Gas Density,kg/m³,
 Hydrate Density,kg/m³,
 CH4 Aqueous Mass Fraction,,
 CH4 Gas Mass Fraction,,
 CH4 Hydrate Mass Fraction,,
 Aqueous Saturation,,
 Gas Saturation,,
 Hydrate Saturation,,
 Integrated CH4 Mass,gm,
 Integrated H2O Mass,gm,
 Integrated Hydrate CH4 Mass,gm,
 Integrated Hydrate H2O Mass,gm,
 0,
 12,
 Temperature,C,
 Gas Pressure,MPa,
 Aqueous Pressure,MPa,
 Aqueous Density,kg/m³,
 Gas Density,kg/m³,
 Hydrate Density,kg/m³,
 CH4 Aqueous Mass Fraction,,
 CH4 Gas Mass Fraction,,
 CH4 Hydrate Mass Fraction,,
 Aqueous Saturation,,
 Gas Saturation,,
 Hydrate Saturation,,

Input File for Hydrate Formation #3 (Second Pressurization and Methane Injection)

~Simulation Title Card

1,
 Hydrate Formation #3,
 Mark White and Won Suk Lee,
 PNNL and KIGAM,
 26 February 2013,
 13:30 PST,
 3,
 Pressurization with the injection of 23250.47 scc of methane
 or 16.67 gm, using a standard pressure and temperature density
 of 0.717 kg/m³. An injection period of 10 minute was assumed.

~Solution Control Card

Restart,
 HYDT-KE w/NaCl w/Isobrine,
 1,
 0.0,sec,600.0,sec,0.01,sec,1.0,sec,1.25,16,1.e-06,
 10000,
 Variable Aqueous Diffusion,
 Variable Gas Diffusion,
 Variable Nonaqueous Liquid Diffusion,
 8.e-6,kmol/s m³,1.e-2,kmol/s m³,1.e-2,kmol/s m³,2.5,
 0,

~Grid Card

Cartesian,
 1,1,100,
 0,cm,4.874248,cm,
 0,cm,4.874248,cm,
 0,cm,100@0.46,cm,

~Rock/Soil Zonation Card
 1,
 Sand,1,1,1,1,1,100,

~Mechanical Properties Card
 Sand,2.633,g/cm³,0.3346,0.3346,compressibility,1.e-12,1/Pa,,,Millington and Quirk,,,

~Hydraulic Properties Card
 Sand,0.202,darcy,0.202,darcy,0.202,darcy,

~Saturation Function Card
 72.0,dynes/cm,24.0,dynes/cm,,,26.7,dynes/cm,
 Sand,van Genuchten w/Webb,0.0341,1/cm,1.422,0.0,,72.0,dynes/cm,0.0,

~Aqueous Relative Permeability Card
 Sand,Free Corey,1.0,3.0,0.3,0.0,

~Gas Relative Permeability Card
 Sand,Free Corey,1.0,3.0,0.3,0.0,

~Nonaqueous Liquid Relative Permeability Card
 Sand,Free Corey,1.0,3.0,0.3,0.0,

~Thermal Properties Card
 Sand,Parallel,2.86,W/m K,2.86,W/m K,2.86,W/m K,700,J/kg K,

~Salt Transport Card
 Sand,0.0,ft,0.0,ft,

~Source Card
 1,
 Nonaqueous Fluid Mass Source,1,1,1,1,100,100,1,
 0,min,0.028,gm/s,1.0,C,0.0,1.0,1.0,

~Boundary Conditions Card
 6,
 Top,Dirichlet Energy,Zero Flux Aqueous,Zero Flux Nonaqueous,
 1,1,1,1,100,100,1,
 0,hr,1.0,C,
 Bottom,Dirichlet Energy,Zero Flux Aqueous,Zero Flux Nonaqueous,
 1,1,1,1,1,1,1,
 0,hr,1.0,C,
 East,Dirichlet Energy,Zero Flux Aqueous,Zero Flux Nonaqueous,
 1,1,1,1,1,100,1,
 0,hr,1.0,C,
 West,Dirichlet Energy,Zero Flux Aqueous,Zero Flux Nonaqueous,
 1,1,1,1,1,100,1,
 0,hr,1.0,C,
 North,Dirichlet Energy,Zero Flux Aqueous,Zero Flux Nonaqueous,
 1,1,1,1,1,100,1,
 0,hr,1.0,C,
 South,Dirichlet Energy,Zero Flux Aqueous,Zero Flux Nonaqueous,
 1,1,1,1,1,100,1,
 0,hr,1.0,C,

~Output Control Card
 11,
 1,1,1,
 1,1,10,

1,1,20,
 1,1,30,
 1,1,40,
 1,1,50,
 1,1,60,
 1,1,70,
 1,1,80,
 1,1,90,
 1,1,100,
 1,1,s,cm,6,6,6,
 16,
 Temperature,C,
 Gas Pressure,MPa,
 Aqueous Pressure,MPa,
 Aqueous Density,kg/m^3,
 Gas Density,kg/m^3,
 Hydrate Density,kg/m^3,
 CH4 Aqueous Mass Fraction,,
 CH4 Gas Mass Fraction,,
 CH4 Hydrate Mass Fraction,,
 Aqueous Saturation,,
 Gas Saturation,,
 Hydrate Saturation,,
 Integrated CH4 Mass,gm,
 Integrated H2O Mass,gm,
 Integrated Hydrate CH4 Mass,gm,
 Integrated Hydrate H2O Mass,gm,
 0,
 12,
 Temperature,C,
 Gas Pressure,MPa,
 Aqueous Pressure,MPa,
 Aqueous Density,kg/m^3,
 Gas Density,kg/m^3,
 Hydrate Density,kg/m^3,
 CH4 Aqueous Mass Fraction,,
 CH4 Gas Mass Fraction,,
 CH4 Hydrate Mass Fraction,,
 Aqueous Saturation,,
 Gas Saturation,,
 Hydrate Saturation,,

Input File for Hydrate Formation #4 (Second Sealed Temperature Reduction)

~Simulation Title Card

1,
 Hydrate Formation #4,
 Mark White and Won Suk Lee,
 PNNL and KIGAM,
 26 February 2013,
 11:15 PST,
 2,
 Temperature reduction to 1 C, starting with the conditions
 after the hydrate formation #3 simulation.

~Solution Control Card

Restart,
 HYDT-KE w/NaCl w/Isobrine,
 1,
 0,sec,12,hr,0.01,sec,0.1,hr,1.25,16,1.e-06,
 10000,
 Variable Aqueous Diffusion,
 Variable Gas Diffusion,
 Variable Nonaqueous Liquid Diffusion,

8.e-6,kmol/s m^3,1.e-2,kmol/s m^3,1.e-2,kmol/s m^3,2.5,
0,

~Grid Card

Cartesian,
1,1,100,
0,cm,4.874248,cm,
0,cm,4.874248,cm,
0,cm,100@0.46,cm,

~Rock/Soil Zonation Card

1,
Sand,1,1,1,1,1,100,

~Mechanical Properties Card

Sand,2.633,g/cm^3,0.3346,0.3346,compressibility,1.e-12,1/Pa,,,Millington and Quirk,,,

~Hydraulic Properties Card

Sand,0.202,darcy,0.202,darcy,0.202,darcy,

~Saturation Function Card

72.0,dynes/cm,24.0,dynes/cm,,,26.7,dynes/cm,
Sand,van Genuchten w/Webb,0.0341,1/cm,1.422,0.0,,72.0,dynes/cm,0.0,

~Aqueous Relative Permeability Card

Sand,Free Corey,1.0,3.0,0.3,0.0,

~Gas Relative Permeability Card

Sand,Free Corey,1.0,3.0,0.3,0.0,

~Nonaqueous Liquid Relative Permeability Card

Sand,Free Corey,1.0,3.0,0.3,0.0,

~Thermal Properties Card

Sand,Parallel,2.86,W/m K,2.86,W/m K,2.86,W/m K,700,J/kg K,

~Salt Transport Card

Sand,0.0,ft,0.0,ft,

~Boundary Conditions Card

6,
Top,Dirichlet Energy,Zero Flux Aqueous,Zero Flux Nonaqueous,
1,1,1,1,100,100,1,
0,hr,1.0,C,
Bottom,Dirichlet Energy,Zero Flux Aqueous,Zero Flux Nonaqueous,
1,1,1,1,1,1,1,
0,hr,1.0,C,
East,Dirichlet Energy,Zero Flux Aqueous,Zero Flux Nonaqueous,
1,1,1,1,1,100,1,
0,hr,1.0,C,
West,Dirichlet Energy,Zero Flux Aqueous,Zero Flux Nonaqueous,
1,1,1,1,1,100,1,
0,hr,1.0,C,
North,Dirichlet Energy,Zero Flux Aqueous,Zero Flux Nonaqueous,
1,1,1,1,1,100,1,
0,hr,1.0,C,
South,Dirichlet Energy,Zero Flux Aqueous,Zero Flux Nonaqueous,
1,1,1,1,1,100,1,
0,hr,1.0,C,

~Output Control Card

11,
1,1,1,
1,1,10,
1,1,20,

1,1,30,
 1,1,40,
 1,1,50,
 1,1,60,
 1,1,70,
 1,1,80,
 1,1,90,
 1,1,100,
 1,1,s,cm,6,6,6,
 16,
 Temperature,C,
 Gas Pressure,MPa,
 Aqueous Pressure,MPa,
 Aqueous Density,kg/m³,
 Gas Density,kg/m³,
 Hydrate Density,kg/m³,
 CH4 Aqueous Mass Fraction,,
 CH4 Gas Mass Fraction,,
 CH4 Hydrate Mass Fraction,,
 Aqueous Saturation,,
 Gas Saturation,,
 Hydrate Saturation,,
 Integrated CH4 Mass,gm,
 Integrated H2O Mass,gm,
 Integrated Hydrate CH4 Mass,gm,
 Integrated Hydrate H2O Mass,gm,
 0,
 12,
 Temperature,C,
 Gas Pressure,MPa,
 Aqueous Pressure,MPa,
 Aqueous Density,kg/m³,
 Gas Density,kg/m³,
 Hydrate Density,kg/m³,
 CH4 Aqueous Mass Fraction,,
 CH4 Gas Mass Fraction,,
 CH4 Hydrate Mass Fraction,,
 Aqueous Saturation,,
 Gas Saturation,,
 Hydrate Saturation,,

Input File for Hydrate Formation #5 (Third Pressurization and Methane Injection)

~Simulation Title Card

1,
 Hydrate Formation #5,
 Mark White and Won Suk Lee,
 PNNL and KIGAM,
 26 February 2013,
 11:20 PST,
 3,
 Adjustment to swapping pressure of 1414.7 psia.

~Solution Control Card

Restart,
 HYDT-KE w/NaCl w/Isobrine,
 1,
 0.0,sec,600.0,sec,0.001,sec,10.0,sec,1.25,16,1.e-06,
 10000,
 Variable Aqueous Diffusion,
 Variable Gas Diffusion,
 Variable Nonaqueous Liquid Diffusion,
 8.e-6,kmol/s m³,1.e-2,kmol/s m³,1.e-2,kmol/s m³,2.5,
 0,

```

~Grid Card
Cartesian,
1,1,100,
0,cm,4.874248,cm,
0,cm,4.874248,cm,
0,cm,100@0.46,cm,

~Rock/Soil Zonation Card
1,
Sand,1,1,1,1,1,100,

~Mechanical Properties Card
Sand,2.633,g/cm^3,0.3346,0.3346,compressibility,1.e-12,1/Pa,,,Millington and Quirk,,,

~Hydraulic Properties Card
Sand,0.202,darcy,0.202,darcy,0.202,darcy,

~Saturation Function Card
72.0,dynes/cm,24.0,dynes/cm,,,26.7,dynes/cm,
Sand,van Genuchten w/Webb,0.0341,1/cm,1.422,0.0,,72.0,dynes/cm,0.0,

~Aqueous Relative Permeability Card
Sand,Free Corey,1.0,3.0,0.3,0.0,

~Gas Relative Permeability Card
Sand,Free Corey,1.0,3.0,0.3,0.0,

~Nonaqueous Liquid Relative Permeability Card
Sand,Free Corey,1.0,3.0,0.3,0.0,

~Thermal Properties Card
Sand,Parallel,2.86,W/m K,2.86,W/m K,2.86,W/m K,700,J/kg K,

~Salt Transport Card
Sand,0.0,ft,0.0,ft,

~Boundary Conditions Card
6,
Top,Dirichlet Energy,Zero Flux Aqueous,Dirichlet Nonaqueous,
1,1,1,1,100,100,1,
0,hr,1.0,C,1414.7,psi,0.0,1.0,1.0,
Bottom,Dirichlet Energy,Zero Flux Aqueous,Zero Flux Nonaqueous,
1,1,1,1,1,1,1,
0,hr,1.0,C,
East,Dirichlet Energy,Zero Flux Aqueous,Zero Flux Nonaqueous,
1,1,1,1,1,100,1,
0,hr,1.0,C,
West,Dirichlet Energy,Zero Flux Aqueous,Zero Flux Nonaqueous,
1,1,1,1,1,100,1,
0,hr,1.0,C,
North,Dirichlet Energy,Zero Flux Aqueous,Zero Flux Nonaqueous,
1,1,1,1,1,100,1,
0,hr,1.0,C,
South,Dirichlet Energy,Zero Flux Aqueous,Zero Flux Nonaqueous,
1,1,1,1,1,100,1,
0,hr,1.0,C,

~Output Control Card
11,
1,1,1,
1,1,10,
1,1,20,
1,1,30,
1,1,40,

```

1,1,50,
 1,1,60,
 1,1,70,
 1,1,80,
 1,1,90,
 1,1,100,
 1,1,s,cm,6,6,6,
 16,
 Temperature,C,
 Gas Pressure,MPa,
 Aqueous Pressure,MPa,
 Aqueous Density,kg/m³,
 Gas Density,kg/m³,
 Hydrate Density,kg/m³,
 CH4 Aqueous Mass Fraction,,
 CH4 Gas Mass Fraction,,
 CH4 Hydrate Mass Fraction,,
 Aqueous Saturation,,
 Gas Saturation,,
 Hydrate Saturation,,
 Integrated CH4 Mass,gm,
 Integrated H2O Mass,gm,
 Integrated Hydrate CH4 Mass,gm,
 Integrated Hydrate H2O Mass,gm,
 0,
 12,
 Temperature,C,
 Gas Pressure,MPa,
 Aqueous Pressure,MPa,
 Aqueous Density,kg/m³,
 Gas Density,kg/m³,
 Hydrate Density,kg/m³,
 CH4 Aqueous Mass Fraction,,
 CH4 Gas Mass Fraction,,
 CH4 Hydrate Mass Fraction,,
 Aqueous Saturation,,
 Gas Saturation,,
 Hydrate Saturation,,

Input File for Swapping Production (First Cycle)

~Simulation Title Card

1,
 Constant Flow Rate Swapping #1,
 Mark White and Won Suk Lee,
 PNNL and KIGAM,
 27 February 2013,
 07:56 PST,
 3,
 Constant flow rate of 480 sccm (8:2 by volume CO2:N2).
 789.48 min simulation time.

~Solution Control Card

Restart,
 HYDT-KE w/NaCl w/Isobrine,
 1,
 0.0,sec,789.48,min,0.01,sec,10.0,min,1.25,16,1.e-06,
 10000,
 Variable Aqueous Diffusion,
 Variable Gas Diffusion,
 Variable Nonaqueous Liquid Diffusion,
 8.e-6,kmol/s m³,1.e-2,kmol/s m³,1.e-2,kmol/s m³,2.5,
 0,

```

~Grid Card
Cartesian,
1,1,100,
0,cm,4.874248,cm,
0,cm,4.874248,cm,
0,cm,100@0.46,cm,

~Rock/Soil Zonation Card
1,
Sand,1,1,1,1,1,100,

~Mechanical Properties Card
Sand,2.633,g/cm^3,0.3346,0.3346,compressibility,1.e-12,1/Pa,,,Millington and Quirk,,,

~Hydraulic Properties Card
Sand,0.202,darcy,0.202,darcy,0.202,darcy,

~Saturation Function Card
72.0,dynes/cm,24.0,dynes/cm,,,26.7,dynes/cm,
Sand,van Genuchten w/Webb,0.0341,1/cm,1.422,0.0,,72.0,dynes/cm,0.0,

~Aqueous Relative Permeability Card
Sand,Free Corey,1.0,3.0,0.3,0.0,

~Gas Relative Permeability Card
Sand,Free Corey,1.0,3.0,0.3,0.0,

~Nonaqueous Liquid Relative Permeability Card
Sand,Free Corey,1.0,3.0,0.3,0.0,

~Thermal Properties Card
Sand,Parallel,2.86,W/m K,2.86,W/m K,2.86,W/m K,700,J/kg K,

~Salt Transport Card
Sand,0.0,ft,0.0,ft,

~Source Card
1,
Nonaqueous Fluid Mass Source,1,1,1,1,100,100,1,
0,hr,0.879,gm/min,1.0,C,0.801,0.0,0.0,

~Boundary Conditions Card
6,
Bottom,Dirichlet Energy,Dirichlet-Outflow Aqueous,Dirichlet-Outflow Nonaqueous,
1,1,1,1,1,1,1,
0,hr,1.0,C,1414.7,psi,1414.7,psi,
Top,Dirichlet Energy,Zero Flux Aqueous,Zero Flux Nonaqueous,
1,1,1,1,100,100,1,
0,hr,1.0,C,
East,Dirichlet Energy,Zero Flux Aqueous,Zero Flux Nonaqueous,
1,1,1,1,1,100,1,
0,hr,1.0,C,
West,Dirichlet Energy,Zero Flux Aqueous,Zero Flux Nonaqueous,
1,1,1,1,1,100,1,
0,hr,1.0,C,
North,Dirichlet Energy,Zero Flux Aqueous,Zero Flux Nonaqueous,
1,1,1,1,1,100,1,
0,hr,1.0,C,
South,Dirichlet Energy,Zero Flux Aqueous,Zero Flux Nonaqueous,
1,1,1,1,1,100,1,
0,hr,1.0,C,

~Output Control Card
11,
1,1,1,

```

1,1,10,
 1,1,20,
 1,1,30,
 1,1,40,
 1,1,50,
 1,1,60,
 1,1,70,
 1,1,80,
 1,1,90,
 1,1,100,
 1,1,s,cm,6,6,6,
 29,
 Temperature,C,
 Gas Pressure,MPa,
 #Aqueous Pressure,MPa,
 Aqueous Density,kg/m^3,
 Gas Density,kg/m^3,
 Hydrate Density,kg/m^3,
 CO2 Aqueous Mass Fraction,,
 CO2 Nonaqueous Liquid Mass Fraction,,
 CO2 Gas Mass Fraction,,
 CO2 Hydrate Mass Fraction,,
 CH4 Aqueous Mass Fraction,,
 CH4 Nonaqueous Liquid Mass Fraction,,
 CH4 Gas Mass Fraction,,
 CH4 Hydrate Mass Fraction,,
 N2 Aqueous Mass Fraction,,
 N2 Nonaqueous Liquid Mass Fraction,,
 N2 Gas Mass Fraction,,
 N2 Hydrate Mass Fraction,,
 Aqueous Saturation,,
 Gas Saturation,,
 Hydrate Saturation,,
 Nonaqueous Liquid Saturation,,
 Integrated CO2 Mass,gm,
 Integrated CH4 Mass,gm,
 Integrated N2 Mass,gm,
 Integrated H2O Mass,gm,
 Integrated Hydrate CO2 Mass,gm,
 Integrated Hydrate CH4 Mass,gm,
 Integrated Hydrate N2 Mass,gm,
 Integrated Hydrate H2O Mass,gm,
 0,
 18,
 Temperature,C,
 Gas Pressure,MPa,
 #Aqueous Pressure,MPa,
 Aqueous Density,kg/m^3,
 Gas Density,kg/m^3,
 Hydrate Density,kg/m^3,
 CH4 Aqueous Mass Fraction,,
 CH4 Gas Mass Fraction,,
 CH4 Hydrate Mass Fraction,,
 CO2 Aqueous Mass Fraction,,
 CO2 Gas Mass Fraction,,
 CO2 Hydrate Mass Fraction,,
 N2 Aqueous Mass Fraction,,
 N2 Gas Mass Fraction,,
 N2 Hydrate Mass Fraction,,
 Aqueous Saturation,,
 Gas Saturation,,
 Hydrate Saturation,,
 Nonaqueous Liquid Saturation,,

~Surface Flux Card

10,
 Total CO2 Mass Flux,gm/s,gm,Bottom,1,1,1,1,1,1,
 Total CH4 Mass Flux,gm/s,gm,Bottom,1,1,1,1,1,1,
 Total N2 Mass Flux,gm/s,gm,Bottom,1,1,1,1,1,1,
 Gas CO2 Mass Flux,gm/s,gm,Bottom,1,1,1,1,1,1,
 Gas CH4 Mass Flux,gm/s,gm,Bottom,1,1,1,1,1,1,
 Gas N2 Mass Flux,gm/s,gm,Bottom,1,1,1,1,1,1,
 Nonaqueous Liquid CO2 Mass Flux,gm/s,gm,Bottom,1,1,1,1,1,1,
 Nonaqueous Liquid CH4 Mass Flux,gm/s,gm,Bottom,1,1,1,1,1,1,
 Gas Mass Flux,gm/s,gm,Bottom,1,1,1,1,1,1,
 Nonaqueous Liquid Mass Flux,gm/s,gm,Bottom,1,1,1,1,1,1,

Input File for Swapping Production (Second Cycle)

~Simulation Title Card

1,
 Constant Flow Rate Swapping #1,
 Mark White and Won Suk Lee,
 PNNL and KIGAM,
 27 February 2013,
 08:16 PST,
 3,
 Constant flow rate of 480 sccm (8:2 by volume CO2:N2).
 789.48 min simulation time.

~Solution Control Card

Restart,
 HYDT-KE w/NaCl w/Isobrine,
 2,
 0.0,sec,120.0,min,0.01,sec,10.0,min,1.25,16,1.e-06,
 120.0,min,165.50,min,0.01,sec,10.0,min,1.25,16,1.e-06,
 10000,
 Variable Aqueous Diffusion,
 Variable Gas Diffusion,
 Variable Nonaqueous Liquid Diffusion,
 8.e-6,kmol/s m^3,1.e-2,kmol/s m^3,1.e-2,kmol/s m^3,2.5,
 0,

~Grid Card

Cartesian,
 1,1,100,
 0,cm,4.874248,cm,
 0,cm,4.874248,cm,
 0,cm,100@0.46,cm,

~Rock/Soil Zonation Card

1,
 Sand,1,1,1,1,1,100,

~Mechanical Properties Card

Sand,2.633,g/cm^3,0.3346,0.3346,compressibility,1.e-12,1/Pa,,Millington and Quirk,,,

~Hydraulic Properties Card

Sand,0.202,darcy,0.202,darcy,0.202,darcy,

~Saturation Function Card

72.0,dynes/cm,24.0,dynes/cm,,26.7,dynes/cm,
 Sand,van Genuchten w/Webb,0.0341,1/cm,1.422,0.0,,72.0,dynes/cm,0.0,

~Aqueous Relative Permeability Card

Sand,Free Corey,1.0,3.0,0.3,0.0,

~Gas Relative Permeability Card

Sand,Free Corey,1.0,3.0,0.3,0.0,

~Nonaqueous Liquid Relative Permeability Card

Sand,Free Corey,1.0,3.0,0.3,0.0,

~Thermal Properties Card

Sand,Parallel,2.86,W/m K,2.86,W/m K,2.86,W/m K,700,J/kg K,

~Salt Transport Card

Sand,0.0,ft,0.0,ft,

~Source Card

1,

Nonaqueous Fluid Mass Source,1,1,1,1,100,100,1,

120.0,min,0.879,gm/min,1.0,C,0.801,0.0,0.0,

~Boundary Conditions Card

6,

Bottom,Dirichlet Energy,Dirichlet-Outflow Aqueous,Dirichlet-Outflow Nonaqueous,

1,1,1,1,1,1,1,

120.0,min,1.0,C,1414.7,psi,1414.7,psi,

Top,Dirichlet Energy,Zero Flux Aqueous,Zero Flux Nonaqueous,

1,1,1,1,100,100,1,

0.0,min,1.0,C,

East,Dirichlet Energy,Zero Flux Aqueous,Zero Flux Nonaqueous,

1,1,1,1,1,100,1,

0.0,min,1.0,C,

West,Dirichlet Energy,Zero Flux Aqueous,Zero Flux Nonaqueous,

1,1,1,1,1,100,1,

0.0,min,1.0,C,

North,Dirichlet Energy,Zero Flux Aqueous,Zero Flux Nonaqueous,

1,1,1,1,1,100,1,

0.0,min,1.0,C,

South,Dirichlet Energy,Zero Flux Aqueous,Zero Flux Nonaqueous,

1,1,1,1,1,100,1,

0.0,min,1.0,C,

~Output Control Card

11,

1,1,1,

1,1,10,

1,1,20,

1,1,30,

1,1,40,

1,1,50,

1,1,60,

1,1,70,

1,1,80,

1,1,90,

1,1,100,

1,1,s,cm,6,6,6,

29,

Temperature,C,

Gas Pressure,MPa,

#Aqueous Pressure,MPa,

Aqueous Density,kg/m^3,

Gas Density,kg/m^3,

Hydrate Density,kg/m^3,

CO2 Aqueous Mass Fraction,,

CO2 Nonaqueous Liquid Mass Fraction,,

CO2 Gas Mass Fraction,,

CO2 Hydrate Mass Fraction,,

CH4 Aqueous Mass Fraction,,

CH4 Nonaqueous Liquid Mass Fraction,,

CH4 Gas Mass Fraction,,

CH4 Hydrate Mass Fraction,,

N2 Aqueous Mass Fraction,,
 N2 Nonaqueous Liquid Mass Fraction,,
 N2 Gas Mass Fraction,,
 N2 Hydrate Mass Fraction,,
 Aqueous Saturation,,
 Gas Saturation,,
 Hydrate Saturation,,
 Nonaqueous Liquid Saturation,,
 Integrated CO2 Mass,gm,
 Integrated CH4 Mass,gm,
 Integrated N2 Mass,gm,
 Integrated H2O Mass,gm,
 Integrated Hydrate CO2 Mass,gm,
 Integrated Hydrate CH4 Mass,gm,
 Integrated Hydrate N2 Mass,gm,
 Integrated Hydrate H2O Mass,gm,
 0,
 18,
 Temperature,C,
 Gas Pressure,MPa,
 #Aqueous Pressure,MPa,
 Aqueous Density,kg/m^3,
 Gas Density,kg/m^3,
 Hydrate Density,kg/m^3,
 CH4 Aqueous Mass Fraction,,
 CH4 Gas Mass Fraction,,
 CH4 Hydrate Mass Fraction,,
 CO2 Aqueous Mass Fraction,,
 CO2 Gas Mass Fraction,,
 CO2 Hydrate Mass Fraction,,
 N2 Aqueous Mass Fraction,,
 N2 Gas Mass Fraction,,
 N2 Hydrate Mass Fraction,,
 Aqueous Saturation,,
 Gas Saturation,,
 Hydrate Saturation,,
 Nonaqueous Liquid Saturation,,

~Surface Flux Card

10,
 Total CO2 Mass Flux,gm/s,gm,Bottom,1,1,1,1,1,1,
 Total CH4 Mass Flux,gm/s,gm,Bottom,1,1,1,1,1,1,
 Total N2 Mass Flux,gm/s,gm,Bottom,1,1,1,1,1,1,
 Gas CO2 Mass Flux,gm/s,gm,Bottom,1,1,1,1,1,1,
 Gas CH4 Mass Flux,gm/s,gm,Bottom,1,1,1,1,1,1,
 Gas N2 Mass Flux,gm/s,gm,Bottom,1,1,1,1,1,1,
 Nonaqueous Liquid CO2 Mass Flux,gm/s,gm,Bottom,1,1,1,1,1,1,
 Nonaqueous Liquid CH4 Mass Flux,gm/s,gm,Bottom,1,1,1,1,1,1,
 Gas Mass Flux,gm/s,gm,Bottom,1,1,1,1,1,1,
 Nonaqueous Liquid Mass Flux,gm/s,gm,Bottom,1,1,1,1,1,1,

Input File for Swapping Production (Third Cycle)

~Simulation Title Card

1,
 Constant Flow Rate Swapping #1,
 Mark White and Won Suk Lee,
 PNNL and KIGAM,
 27 February 2013,
 09:38 PST,
 3,
 Constant flow rate of 480 sccm (8:2 by volume CO2:N2).
 789.48 min simulation time.

```

~Solution Control Card
Restart,
HYDT-KE w/NaCl w/Isobrine,
2,
0.0,sec,120.0,min,0.01,sec,10.0,min,1.25,16,1.e-06,
120.0,min,153.13,min,60,sec,10.0,min,1.25,16,1.e-06,
10000,
Variable Aqueous Diffusion,
Variable Gas Diffusion,
Variable Nonaqueous Liquid Diffusion,
8.e-6,kmol/s m^3,1.e-2,kmol/s m^3,1.e-2,kmol/s m^3,2.5,
0,

~Grid Card
Cartesian,
1,1,100,
0,cm,4.874248,cm,
0,cm,4.874248,cm,
0,cm,100@0.46,cm,

~Rock/Soil Zonation Card
1,
Sand,1,1,1,1,1,100,

~Mechanical Properties Card
Sand,2.633,g/cm^3,0.3346,0.3346,compressibility,1.e-12,1/Pa,,,Millington and Quirk,,,

~Hydraulic Properties Card
Sand,0.202,darcy,0.202,darcy,0.202,darcy,

~Saturation Function Card
72.0,dynes/cm,24.0,dynes/cm,,,26.7,dynes/cm,
Sand,van Genuchten w/Webb,0.0341,1/cm,1.422,0.0,,72.0,dynes/cm,0.0,

~Aqueous Relative Permeability Card
Sand,Free Corey,1.0,3.0,0.3,0.0,

~Gas Relative Permeability Card
Sand,Free Corey,1.0,3.0,0.3,0.0,

~Nonaqueous Liquid Relative Permeability Card
Sand,Free Corey,1.0,3.0,0.3,0.0,

~Thermal Properties Card
Sand,Parallel,2.86,W/m K,2.86,W/m K,2.86,W/m K,700,J/kg K,

~Salt Transport Card
Sand,0.0,ft,0.0,ft,

~Source Card
1,
Nonaqueous Fluid Mass Source,1,1,1,1,100,100,1,
120.0,min,0.879,gm/min,1.0,C,0.801,0.0,0.0,

~Boundary Conditions Card
6,
Bottom,Dirichlet Energy,Dirichlet-Outflow Aqueous,Dirichlet-Outflow Nonaqueous,
1,1,1,1,1,1,1,
120.0,min,1.0,C,1414.7,psi,1414.7,psi,
Top,Dirichlet Energy,Zero Flux Aqueous,Zero Flux Nonaqueous,
1,1,1,1,100,100,1,
0.0,min,1.0,C,
East,Dirichlet Energy,Zero Flux Aqueous,Zero Flux Nonaqueous,
1,1,1,1,1,100,1,
0.0,min,1.0,C,

```

West,Dirichlet Energy,Zero Flux Aqueous,Zero Flux Nonaqueous,
 1,1,1,1,1,100,1,
 0.0,min,1.0,C,
 North,Dirichlet Energy,Zero Flux Aqueous,Zero Flux Nonaqueous,
 1,1,1,1,1,100,1,
 0.0,min,1.0,C,
 South,Dirichlet Energy,Zero Flux Aqueous,Zero Flux Nonaqueous,
 1,1,1,1,1,100,1,
 0.0,min,1.0,C,

~Output Control Card

11,
 1,1,1,
 1,1,10,
 1,1,20,
 1,1,30,
 1,1,40,
 1,1,50,
 1,1,60,
 1,1,70,
 1,1,80,
 1,1,90,
 1,1,100,
 1,1,s,cm,6,6,6,
 29,
 Temperature,C,
 Gas Pressure,MPa,
 #Aqueous Pressure,MPa,
 Aqueous Density,kg/m^3,
 Gas Density,kg/m^3,
 Hydrate Density,kg/m^3,
 CO2 Aqueous Mass Fraction,,
 CO2 Nonaqueous Liquid Mass Fraction,,
 CO2 Gas Mass Fraction,,
 CO2 Hydrate Mass Fraction,,
 CH4 Aqueous Mass Fraction,,
 CH4 Nonaqueous Liquid Mass Fraction,,
 CH4 Gas Mass Fraction,,
 CH4 Hydrate Mass Fraction,,
 N2 Aqueous Mass Fraction,,
 N2 Nonaqueous Liquid Mass Fraction,,
 N2 Gas Mass Fraction,,
 N2 Hydrate Mass Fraction,,
 Aqueous Saturation,,
 Gas Saturation,,
 Hydrate Saturation,,
 Nonaqueous Liquid Saturation,,
 Integrated CO2 Mass,gm,
 Integrated CH4 Mass,gm,
 Integrated N2 Mass,gm,
 Integrated H2O Mass,gm,
 Integrated Hydrate CO2 Mass,gm,
 Integrated Hydrate CH4 Mass,gm,
 Integrated Hydrate N2 Mass,gm,
 Integrated Hydrate H2O Mass,gm,
 0,
 18,
 Temperature,C,
 Gas Pressure,MPa,
 #Aqueous Pressure,MPa,
 Aqueous Density,kg/m^3,
 Gas Density,kg/m^3,
 Hydrate Density,kg/m^3,
 CH4 Aqueous Mass Fraction,,
 CH4 Gas Mass Fraction,,

CH4 Hydrate Mass Fraction,,
CO2 Aqueous Mass Fraction,,
CO2 Gas Mass Fraction,,
CO2 Hydrate Mass Fraction,,
N2 Aqueous Mass Fraction,,
N2 Gas Mass Fraction,,
N2 Hydrate Mass Fraction,,
Aqueous Saturation,,
Gas Saturation,,
Hydrate Saturation,,
Nonaqueous Liquid Saturation,,

~Surface Flux Card

10,

Total CO2 Mass Flux,gm/s,gm,Bottom,1,1,1,1,1,1,
Total CH4 Mass Flux,gm/s,gm,Bottom,1,1,1,1,1,1,
Total N2 Mass Flux,gm/s,gm,Bottom,1,1,1,1,1,1,
Gas CO2 Mass Flux,gm/s,gm,Bottom,1,1,1,1,1,1,
Gas CH4 Mass Flux,gm/s,gm,Bottom,1,1,1,1,1,1,
Gas N2 Mass Flux,gm/s,gm,Bottom,1,1,1,1,1,1,
Nonaqueous Liquid CO2 Mass Flux,gm/s,gm,Bottom,1,1,1,1,1,1,
Nonaqueous Liquid CH4 Mass Flux,gm/s,gm,Bottom,1,1,1,1,1,1,
Gas Mass Flux,gm/s,gm,Bottom,1,1,1,1,1,1,
Nonaqueous Liquid Mass Flux,gm/s,gm,Bottom,1,1,1,1,1,1,

4.0 References

- Andersen, G., Probst, A., Murray, L., Butler, S., 1992. "An accurate PVT model for geothermal fluids as represented by H₂O-CO₂-NaCl mixtures." In Proceedings of Seventeenth Workshop on Geothermal Reservoir Engineering, Stanford University, Stanford, California.
- ASHRAE, 1977; Psychrometric Tables given by *ASHRAE Handbook 1977 Fundamentals*, American Society of Heating, Refrigerating and Conditioning Engineering, Inc., 345 East 47th Street, New, N.Y.
- Battistelli, A., C. Claudio, and K. Pruess. 1997. "The simulator TOUGH2/EWASG for modelling geothermal reservoirs with brines and noncondensable gas." *Geothermics*, 26(4):437-464.
- Booth, J.S., Rowe, M.M., Fischer, K.M. 1996. "Offshore gas hydrate sample database with an overview and preliminary analysis." *U.S. Geological Survey, Open File Report 96-272*, Denver, Colorado.
- Bromley, L.A. 1973. "Thermodynamic properties of strong electrolytes in aqueous solutions." *AIChE Journal*, 19(2):313-320.
- Brooks, R. H., Corey, A. T., 1964. "Hydraulic Properties of Porous Media." *Colorado State University, Hydrology Paper, No. 3*, Fort Collins, Colorado.
- Brun, M., Lallemand, A., Quinson, J. F., Eyraud, C., 1977. A new method for the Kluda, J. B., Sandler, S. I., 2001. Modeling gas hydrate phase equilibria in laboratory and natural porous media. *Industrial Engineering Chemical Research*, 40:4197-4208.
- Castaldi, M.J., Y. Zhou, and T.M. Yegulalp. 2007. "Down-hole combustion method for gas production from methane hydrates." *Journal of Petroleum Science and Engineering*, 56:176-185.
- Dickerson, R. W., Jr., 1969. Thermal properties of food, in *The Freezing Preservation of Foods*, 4th ed., Vol. 2, D. K. Tressler, W. B. Van Arnsdel, and M. J. Copley (Editors), AVI Publishing Co., Westport, Conn.
- Elliot, J.R. and C.T. Lira. 1998. *Introductory Chemical Engineering Thermodynamics*, Prentice Hall International Series in the Physical and Chemical Engineering Sciences, ISBN 0-13-011386-7.
- Englezos, P. 1993. "Clathrate hydrates." *Industrial Engineering Chemical Research*, 32: 1251-1274.
- Ferraresi, M. 1989. "An integrated finite difference model for groundwater flow and quality simulation." *Groundwater Management Quantity and Quality*, (Proceedings of the Benidorm Symposium, Oct. 1989). IAHS Pub. No. 188:321-330.
- Fenghour, A., W. A. Wakeham, V. Vesovic. 1998. "The viscosity of carbon dioxide." *J. Phys. Chem. Ref. Data*, 27(1):31-41.
- Garapati, N., Anderson, B.J. 2009. "Predictions of Mixed Hydrate Phase Equilibria and the Swapping of CH₄ Hydrate with CO₂ and CO₂+N₂ Mixtures" AIChE National Meeting, Nashville, TN, November, 2009.
- Garapati, N., Anderson, B.J. 2010. "Predictions of Phase Equilibrium Data of Mixed Hydrates Using the Cell Potential Method," West Virginia Academy of Science 85th Annual Meeting, Morgantown, WV, April 10, 2010.
- Gudmundsson, J.S., and H. Thrainsson. 1989. "Power potential of two-phase geothermal wells." *Geothermics* 18(3):357-366.

- Hanley, H.J.M., W.M. Haynes, and R.D. McCarty. 1997. "The viscosity and thermal conductivity coefficients for dense gaseous and liquid methane." *J. Phys. Chem. Ref. Data*, 6(2):597-609.
- Hirohama, S., Y. Shimoyama, A. Wakabayashi, S. Tatsuta, and N. Nishida. 1996. "Conversion of CH₄-hydrate to CO₂-hydrate in liquid CO₂." *Journal of Chemical Engineering of Japan*, 29(6):1014-1020.
- Klauda, J.B., and S.I. Sandler. 2003. Phase behavior of clathrate hydrates: a model for single and multiple gas component hydrates. *Chemical Engineering Science*, 58:27-41.
- Komai, T.; Yamamoto, Y.; and Ikegami, S. 1997. "Equilibrium properties and kinetics of methane and carbon dioxide gas hydrate formation/dissociation." *Proceedings of American Chemical Society Fuel Chemistry Division*, 42(2):568-572.
- Lemmon, E.W., and R.T. Jacobsen. 2004. "Viscosity and thermal equations for nitrogen, oxygen, argon, and air," *International Journal of Thermophysics* 25(1):21-69.
- McGrail, B.P., T. Zhu, R.B. Hunter, M.D. White, S.L. Patil, and A.S. Kulkarni. 2004. "A new method for enhanced production of gas hydrates with CO₂." *Gas Hydrates: Energy Resource Potential and Associated Geologic Hazards*, American Association of Petroleum Geologists.
- Michlesen, M.L. 1980. "Calculation of phase envelopes and critical points for multicomponent mixtures." *Fluid Phase Equilibria*, 4:1-10.
- Michelsen, M.L. 1986. "Simplified Flash Calculations for Cubic Equations of State." *Industrial Engineering Chemical Process Design and Development*, 25:184-188.
- Meyer, C.A., R.B. McClintock, G.J. Silvestri, and R.C. Spencer. 1993. *ASME Steam Tables*, The American Society of Mechanical, New York.
- Nakano, S., K. Yamamoto, and K. Ohgaki. 1998. "Natural gas exploitation by carbon dioxide from gas hydrate fields - High-pressure phase equilibrium for an ethane hydrate system." In *Proceedings of the Institution of Mechanical Engineers*, 212:159-163.
- Nickalls, R.W.D. 1993. "A new approach to solving the cubic: Cardin's solution revealed." *Math. Gaz.*, 77:354-359.
- Ohgaki, K., K. Takano, H. Sangawa, T. Matsubara, and S. Nakano. 1996. "Methane exploitation by carbon dioxide from gas hydrates – Phase equilibria for CO₂-CH₄ mixed hydrate system." *Journal of Chemical Engineering of Japan*, 29(3):478-483.
- Østergaard, K.K., R. Masoudi, B. Tohidi, A. Danesh, and A.C. Todd. 2005. A general correlation for predicting the suppression of hydrate dissociation temperature in the presence of thermodynamic inhibitors. *Journal of Petroleum Science and Engineering*, 48(1-2):70-80.
- Ozbek, H. and S.L. Phillips. 1980. "Thermal conductivity of aqueous sodium chloride solutions from 20 to 330 C." *J. Chem. Engr. Data*, 25:263-267.
- Peng, D-Y. and D. B. Robinson. 1976. "A New Two-Constant Equation of State." *Industrial Engineering Chemical Fundamentals*, 15:59-64.
- Pedersen, K.S. and P.L. Christensen. 2007. *Phase Behavior of Petroleum Reservoir Fluids*, CRC Press, ISBN 0-8247-0694-3.

- Phillips, S.L., A. Igbene, J.A. Fair, H. Ozbek, and M. Tavana. 1981. *A Technical Databook for Geothermal Energy Utilization*, LBL-12810, UC-66a, Lawrence Berkeley Laboratory, University of California, Berkeley, California.
- Press, W.H., B.P. Flannery, S.A. Teukolsky, and W.T. Vetterling. 1986. *Numerical Recipes, The Art of Scientific Computing*, Cambridge University Press, Cambridge.
- Renner, T.A. 1988. "Measurement and Correlation of Diffusion Coefficients for CO₂ and Rich-Gas Applications." *SPE Reservoir Engineering*, pp:517-523.
- Rice, W. 2003. "Proposed system for hydrogen production from methane hydrate with sequestering of carbon dioxide hydrate." *Journal of Energy Resource Technology (ASME)*, 125(4):253–256.
- Rice, W. 2006. "Hydrogen production from methane hydrate with sequestering of carbon dioxide." *International Journal of Hydrogen Energy*, 31(14):1955-1963.
- Setzmann, U., and W. Wagner. 1991. A new equation of state and tables of thermodynamic properties for methane covering the range from the melting line to 625 K at pressures up to 1000 MPa. *Journal of Physical and Chemical Reference Data*, 20(6):1061-1155.
- Sloan, E.D., Jr. 1998. *Clathrate Hydrates of Natural Gases*, 2nd ed., Marcel Dekker, Inc., New York.
- Sloan, E.D., Jr., 2000. Clathrate hydrates: The other common solid water phase. *Industrial Engineering and Chemical Research*, 39:3123-3129.
- Span, R., E. W. Lemmon, R. T. Jacobsen, W. Wagner, and A. Yokozeki. 2000. "A reference equation of state for the thermodynamic properties of nitrogen for temperatures from 63.151 to 1000 K and pressures to 2200 MPa." *J. Phys. Chem. Ref. Data*, 29(6):1361-1433.
- Span, R. and W. Wagner. 1996. A new equation of state for carbon dioxide covering the fluid region from the triple-point to 1100 K at pressures up to 800 MPa. *Journal of Physical and Chemical Reference Data*, 25(6):1509-1588.
- U.S. Environmental Protection Agency. 2006. "The significance of methane and activities to reduce methane emissions." *Methane to Markets Bulletin*, www.methanetomarkets.org.
- van Genuchten, M.T.A. 1980. A closed-form equation for predicting the hydraulic conductivity of unsaturated soils. *Soil Science Society of America Journal*, 44:892-898.
- Vesovic, V., W.A. Wakeman, G.A. Olchow, J.V. Sengers, J.T.R. Watson, and J. Millat. 1990. "The transport properties of carbon dioxide." *J. Phys. Chem. Ref. Data*, 19(3):763-808.
- Waite, W.F., L.A. Stern, S.H. Kirby, W.J., Winters, and D.H. Mason 2007. "Simultaneous determination of thermal conductivity, thermal diffusivity, and specific heat in sI methane hydrate." *Geophysical Journal International*, 169:767-774, doi:10.1111/j.1365-246X.2007.03382.x.
- Webb, S.W. 2000. "A simple extension of two-phase characteristic curves to include the dry region." *Water Resources Research*, 36:1425-1430.
- White, M.D., and M. Oostrom. 2000. *STOMP Subsurface Transport Over Multiple Phases, Version 2.0, Theory Guide*, PNNL-12030, UC-2010, Pacific Northwest National Laboratory, Richland, Washington.

- White, M.D. and B.P. McGrail. 2006. "STOMP-HYD: A new numerical simulator for analysis of methane hydrate production from geologic formations." In Proceedings of 2nd International Symposium on Gas Hydrate Technology, 1-2 November 2006, KIGAM, Daejeon, Korea.
- White, M.D. and B.P. McGrail. 2008. "Numerical simulation of methane hydrate production from geologic formations via carbon dioxide injection." In Proceedings of 2008 Offshore Technology Conference, 5-8 May 2008, Houston, Texas, U.S.A.
- Wösten, J.H.M., Ya.A. Pachepsky, and W.J. Rawls. 2001. "Pedotransfer functions: bridging the gap between available basic soil data and missing soil hydraulic characteristics." *Journal of Hydrology*, 251:123-150.
- Yoon, J. Y. Yamamoto, T. Komai, and H. Haneda. 2003. "Rigorous approach to the prediction of the heat of dissociation of gas hydrates." *Ind. Eng. Chem. Res.*, 42:1111-1114.



Pacific Northwest
NATIONAL LABORATORY

902 Battelle Boulevard
P.O. Box 999
Richland, WA 99352
1-888-375-PNNL (7665)

www.pnl.gov



U.S. DEPARTMENT OF
ENERGY